New 40AR/39AR Age Constraints on the Timing of Metamorphism and Deformation in the Western Nashoba Terrane, Eastern Massachusetts

Author: Erin C. Reynolds

Boston College

The Graduate School of Arts and Sciences

Department of Earth and Environmental Sciences

NEW $^{40}AR/^{39}AR$ AGE CONSTRAINTS ON THE TIMING OF METAMORPHISM AND DEFORMATION IN THE WESTERN NASHOBA TERRANE, EASTERN MASSACHUSETTS

A Thesis by

ERIN C. REYNOLDS

Submitted in partial fulfillment of the requirements

for the degree of

Master of Science

May 2012

NEW ^{40}AR/^{39}AR AGE CONSTRAINTS ON THE TIMING OF METAMORPHISM AND DEFORMATION IN THE WESTERN NASHOBA TERRANE, EASTERN MASSACHUSETTS

Erin Reynolds

ABSTRACT

^{40}Ar/^{39}Ar single-grain total-fusion ages of muscovite and biotite and one ^{40}Ar/^{39}Ar furnace step-heating age of hornblende from the Tadmuck Brook Schist, Nashoba Formation, and Ball Hill mylonite zone are used to reconstruct the late tectonic and metamorphic history of the Nashoba terrane in eastern Massachusetts. The data fall into three age populations. Age population I (~376-330 Ma) is interpreted as cooling after a migmatization event in the Nashoba terrane, population II (~300 Ma) may be associated with normal movement on the Clinton-Newbury fault, and population III (~267 Ma) is possibly related to cooling of the Rocky Pond Granite. No younger Alleghanian overprint was observed.

ACKNOWLEDGEMENTS

I would like to express my deepest gratitude to Yvette Kuiper and Chris Hepburn for their guidance in this journey. They had the patience and strength to stick by me for six years. I cannot even begin to convene how much I have learned from them or how greatly I appreciate all that they have done for me.

William Olszewski, thank you for teaching me about the various ins and outs of the $^{40}Ar/^{39}Ar$ technique and for allowing me to be a part of the analytical process at the Argon Lab at MIT.

My fellow New England Appalachian colleagues also deserve my thanks. MaryEllen Loan, Andrew Kay, and Kristin Sorota, thank you for insightful conversations about the Nashoba and Merrimack terranes. Your ideas helped drive my research and I hope that I was able to do the same for you.

Thank you to my parents and sister, Edward, Michelle, and Megan Reynolds, as well as the rest of the Reynolds Clan. You were always so understanding and encouraging while I was on this journey. I could not have done it without your continued support and love (as well as all of the rock jokes that you threw my way!).

Hosanna Lillydahl-Schroeder, you have been my partner in crime these past few years. I am so lucky and happy to have met you during our tenure here at Boston College. Thank you so much for the sacrifices that you have made to help me finish, as well as the love and knowledge that you have shared. I promise to do the same for you as you complete your thesis. (Although you may be on your own when it comes to the laundry).

Tourmaline and Gypsy, thank you for being two wonderful cats. You provided the perfect amount of distraction when it was needed the most.

TABLE OF CONTENTS

FIGURES

TABLES

Chapter 1. INTRODUCTION

A. INTRODUCTION TO THE APPALACHIANS

The Appalachian Mountain Belt stretches from Newfoundland in Canada southwestward to Alabama in the United States. This mountain belt resulted from five major orogenic events during the Paleozoic. These orogenic events, the Taconic (Ordovician), Salinic (Silurian), Acadian (Devonian), Neo-Acadian (Mississippian) and A llleghanian (Pennsylvanian-Permian) are all believed to have been the result of unique terrane accretions (Hatcher, 2010; Rankin, 1994; Robinson et al., 1998; van Staal et al., 2009; Zagorevski et al., 2007). It is important to note the tectonic and metamorphic implications of these collisions are not uniform throughout the Appalachians. Thus, some areas show complex polymetamorphic and polydeformational histories, while others only record a single accretionary event.

B. TECTONIC HISTORY OF MASSACHUSETTS

During the Taconic orogeny in southeast New England, the passive margin of Laurentia was subducted under a magmatic arc, resulting in accretion of the arc to Laurentia (Fig. 1.1). Today this arc, Shelburne Falls Arc (Fig. 1.1), is found in Vermont, western Massachusetts, and Connecticut (Karabinos et al., 1998).

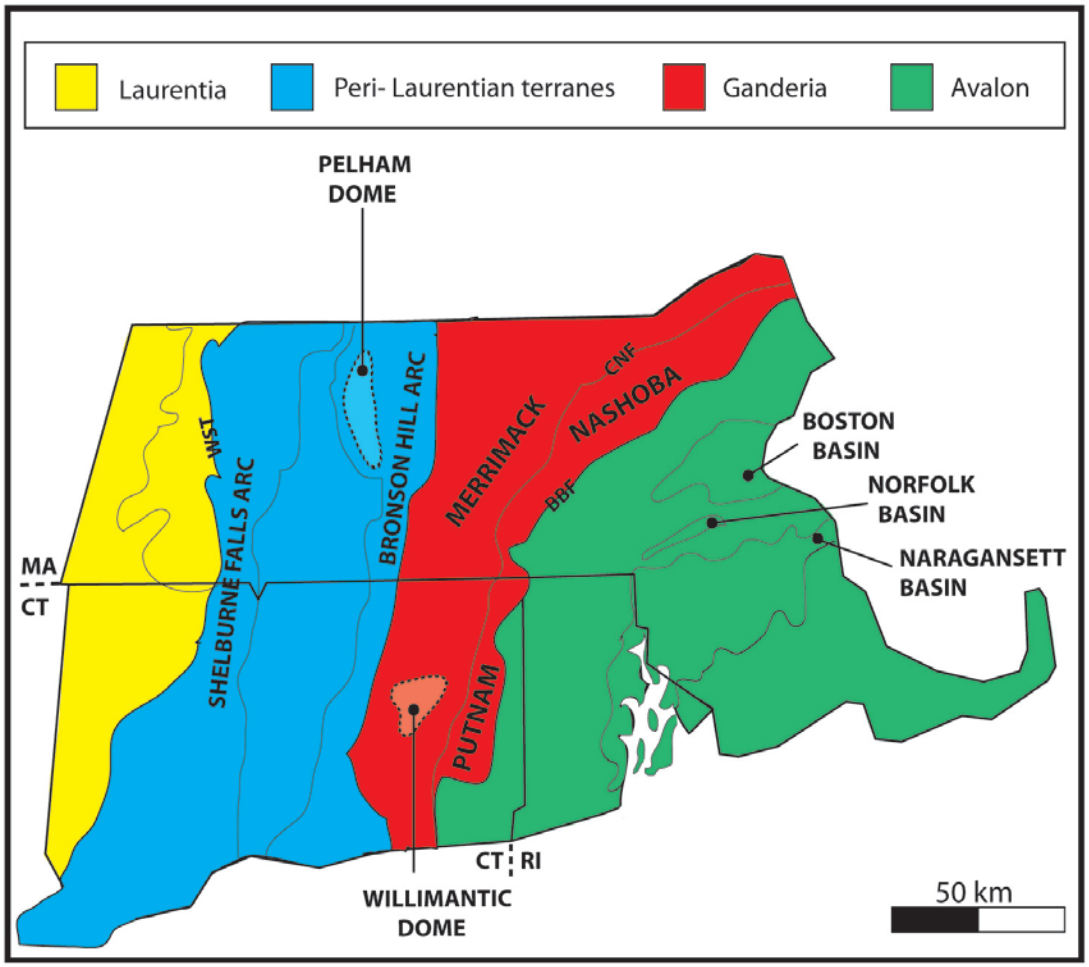

Figure 1.1 Simplified tectonic map of southern New England. Modeled after Aleinikoff et al. (2007), Hepburn et al., (1987a), Karabinos et al. (1998), Moecher (1999), and Pollack et al. (2007). BBF = Bloody Bluff fault, CNF = Clinton-Newbury fault zone, WST=Whitcomb Summit thrust zone.

“Ganderia” has been used to describe the peri-Gondwanan terranes that accreted onto Laurentia after the peri-Laurentian terranes and before Avalon (van Staal et al., 2009). Recent studies have suggested that the Nashoba and Merrimack terranes were both part of Ganderia (Fig. 1.1; Kay et al., 2011; Loan, 2011; Sorota et al., 2012). The Salinic orogeny is characterized by the accretion of Ganderia onto Laurentia during the Silurian (Fig. 1.1; Fig. 1.2). Deposition of the units analyzed in this study also occurred during this time period (Loan, 2011).

Next, the Acadian orogeny occurred during the Devonian, when Avalon collided with and accreted onto Laurentia (Fig. 1.2). This was a period of migmatization and sillimanite-grade metamorphism in the Nashoba terrane.

In central Massachusetts, the Neo-Acadian orogeny was a period of intense metamorphism up to granulite facies with associated magmatism and severe deformation. The Meguma terrane accreted in the northern Appalachians at this time (Hibbard et al., 2007; van Staal et al., 2009). However, accretion does not seem to be a cause of deformation in Massachusetts because Avalon, the easternmost terrane in the field area, remains relatively undeformed (Markwort, 2007). The deformation that occurred in the Nashoba terrane at this time may be related to post-amalgamation motion among the Merrimack, Nashoba, and Avalon terranes (Markwort, 2007).

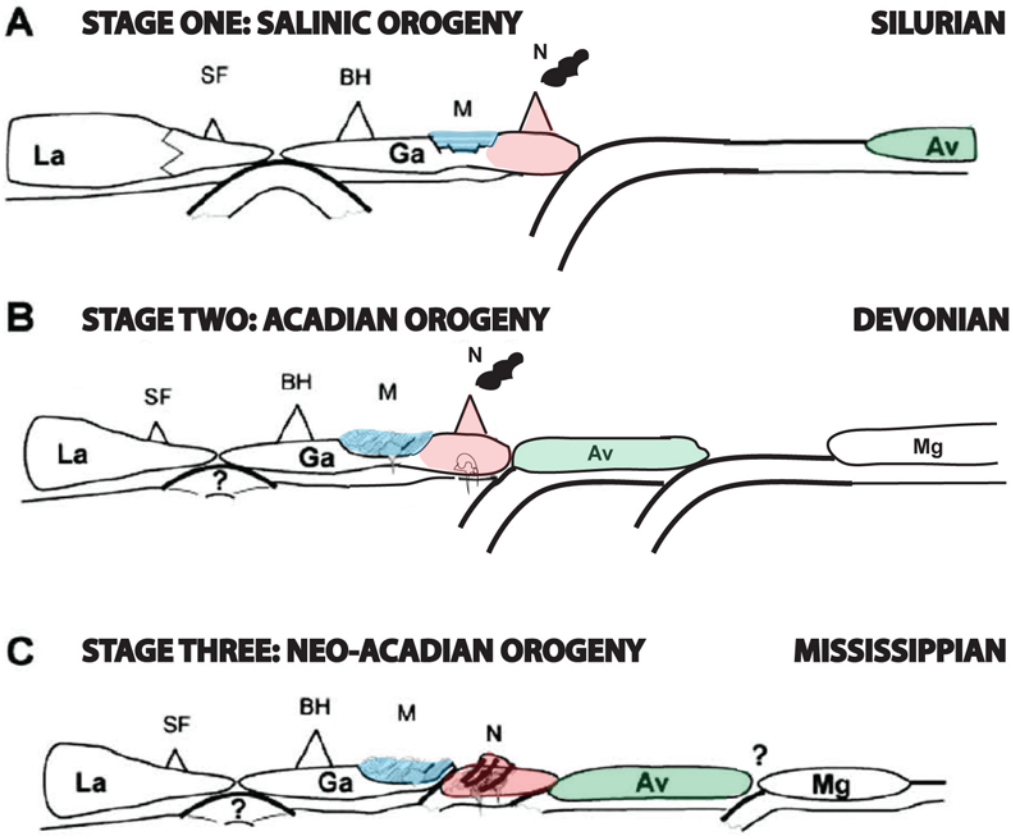

Figure 1.2 Accretionary history of the Merrimack, Nashoba, and Avalon terranes. La = Laurentia; Ga=Gander; Av=Avalon; Mg=Meguma; SF=Shelburne Falls Arc; BH=Bronson Hills Arc; M=Merrimack; N=Nashoba (Markwort, 2007; van Staal et al., 2009; Zagorevski et al., 2007)

The Alleghanian orogeny is related to the collision of Laurentia with Africa. The orogeny caused metamorphism, deformation, and magmatism in gneiss domes, such as the Pelham and Willimantic Domes in western Massachusetts and eastern Connecticut, respectively (Fig. 1.1; Moecher, 1999). In the southern Appalachians, structural reworking and metamorphism from the Alleghanian orogeny is common. Alleghanian overprinting is not as pronounced in southern New England, but is observed in the Avalon terrane and western Massachusetts, and weakly in the Nashoba terrane (Wintsch, 1992; Wintsch et al., 2003; Wintsch et al., 2010; Zartman et al., 1970). At present, it is unclear what effect the Alleghanian orogeny had on the Nashoba terrane (Wintsch et al., 2003), a question this study sought to answer.

C. LOCATION OF STUDY AREA

The investigation encompassed a region approximately 8km x 40km in eastern Massachusetts (red box in Fig. 1.3), northwest of Boston. This study is focused mainly on the Nashoba terrane (see Chapter 2). The area included parts of the towns of Marlborough, Berlin, Boylston, Harvard, and Littleton. The study area is bounded to the northwest by the Clinton-Newbury fault (CNFZ in Fig. 1.3).

D. PURPOSE

Multiple studies have documented the presence of Carboniferous and younger geochronological overprinting in southern New England, which they

have attributed to the Alleghanian orogeny (Wintsch, 1992; Wintsch et al., 2003; Wintsch et al., 2010). However, it has been suggested that the effect of the Alleghanian orogeny in Massachusetts was largely limited to the Avalon terrane, with little apparent overprinting in the Nashoba terrane (Wintsch et al., 2003). The purpose of this study was to determine (1) the age and nature of the youngest metamorphic and deformation events affecting the Nashoba terrane and (2) if these events were related to the Alleghanian orogeny.

The $^{40}Ar/^{39}Ar$ technique was used to date samples because it is useful for dating overprinted, low-temperature (<350 °C) metamorphic events (Hames et al., 1991; Murphy and Collins, 2008; see Chapter 3 for background on $^{40}Ar/^{39}Ar$ geochronology). Samples were collected along the western boundary of the Nashoba terrane, and include the Nashoba Formation, Tadmuck Brook Schist, and Ball Hill mylonite. These units/formations were chosen because: (1) they contain abundant K-bearing minerals, such as biotite, muscovite, and hornblende, all of which may be dated using the $^{40}Ar/^{39}Ar$ method, (2) the minerals to be dated were large enough to separate from the matrix, and (3) the units/ formations were originally believed to be unaffected by late, discrete igneous activity.

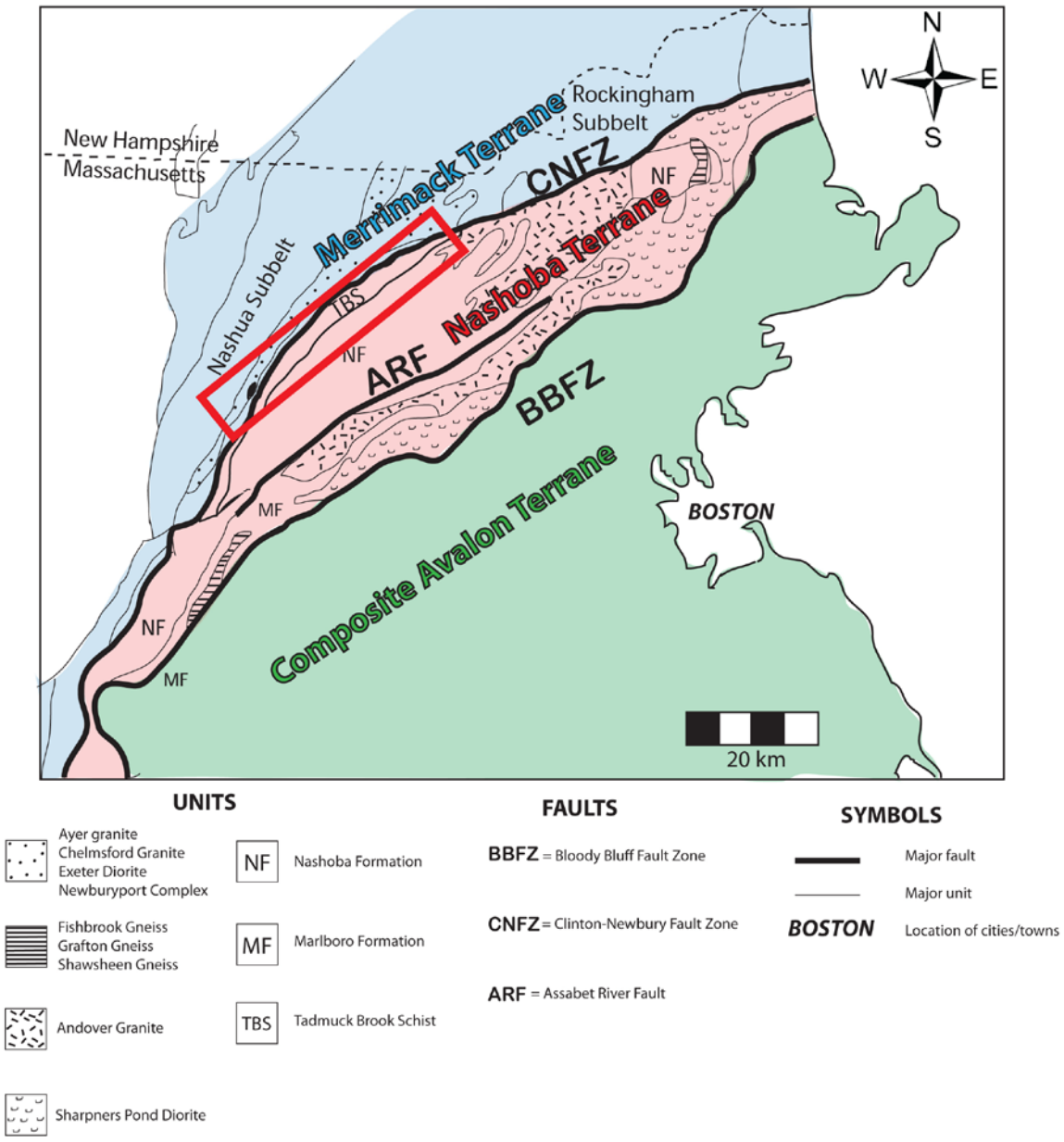

Figure 1.3 Field area (shown by red box) in eastern Massachusetts. Map is adapted from Goldsmith (1991).

Chapter 2. PREVIOUS WORK

A. TERRANES IN EASTERN MASSACHUSETTS

I. Introduction to terranes

Terranes are discrete crustal blocks or fragments that may become attached to a continent as a result of a collision. The northern Appalachian Mountains are a result of at least three unique terrane accretions or agglomerations: Ganderia (Salinic Orogeny), Avalonia (Acadian Orogeny), and Meguma (Neo-Acadian Orogeny) (Fig. 1.2; Hatcher, 2010; Rankin, 1994; Robinson et al., 1998; van Staal et al., 2009; Zagorevski et al., 2007). There are three terranes in eastern Massachusetts. From east to west they are the Avalon, Nashoba, and Merrimack terranes (Fig. 1.3). Each of these terranes is described below.

II. Avalon terrane

There are three basins within the Avalon terrane of southeast New England that mostly consist of sedimentary and metasedimentary rocks: (1) Boston Basin (late Proterozoic-early Paleozoic), (2) Norfolk Basin (Carboniferous) and (3) Narragansett Basin (Carboniferous) (Fig. 1.1; Bell and Alvord, 1976; Hepburn et al., 1987a). The Avalon terrane was intruded by late Proterozoic plutons and alkalic to peralkaline mid-Paleozoic to Carboniferous plutons and volcanic rocks (Hepburn et al., 1993; Zartman and Naylor, 1984). The late Proterozoic plutons were mostly arc derived (Goldsmith, 1991).

In eastern Massachusetts, the Avalon terrane is weakly metamorphosed and seems unaffected by the Acadian orogeny (Rast and Skehan, 1993). Avalon experienced upper greenschist facies metamorphism (Grimes and Skehan, 1995), much lower than that experienced by the Nashoba terrane.

The western border of the Avalon terrane (Fig. 1.3) is defined by the Bloody Bluff-Lake Char-Honey Hill fault system, an array of mylonitic shear zones and brittle faults. This fault system forms the boundary between the Avalon and Nashoba terranes.

III. Merrimack terrane

The Merrimack belt (Zen et al., 1983; Fig. 1.3) is believed to correlate with the Gander terrane of Newfoundland and extends from south-central Connecticut to the Gulf of Maine (Wintsch et al., 2007). The eastern portion of the belt, part of the study area, consists of a thick sequence of metasedimentary rocks including impure quartzites, metapelites, and calcareous metasiltstones of Ordovician to Devonian age (Sorota et al., 2011; Wintsch et al., 2007; Zen et al., 1983).

The Merrimack terrane was multiply deformed and metamorphosed during the Acadian orogeny (Osberg et al., 1989). The metasedimentary rocks have been metamorphosed to greenschist facies in the east (in the study area) and to amphibolite facies along the western boundary of the terrane (Zen et al., 1983). They were later intruded by middle to late Paleozoic granites, diorites, and tonalities (Robinson and Goldsmith, 1991). The terrane is bounded to the east by the Clinton-Newbury fault.

Sorota et al. (2011) dated detrital zircons from the Merrimack terrane in Massachusetts and southeast New Hampshire and determined that deposition occurred between the mid-Silurian and early-Devonian. Similar ages of deposition were found by Wintsch et al. (2007) in a study of detrital, metamorphic and magmatic zircons and metamorphic monazite and titanite from the Merrimack terrane in Connecticut and Maine. The timing of sedimentation suggests that much of the detritus was generated during the Salinic orogeny (Sorota et al., 2011).

IV. Nashoba terrane

The Nashoba terrane (Fig. 1.3; Fig 2.1) is bounded by the Bloody Bluff fault to the east and by the Clinton-Newbury fault to the west. In Massachusetts the Clinton-Newbury fault can be traced from Newburyport, along the northeast coast, to Oxford, near the Connecticut border. Past studies have suggested the Clinton-Newbury fault experienced a late, normal west-down movement (Goldstein, 1994).

The Nashoba terrane is composed of Cambrian to Ordovician arc-related rocks (Hepburn et al., 1995; Loan, 2011; Walsh and Wintsch, 2011). No lithologies can be correlated across the terrane bounding faults. There are major faults and shear zones throughout the terrane, suggesting that it represents a tectonic assemblage and not an original stratigraphic sequence (Hepburn et al., 1995; Zen et al., 1983). The formations and units that make up the Nashoba

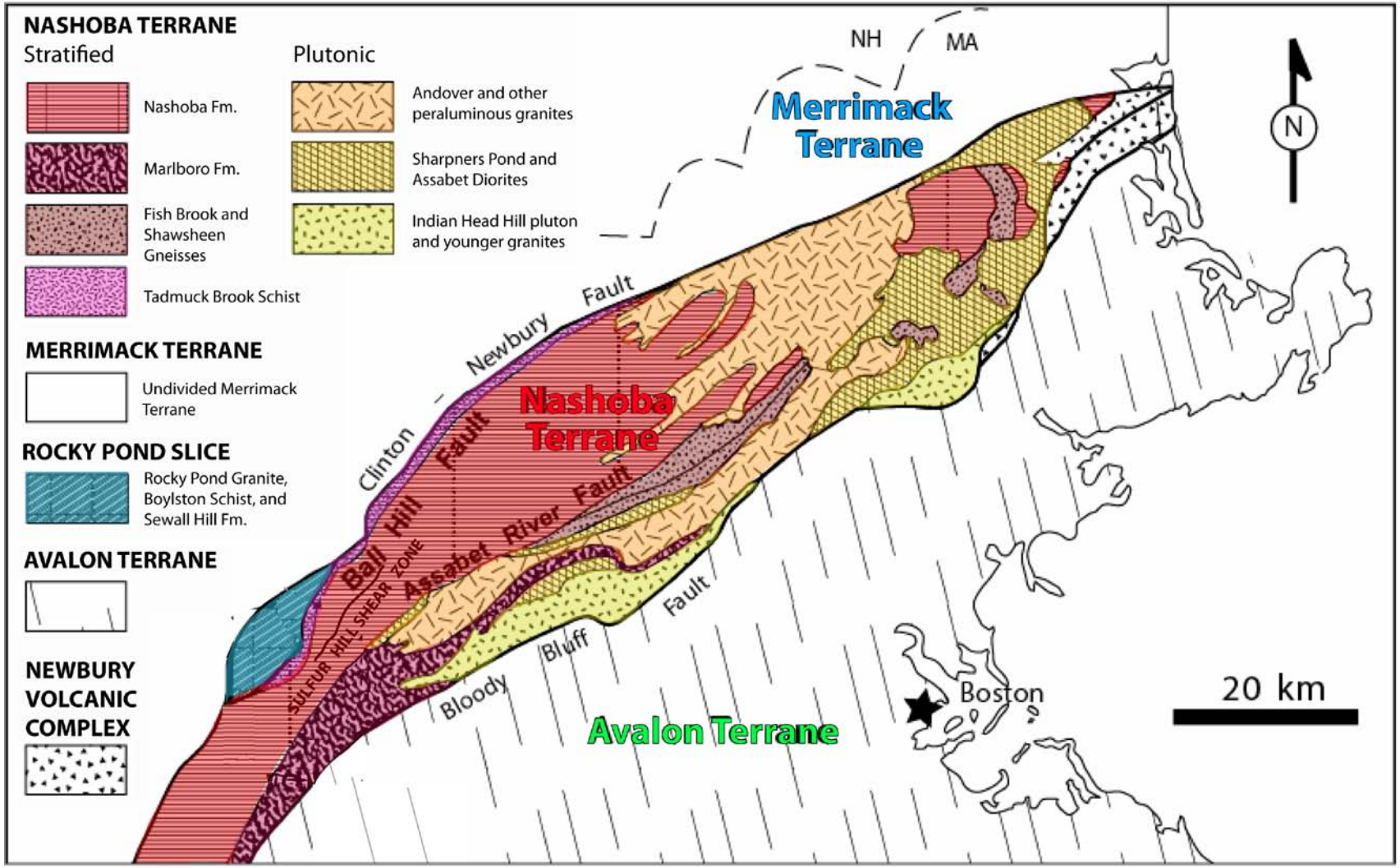

Figure 2.1 Geologic map of the Nashoba Terrane (modified after Markwort, 2007; Zen et al., 1983; basemap modified from Hepburn et al., 1995)

terrane include the Marlboro Formation, Fish Brook Gneiss, Nashoba Formation, Shawsheen Gneiss, and Tadmuck Brook Schist.

The Marlboro Formation (Fig. 2.1) is located in the southeastern part of the terrane. This formation is composed of biotite-hornblende quartzofeldspathic gneisses and amphibolites (Goldsmith, 1991), the latter are thought to have mafic volcanic protoliths (Hepburn et al., 1995). The Grafton Gneiss cross-cuts the Marlboro Formation and has a SHRIMP U-Pb age of 515 ± 4 Ma, constraining the age of the Marlboro Formation to Early Cambrian or older (Walsh et al., 2009). Sm/Nd geochemistry suggests the Marlboro Formation had an ocean island arc/back arc origin (Kay et al., 2009).

The Fish Brook Gneiss (Fig. 2.1) has been mapped as an orthogneiss (Bell and Alvord, 1976; Zen et al., 1983) and incorporates material originating from an older continental source of unknown origin (Kay et al., 2009). Sm/Nd values suggest the Nashoba terrane may have formed on the edge of a continent, Ganderia (Kay et al., 2011). The Fish Brook Gneiss has a U/Pb zircon date of 499 +6/-3 Ma (Hepburn et al., 1995). A U-Pb monazite age from the Fish Brook Gneiss of 425 ± 3 Ma (Hepburn et al., 1995) is interpreted as metamorphic.

The Nashoba Formation (Fig.2.1) is a thick deposit of metasedimentary rocks located in the northwestern part of the Nashoba terrane. The Tadmuck Brook Schist (Fig. 2.1) is a rusty, sulfidic schist located in the footwall of the

Clinton-Newbury fault (Goldstein, 1994). The Nashoba Formation and Tadmuck Brook Schist will be discussed further in Section B of this chapter.

V. Rocky Pond Slice

The Rocky Pond Slice is a complex, fault-bounded tectonic slice (Fig. 2.1) separated from the Nashoba terrane by the Rattlesnake Hill fault. The fault exhibits structural evidence for west-side-down normal motion with possible earlier deformation (Markwort, 2007).

The origin of the Rocky Pond Slice is unclear. It may be an upthrust block of the Nashoba terrane caught in the Clinton-Newbury fault zone (Goldsmith, 1991; Munn, 1987) or a part of the low-grade Merrimack terrane (Markwort, 2007). Similar to the Nashoba terrane, parts of the slice experienced amphibolite facies metamorphism (Munn, 1987). The Rocky Pond Slice is composed of schists intruded by the unfoliated Rocky Pond Granite (Markwort, 2007). The Rocky Pond Granite is peraluminous (S-type), based on an abundance of muscovite, tourmaline and garnet, and it likely formed from the melting of sediments (Markwort, 2007; Munn, 1987). The granite is medium-grained to pegmatitic. Several δ-porphyroclasts and an asymmetric extensional shear band fabric observed in a Rocky Pond Granite thin section also indicate a northwest-side-down motion (Markwort, 2007).

Zartman and Naylor (1984) attempted to date the Rocky Pond Granite using the Rb-Sr whole rock isochron method. They were unable to obtain an

acceptable isochron, and believe this was due to a post-crystallization event that disturbed the system, resulting in a partial homogenization of strontium isotopes.

B. UNITS/FORMATIONS STUDIED

I. Nashoba Formation

The Nashoba Formation is bounded to the west by the Ball Hill fault in the southern part of the study area (Fig. 2.1). Protoliths of the Nashoba Formation include volcanoclastic sediments and mafic volcanics interbedded with feldspathic sandstones. These have been polymetamorphosed and multiply deformed under sillimanite and sillimanite-K-feldspar zone metamorphic conditions to amphibolites, schists, and gneisses (Bell and Alvord, 1976; Goldsmith, 1991).

Amphibolites are found throughout the Nashoba terrane in beds up to a few meters thick in the Nashoba Formation (Bober, 1990). One amphibolite unit of the Nashoba Formation from Route 2 in Littleton, MA was analyzed for this study (See Chapter 4).

Schists found within the Nashoba Formation tend to be orange to dark brown in color and are fine- to medium-grained. The schists tend to be in beds much thicker than those of the amphibolites, reaching thicknesses of tens of meters (Bober, 1990). The Nashoba Formation has a maximum deposition age of ~465 Ma (Loan, 2011).

II. Tadmuck Brook Schist

The Tadmuck Brook Schist (TBS) was named by Bell and Alvord (1976) and is located on the eastern side, in the footwall, of the Clinton-Newbury fault (Goldstein, 1994). It is a rusty-weathered sulfidic pelitic phyllite to schist that has been multiply metamorphosed and deformed. A detrital zircon U/Pb age of 450-440 Ma places the deposition of the TBS in the late Ordovician to early Silurian (Loan, 2011).

The TBS is divided into three members of increasing metamorphic grade: northwest, center, and southeast (Jerden, 1997). The isograds in the TBS parallel the main foliation of the unit. In the northwest, bordering the Merrimack terrane, the highest-grade metamorphism seen is andalusite-grade (Jerden, 1997). The same maximum metamorphic grade is visible in the central unit, where the member is more schistose. The TBS eventually reaches sillimanite-grade metamorphism in the southeast, bordering the Nashoba Formation. The decrease in metamorphic grade moving northwest across the unit is not representative of a simple metamorphic grade derived from one metamorphic event. Instead, the unit contains evidence of at least four distinct metamorphic events and three deformation events (Jerden, 1997). It is important to note that not all of the events are recorded by all three members of the TBS.

There has been previous disagreement as to whether the TBS is in the easternmost part of the Merrimack terrane or the westernmost part of the Nashoba terrane. Because the TBS seems to have a conformable relationship

with the Vaughn Hills Quartzite, a member of the Merrimack terrane (Bell and Alvord, 1976), the TBS has been mapped as the eastern-most ~900 meters of the Merrimack terrane (Goldsmith, 1991; Markwort, 2007). However, recent U/Pb detrital zircon dating has shown that the TBS has zircon populations more similar to the Nashoba Formation than the Merrimack terrane (Fig. 2.2; Loan, 2011). Therefore, this study assumes that the TBS is part of the Nashoba terrane.

III. Ball Hill Mylonite Zone

The Ball Hill mylonite zone is located on the Ball Hill fault, which is approximately 25 km long and may merge with the Clinton-Newbury fault north of the study area (Castle et al., 1976). The Ball Hill mylonite has an igneous protolith age of 438 Ma and is exposed along Smith Rd. in Northborough, MA. The mylonite is 10-20 meters wide and varies from mylonitic to ultramylonitic (Markwort, 2007). Counter-clockwise rotated porphyroclasts indicate a sinistral shear sense (Markwort, 2007).

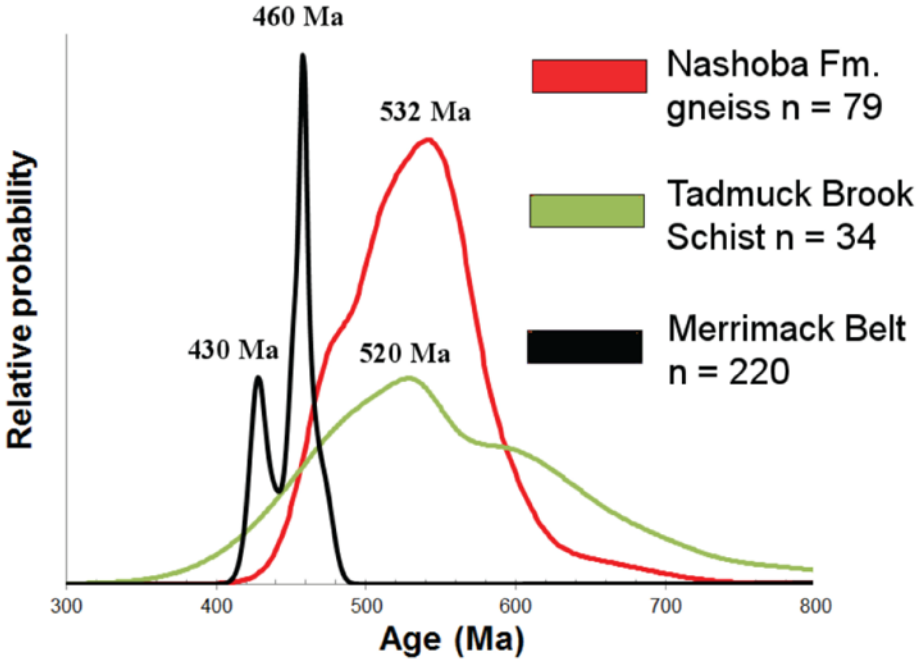

Figure 2.2 Probability density diagram of $^{206}Pb/^{238}U$ ages for detrital zircons <800 Ma. This diagram shows frequency curves of the suites of zircon ages from the Tadmuck Brook schist, Nashoba Formation gneiss, and selected units of the Merrimack belt (Wintsch et al., 2007). The zircon populations found in the Tadmuck Brook schist are more similar to those found in the Nashoba Formation. (Figure from Loan, 2011)

C. AGES OF METAMORPHISM

Stroud et al. (2009) discerned three metamorphic events in the Nashoba terrane by dating monazite in mylonites from the Assabet River fault, Sulfur Hill shear zone, and Ball Hill mylonite zone (Fig. 2.1). Ages of metamorphism are ~435-400 Ma, ~400-385 Ma, and ~385-360 Ma. M_1 (~435-400 Ma) was related to a thermal event because there is no evidence to support deformation during monazite growth at this time. M_1 may have had a peak temperature of 600 ± 50 °C (Bober, 1990). M_2 (~400-385 Ma) is interpreted to be related to widespread migmatization in the Nashoba terrane, especially in the Nashoba Formation (Stroud et al., 2009). A monazite date of 395 ± 2 Ma from a Nashoba Formation migmatite is in agreement with this age range (Hepburn et al., 1995). M_2 had a peak temperature of 600 ± 50 °C and a peak pressure of 4.4 ± 0.5 kbar (Bober, 1990). The youngest age of metamorphism (~385-360 Ma) is related to deformation in the Nashoba terrane (Stroud et al., 2009), and may have been caused by post-amalgamation motion in the Merrimack, Nashoba, and Avalon terranes (Markwort, 2007). Active ductile deformation and shearing in the Nashoba terrane occurred at this time (~376 Ma; Markwort, 2007). Discrete fault reactivation, hydrothermal reactions, and metamorphism occurred from 360-305 Ma (Stroud et al., 2009).

Hepburn et al. (1987b) calculated a $^{40}Ar/^{39}Ar$ plateau age for biotite from the Straw Hollow Diorite at 308 Ma. Thus, by mid-Pennsylvanian the Straw Hollow Diorite must have cooled to ~300 ºC (McDougall and Harrison, 1999).

The cooling age seems to suggest that the Nashoba terrane was not affected by an Alleghanian (Permian aged) thermal event significant enough to cause argon loss from biotite.

K-Ar ages from mica and hornblende revealed a resetting of ages in New England in the Permian (Zartman et al., 1970). K-Ar ages are not as reliable as step-heating $^{40}Ar/^{39}Ar$ because excess argon or argon loss cannot be identified in this method (See Chapter 3). However, these dates have been supported by more recent $^{40}Ar/^{39}Ar$ plateau ages from samples collected in south-central Connecticut (hornblende: 258 Ma) and southern Rhode Island (biotite: 243 Ma) that yielded similar ages (Wintsch and Sutter, 1986).

Ages from Zartman (1970) were plotted using ESRI GIS and data was interpolated to create an age gradient map of southern New England (Fig. 2.3) An area of Permian ages is visible stretching through eastern Connecticut and Rhode Island, central Massachusetts, southeastern New Hampshire, and western Maine (Dashed line; Fig. 2.3). Zartman et al. (1970) hypothesized that these dates could be explained by one of the following: (1) contact metamorphism related to contemporaneous emplacement of igneous plutons, (2) alteration associated with major faulting, (3) regional metamorphism in the late Paleozoic, or (4) burial followed by uplift and erosion. These hypotheses were tested in this study.

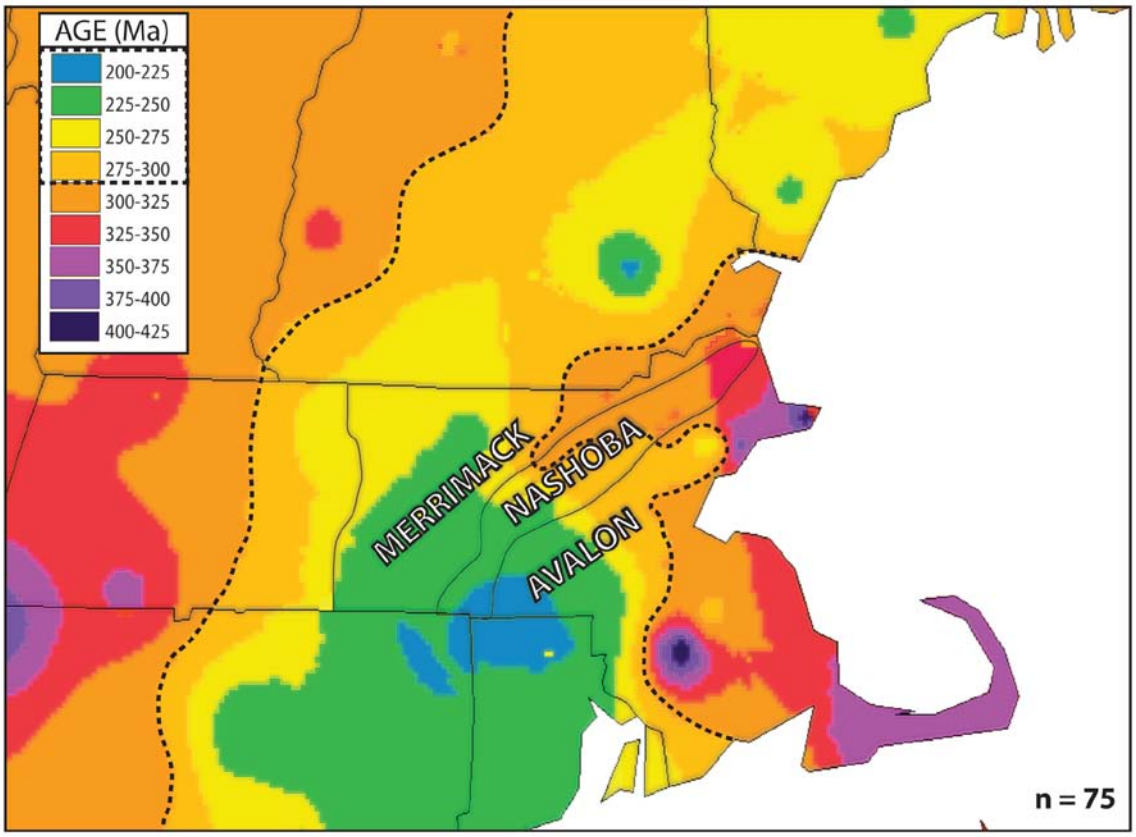

Figure 2.3 K-Ar cooling ages for muscovite and biotite from Zartman (1970). Data was interpolated using ESRI GIS. The dashed lines highlight the Permian and younger age distribution.

Chapter 3. METHODOLOGY

A. $^{40}Ar/^{39}Ar$ GEOCHRONOLOGY BACKGROUND

The $^{40}Ar/^{39}Ar$ geochronometer is based on the $^{40}K/^{40}Ar$ decay system. ^{40}K has a dual mode of decay to ^{40}Ar by electron capture and ^{40}Ca by β-decay. It is not possible to use ^{40}Ca for geochronology since it is the most common isotope of calcium. ^{40}Ar is a much less abundant isotope of argon, so it works well as a geochronometer (McDougall and Harrison, 1999).

The $^{40}Ar^*/^{39}Ar_K$ (* = radiogenic) ratio is proportional to $^{40}Ar^*/^{40}K$, because ^{39}Ar is generated from ^{39}K during irradiation and $^{40}K/^{39}K$ is essentially constant in nature. The $^{40}K/^{39}K$ ratio is assumed to be constant because (1) ^{39}K is a stable isotope, and (2) since ^{40}K has a half-life of 1.250×10^9 years, it will not decay substantially during the "human timescale" (McDougall and Harrison, 1999). Therefore, ^{39}Ar generated from ^{39}K is proportional to the ^{40}K present in the sample. This means that samples can be dated by measuring a ratio of $^{40}Ar^*/^{39}Ar_K$ instead of measuring concentrations of ^{40}K and ^{40}Ar separately.

^{39}Ar is generated by irradiating a sample in a nuclear reactor. During irradiation a neutron interacts with the ^{39}K nucleus, which is then transmuted to ^{39}Ar. During this process a proton is emitted. Following the irradiation process the ratio of ^{40}Ar to ^{39}Ar (that replaces the ratio of D to N in Eq.3.1) is measured.

I. Age equation

The age of a sample depends on its decay constant, λ (i.e. how quickly the parent isotope decays to the daughter isotope), the concentration of the parent isotope (N), and the concentration of the daughter isotope (D), following the basic age equation:

$$t = \frac{1}{\lambda} \ln\left(1 + \frac{D}{N}\right)$$

Equation 3.1 λ = system decay constant; D=concentration of daughter isotope; N=concentration of parent isotope

This equation (Eq. 3.1) can be applied to any radiogenic decay system with the appropriate modifications.

II. Irradiation

When a sample is in the nuclear reactor it receives an unknown amount of integrated neutron flux or fluence, meaning the amount of ^{39}K that is transformed into ^{39}Ar while the sample is being irradiated is unknown. In order to determine the amount of fluence that a sample receives, a standard with a precisely known $^{40}K/^{40}Ar$ age, known as a monitor mineral (see section below) is irradiated along with the sample. This will allow for the amount of fluence, known as the J-value, to be calculated (Eq. 3.2).

$$J \equiv \frac{e^{\lambda t_{mm}} - 1}{\left({}^{40}Ar^{*}/{}^{39}Ar\right)_{mm}}$$

Equation 3.2 J= irradiation parameter; λ=decay constant for ^{40}K; t_{mm}=known age of monitor mineral; $(^{40}Ar^{*}/^{39}Ar)_{mm}$=measured Ar ratio of the monitor mineral

Since irradiation is required to prepare samples for $^{40}Ar/^{39}Ar$ analysis, the irradiation parameter, J (Eq. 3.2), must be accounted for in the age equation. Given this factor, the basic age equation for the $^{40}Ar/^{39}Ar$ geochronometer is:

$$t = \frac{1}{\lambda} \ln\left(1 + J\,\frac{40Ar^{*}}{39Ar_{k}}\right)$$

Equation 3.3 λ = decay constant; *J* = irradiation parameter; $^{40}Ar^{*}$ = radiogenic argon; $^{39}Ar_{k}$ = argon generated from ^{39}K during irradiation

Two monitor samples were used for this project: the McClure Mountain Syenite Hornblende (Renne et al., 1998; Samson and Alexander, 1987; Schoene and Bowring, 2006; Spell and McDougall, 2003) and the Fish Canyon sanidine (Jourdan and Renne, 2007).

III. Dating methods

Two techniques were used for the extraction of argon gas from mineral samples in this study. One sample was dated using resistance furnace step-heating and the remaining samples were dated using the single-grain total-fusion method. The argon gas was analyzed on a MAP 215-50 Mass Spectrometer at MIT. Interpretations of data are explained in the section "Data Interpretation" below.

Resistance Furnace Step-heating

The resistance-furnace has excellent temperature control and it releases the argon gas slowly over 10-20 steps of successively increasing temperatures. This method provides information relating to the spatial distribution of radiogenic argon in a sample since the release of argon is controlled by diffusion and, therefore, argon from the margins of minerals is released before argon from the cores. In hornblende, the only mineral in this study dated with this method due to inconclusive total-fusion results, excess argon tends to be situated at the grain margins and would be released in the first few increments of the step-heating process (McDougall and Harrison, 1999). Figure 3.1 shows an example of a step-heating spectrum which demonstrates excess argon uptake (entirely at the grain margins) that has been superimposed on a small amount of radiogenic argon loss as well as a well-defined plateau (>90% Cumulative $\%^{39}Ar$ released; McDougall and Harrison, 1999). The graphs that result from step-heating makes

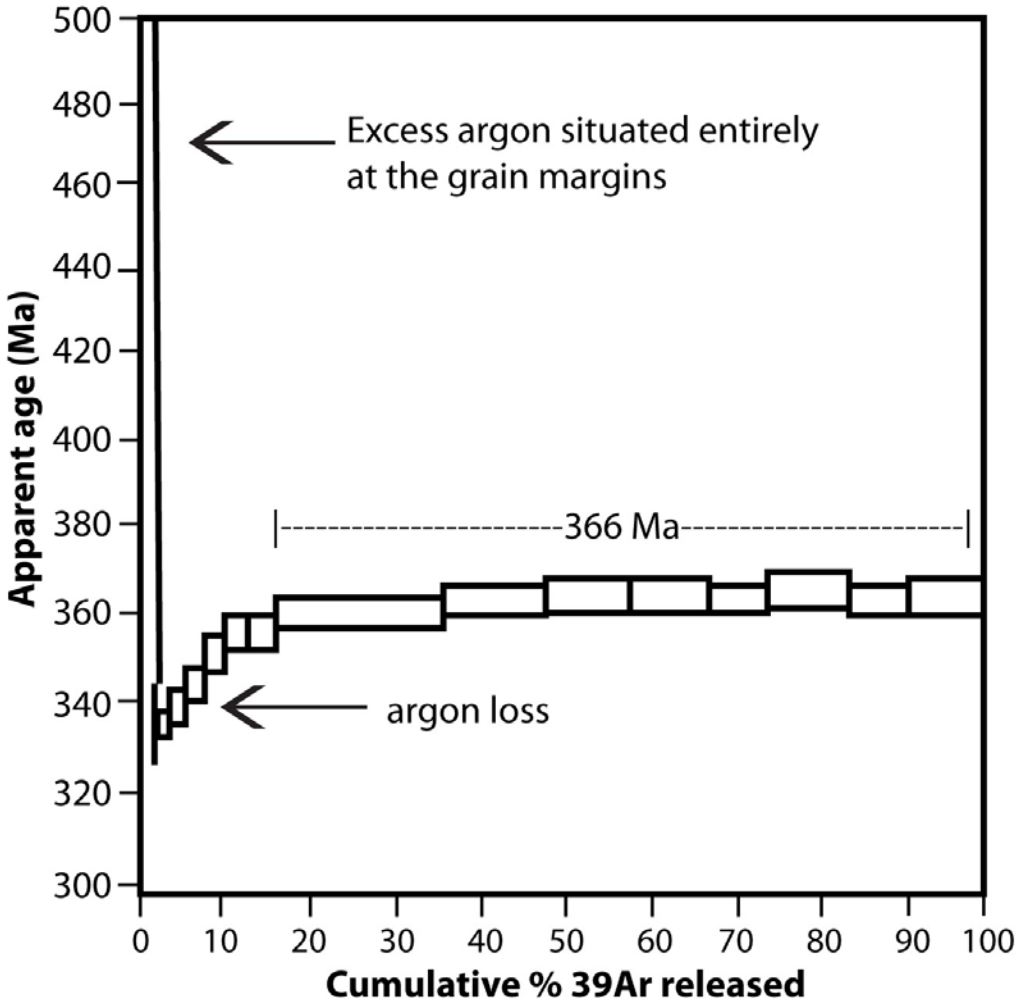

Figure 3.1 Example of a spectrum produced by resistance furnace step-heating (after McDougall and Harrison, 1999).

it easier to identify samples that contain excess or lost argon (see “Data Interpretation” section below; McDougall and Harrison, 1999).

There are a few potential problems with this method: (1) If the entire sample has experienced partial argon loss than the reported age will be meaningless. (2) If the resolution of the analysis is too low (i.e. argon gas is released with fewer steps with larger increases in temperature between each step) then the excess argon gradient would be obscured since excess argon is usually situated entirely at the grain margins in hornblende. (3) The resistance furnace requires a larger quantity of sample than single-grain total fusion. The furnace at MIT requires a sample of at least 1 mg.

Single-grain total-fusion

The single-grain total-fusion method is used if it is possible that more than one generation of mineral growth exists in a sample since it is a less expensive method and allows for more grains to be analyzed. This method utilizes a UV-laser to completely fuse the 1-3 grains that have been placed in a hole of the planchette. All of the argon gas is released and measured in one step, instead of incrementally over 10-30 steps as is usual in step-heating. The graphs from single-grain total fusion dating only provide one age, or one step, per aliquot hole instead of an entire spectrum. This method can discern if excess argon was

present in some of the grains by analyzing the inverse isochron that is constructed from the multiple analyses (see Inverse Isochron Graphs, below).

IV. Data Interpretation

Closure temperature

$^{40}Ar/^{39}Ar$ dates generally represent the time that a mineral cools through its argon closure temperature (T_C), as opposed to the peak of metamorphism, which means that the argon exchange with the environment has ceased. However, micas that form below their argon closure temperature would date mineral growth and the event that created them (Dodson, 1974; McDougall and Harrison, 1999). In this study, the only mineral that possibly could have grown below its closure temperature is muscovite. Muscovite can grow in conditions as low as the greenschist facies and has a closure temperature of 350 ± 50 ºC (McDougall and Harrison, 1999). In metamorphic rocks, biotite typically reflects the time since cooling below a temperature of 300-350 ºC (McDougall and Harrison, 1999). Biotite will only date mineral growth/crystallization in the case of rapidly cooled igneous rocks (McDougall and Harrison, 1999). The closure temperature for hornblende is 500 ºC (McDougall and Harrison, 1999), which is below the minimum temperature of amphibolite facies rocks (~525-550 ºC).

Inverse isochron graphs

Most data (single-grain total-fusion measurements) for this study will be presented in the inverse isochron format. Each data point on an inverse isochron graph represents data from a separate aliquot of the same sample. Inverse isochron graphs can be used for recognizing excess argon because they do not assume a trapped $^{40}Ar/^{36}Ar$ ratio of 295.5 (atmospheric argon composition), unlike step-heating spectra (Kuiper, 2002).

In this study each data point on an inverse isochron graph represents single grains of the same mineral from one sample. If there was no excess ^{40}Ar present in a sample then the y-intercept ($^{36}Ar/^{40}Ar$) should occur at the value of atmospheric argon (~0.0034, which is the inverse of 295.5). However, if there is excess ^{40}Ar present, then the y-intercept will plot below 0.0034 (Fig. 3.2A).

In the case of argon loss (Fig. 3.2B) it is assumed that the argon isotopes do not fractionate as they diffuse out of a mineral, meaning that the $^{36}Ar/^{40}Ar$ ratio will remain unchanged during argon loss and the $^{39}Ar/^{40}Ar$ ratio will increase since ^{39}Ar was created from ^{40}K during irradiation in the lab and it will not change. This will lead to all data points shifting to the right. If argon loss was not complete then the data will probably not plot on a line and (if they do) the inverse isochron age may represent a scientifically insignificant value which lies somewhere between the end of the argon loss event and the cooling event on the x-axis (Kuiper, 2002).

Step-heating graphs

Step-heating graphs, known as age spectra, represent the $^{40}Ar/^{39}Ar$ apparent age vs. the cumulative percentage of ^{39}Ar released. If a sample has a completely flat spectrum (Fig. 3.3A) then it can be assumed that it didn't incorporate excess argon, it remained a closed system and it has not been disturbed since crystallization. There are two main reasons why an age spectrum of a hornblende sample may not yield a perfect plateau (McDougall and Harrison, 1999). First, hornblendes from metamorphic terranes have been shown to incorporate excess argon ($^{40}Ar_E$) in their mineral lattice. In hornblendes $^{40}Ar_E$ tends to be situated at grain margins, showing up early (the first ^{39}Ar released upon heating) in an age spectrum (Fig. 3.3B; McDougall and Harrison, 1999). Second, most systems tend to be an open (complex) system in which there is loss of some of the radiogenic argon ($^{40}Ar^*$). This $^{40}Ar^*$ loss can occur by mineral recrystallization or by volume diffusion. An age "plateau" is defined as a well-defined high furnace temperature plateau for more than 50% of the ^{39}Ar released (McDougall and Harrison, 1999).

Errors

MSWD

MSWD, or mean square of weighted deviates, is commonly used in geochronology in order to assess the "goodness of fit" of multiple data from one sample to a single age. The MSWD values for age for this study were calculated

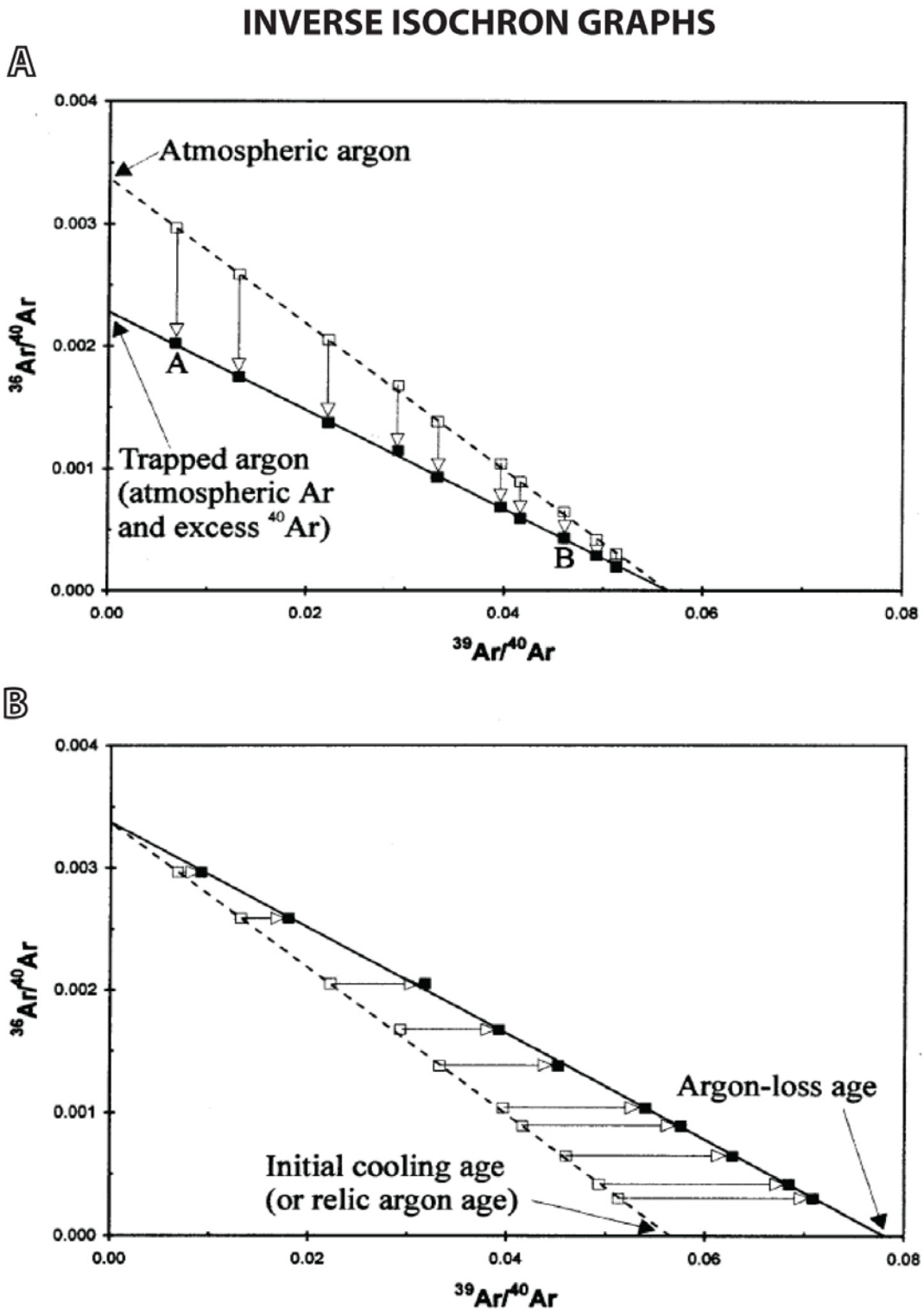

Figure 3.2 Inverse isochron plots showing **A)** excess ^{40}Ar trapped in a mineral lattice and **B)** argon loss from a mineral lattice. (From Kuiper, 2002)

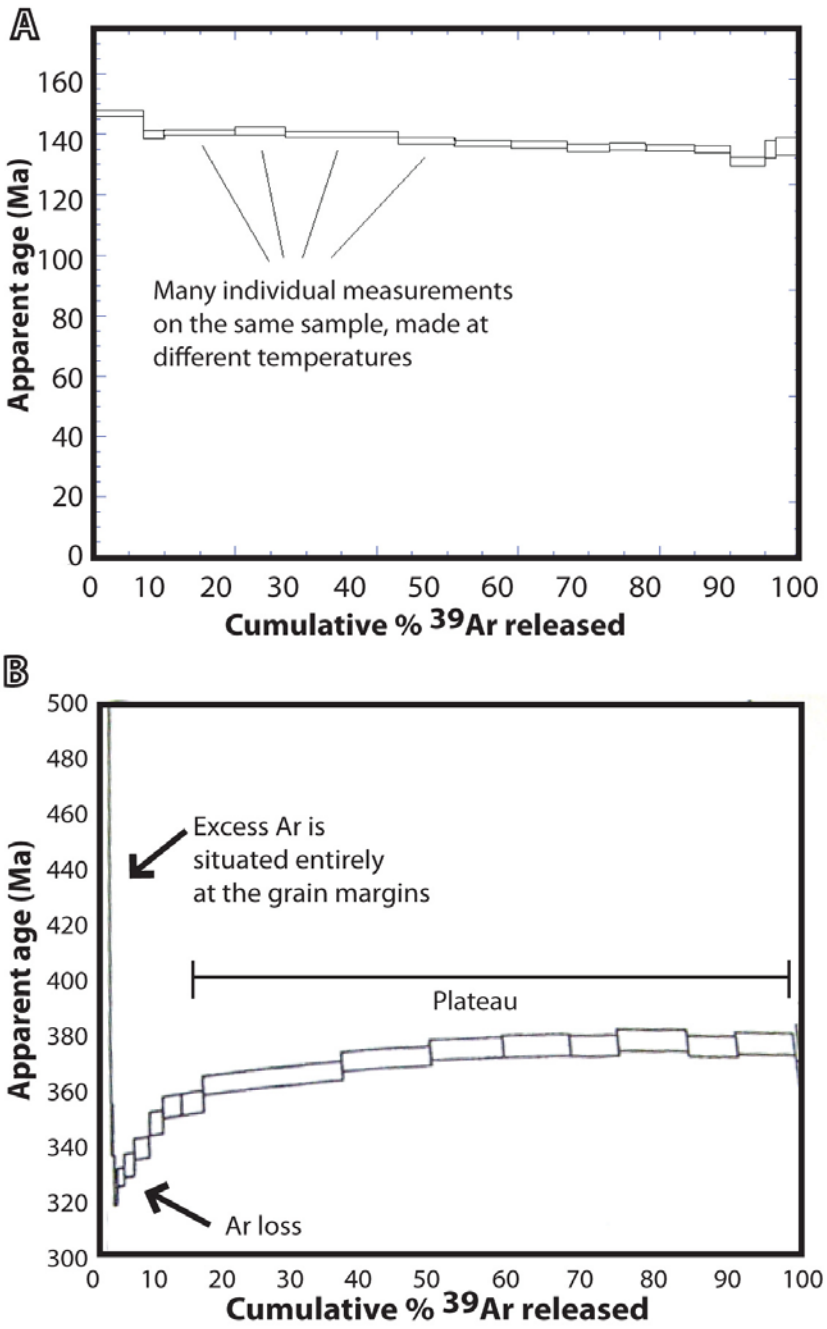

Figure 3.3 Examples of age spectra **A)** Ar/Ar values are uniform throughout this sample, giving a plateau age of ~140 Ma. **B)** Excess argon in a hornblende lying entirely along the margin. The plateau age is ~366 Ma. Plots after McDougall and Harrison (1999).

by Dr. William Olszewski using the ArArCalc program. These values were calculated for 10 measurements (each measurement was composed of 1-3 grains) of each mineral measured from each sample.

MSWD values in this study are used to determine whether all data are measuring the same mean value. An MSWD that is much less than 1 means that more than one line can be fit through the data. If the value of MSWD greatly exceeds 1 then a linear relationship between the data does not exist (Wendt and Carl, 1991). The acceptable range of an MSWD for $^{40}Ar/^{39}Ar$ geochronology falls between the range of 0.17 and 2.5 (McDougall and Harrison, 1999). There are cases in this study where MSWD values exceed 2.5, and further consideration was necessary to determine the usefulness of the calculated ages. This will be visited in the results section of this study.

B. METHODOLOGY

I. Sample Selection

Samples ER1, ER2, ER3, ER4, ER8, ER20, and 25.1 were collected during 2007 and 2008. The Nashoba Formation schist samples (NFS-1 and MLBS-1; Fig. 3.4) were collected by Andrew Kay and MaryEllen Loan for their respective Masters theses. Detailed sample location descriptions can be found in Appendix II.

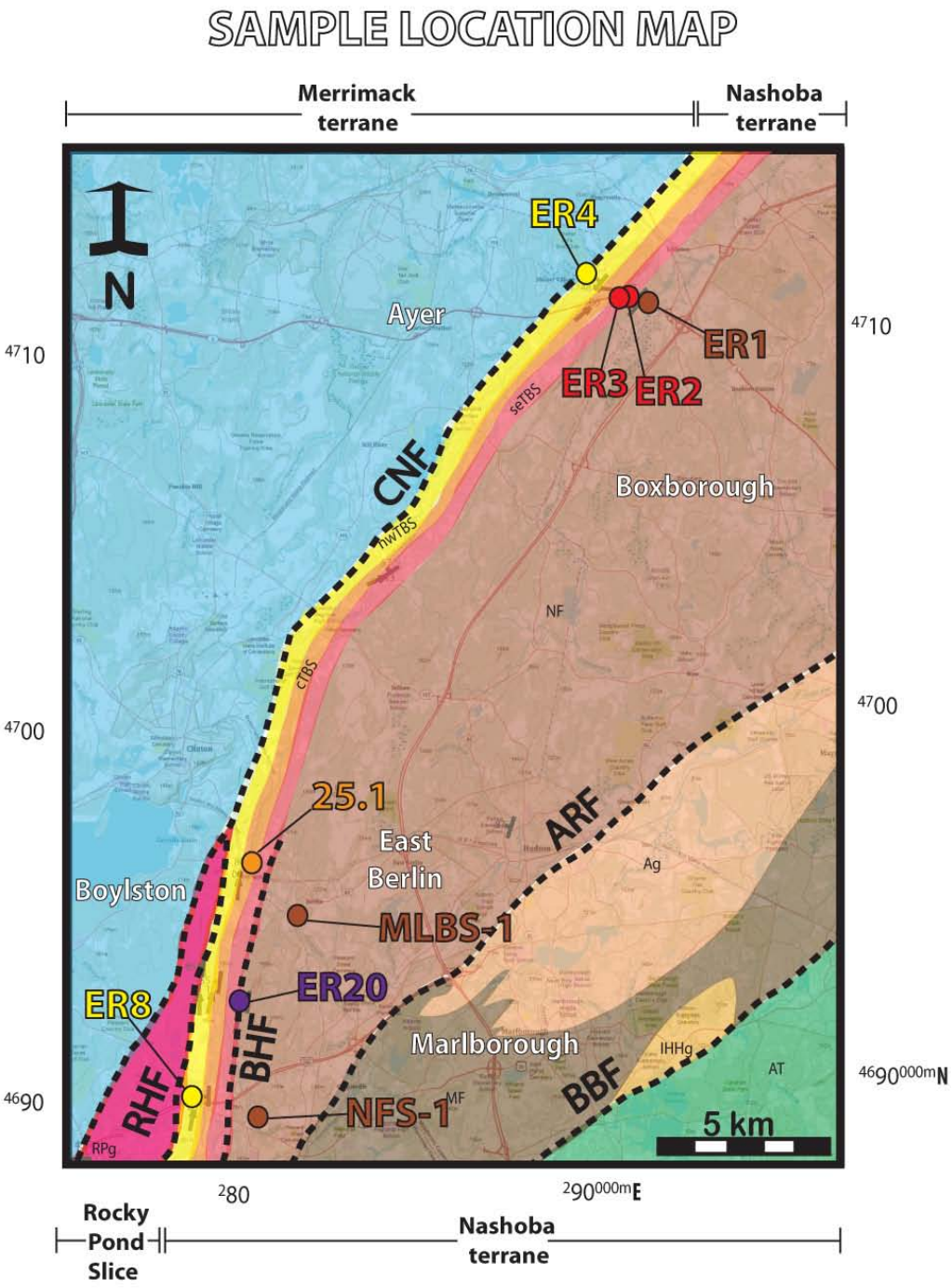

Figure 3.4 Location map of samples analyzed in this study. Approximate locations of units are based off of maps by Jerden (1997), Kopera (2005), Kopera (2006), Kopera et al. (2006), Markwort (2007), and this study.

CNF = Clinton-Newbury Fault; RHF = Rattlesnake Hill Fault; BHF = Ball Hill Fault; ARF = Assabet River Fault; BBF = Bloody Bluff Fault

See next page for complete key.

KEY TO FIGURE 3.4

EXPLANATION OF LITHOLOGIC UNITS

Merrimack Terrane

MT Merrimack Terrane

Stratified Rocks of the Nashoba Terrane

Tadmuck Brook Schist

nwTBS NW member of TBS

cTBS Central member of TBS

seTBS SE member of TBS

NF Nashoba Formation

MF Marlboro Formation

Intrusive Rocks of the Nashoba Terrane

RPg Rocky Pond Granite

Ag Andover Granite

IHHg Indian Head Hill Granite

The Composite Avalon Terrane

AT Avalon Terrane

SAMPLE LOCATIONS

NW member of TBS

Central member of TBS

SE member of TBS

Ball Hill mylonite zone

Nashoba Formation

EXPLANATION OF MAP SYMBOLS

26 Strike and dip of dominant foliation

14 Trend and plunge of mineral lineation

ADDITIONAL SYMBOLS

Boylston Town location

Fault

Hornblende, muscovite and biotite were dated because they are abundant throughout the study area. Also, micas commonly have little initial argon, because argon is fairly incompatible with mica in the mica-water system and will partition strongly into the fluid phase (Mulch and Cosca, 2004). This means that the largest contribution of ^{40}Ar in micas will be from decay of ^{40}K and that the excess argon contribution from water will be insignificant compared to the radiogenic concentration. Although K-feldspar is also common in samples from this study it was not dated, partially due to budget constraints.

Hornblende was dated since its higher closure temperature would allow for a calculation of the cooling rate in the Nashoba terrane when compared with ages of minerals with lower closure temperatures (i.e. biotite and muscovite). The hornblende was first dated using the total-fusion method, but multiple grains had excess argon. Therefore, hornblende was also dated using the furnace step-heating method.

II. Sample Preparation

Samples were crushed using a hand held pestle and mortar. Next, they were rinsed through a 50 μm screen with alcohol to remove particles that were too small to use for dating. The removal of these small particles made the hand separation of the discrete mineral phases to be dated more efficient. The rinsed sample was then placed into a large Petri dish and was dried under a heating lamp.

Once the crushed sample was dry, it was placed under a microscope and the minerals to be dated were selected using tweezers. Minerals with little to no inclusions (Fig. 3.5A) and without other attached minerals (Fig. 3.5B) were selected for analysis (Fig. 3.5C). Roughly 100-300 grains were picked for each mineral sample. Minerals were not separated by grain size in order to analyze various grain size fractions as there was no way to determine if smaller grain sizes were simply pieces from larger grains that had been crushed.

Each mineral sample had to be thoroughly cleaned with acid to dissolve any possible minerals or alteration products attached to it. An ultrasonic cleaner was used for all steps of the cleaning process. All minerals were placed in disposable polypropylene beakers with enough 10% nitric acid to cover all minerals. The nitric acid dissolves the sulfates and carbonates that could possibly be attached to the mineral grains. The samples were left in this solution in the ultra-sonic cleaner for 1-2 hours. The nitric acid was then carefully poured into a waste container. The samples were immediately rinsed three times with deionized water, and then three times with spectral analyzed methanol.

After the samples had dried from the nitric acid rinse, a 6% hydrofluoric acid solution was added to the polypropylene beakers. The minerals were left in this solution for only 5 minutes in the ultra-sonic cleaner. Chlorite and zeolites are dissolved before silicates, but hydrofluoric acid does eventually dissolve silicates. After 5 minutes the hydrofluoric acid was poured into a waste container and the

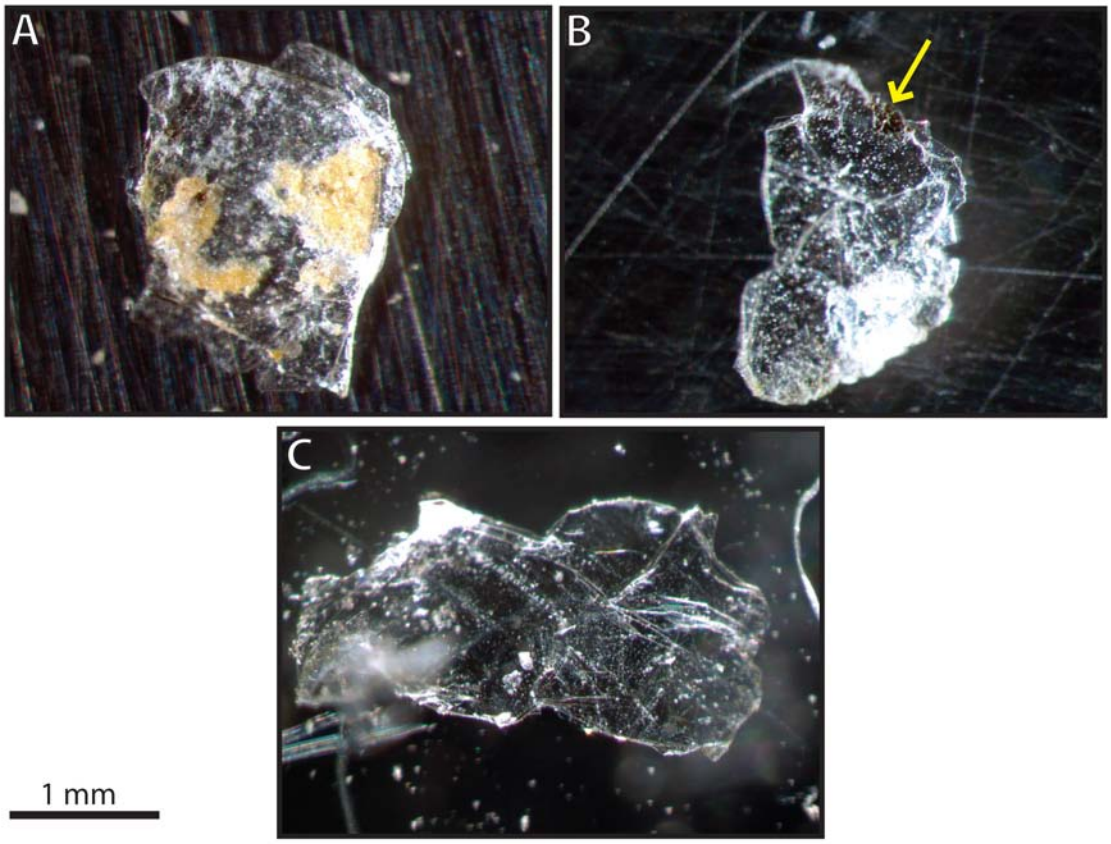

Figure 3.5 Photomicrographs showing examples of muscovite from the southeast member of the TBS. **A)** Inclusions on the surface of this muscovite make it unsuitable for dating. **B)** A small amount of biotite is part of this grain of muscovite. **C)** This grain of muscovite is suitable for dating since it has no inclusions.

samples were once again rinsed with deionized water three times and spectral analyzed methanol three times.

The mica and hornblende samples were packaged up in aluminum capsules approximately the size of a pencil eraser at MIT. These capsules were carefully constructed from aluminum foil using tweezers. Each sample required 1-3 capsules depending on the amount of sample that had been picked. These capsules were loaded and closed using tweezers and a small metal spatula. It

was vital that none of the capsules “leaked”, which was not a simple task considering the fragility of aluminum foil. At times the samples had to be “double-packed” in additional tin foil if they appeared to have a tear. Each capsule was weighed before and after the sample was added so that the sample weight could be attained. Once all of the capsules were loaded they were placed in a glass tube along with monitoring packages. The distance of each sample from the bottom of the tube was measured in order to allow the J-value for each sample to be accurately calculated later. This glass tube was then sent to the McMaster nuclear reactor where it was placed in the nuclear reactor for irradiation for ~30 hours.

After the samples had “cooled down” and were no longer radioactive the packages were opened. A 100-hole planchette to hold the samples was cleaned with compressed air. Next, 1-3 grains were placed into each planchette hole using tweezers. Each mineral type for each sample filled one row of the planchette (i.e. 10-30 grains in 10 holes per mineral type per sample). This planchette was then loaded into the UV-laser compartment and was ready to be analyzed.

Chapter 4. METAMORPHISM AND DEFORMATION

A. PETROLOGY

All thin sections were cut perpendicular to the foliation and parallel to the lineation.

I. Nashoba Formation schists

Two schists were collected from the Nashoba Formation (MLBS-1 and NFS-1 in Fig. 3.4). NFS-1 contains sillimanite, muscovite, fibrolite, plagioclase, garnet, quartz, and biotite (Table 4.1) and it has a silvery sheen due to the presence of fibrolite (Fig. 4.1A). NFS-1 weathers to a rusty orange color in places, suggesting that it is a sulfidic schist (Fig. 4.1A and B). Large grains of biotite and garnet are visible to the naked eye (Fig. 4.1B).

MLBS-1 appears rusty brown in hand sample and is more friable than NFS-1 (Fig. 4.1C). It contains fibrolite, garnet, sillimanite, quartz, muscovite, and biotite (Table 4.1). Both samples have abundant opaque minerals, such as possible arsenopyrite (based on its crystallography and color in reflected light), and sericitization, suggesting the samples experienced hydrothermal alteration (Fig. 4.1 D). Both Nashoba Formation schists had large garnet porphyroblasts up to 1.0 cm in diameter (Fig. 4.1E).

At least two generations of biotite growth were apparent in both samples: (1) earlier grains that composed the S-C fabric, and (2) late “fish-scale” grains that cross-cut the foliation.

THIN SECTION MODES

	Nashoba Fm. Schist		Nashoba Fm. Amphibolite	Northwest Member of TBS				Central Member of TBS	Southeast Member of TBS		Ball Hill Mylonite Zone
	MLBS-1	NFS-1	ER1	ER4B	ER4C	ER4D	ER8	25.1	ER2	ER3	ER20
PORPHYROBLASTS											
size in mm	*1.0-5.0*	*2.0-10.0*	*2.0-3.0*	–	*5.0-7.0*	–	*1.0-4.0*	*3.0-12.0*	*2.0-5.0*	*2.0-4.0*	*3.0-9.0*
Andalusite	–	–	–	–	4	–	5	5	2	5	–
Biotite	12	8	–	–	–	–	–	9	–	–	11
Muscovite	–	–	–	–	–	–	–	–	11	7	–
Quartz	5	–	–	–	–	–	–	8	–	–	24
Hornblende	–	–	7	–	–	–	–	–	–	–	–
Staurolite	–	–	–	–	–	–	24	22	–	–	–
Kspar	–	–	–	–	–	–	–	–	–	–	20
Plagioclase	–	–	–	–	–	–	–	–	–	–	11
Garnet	8	13	–	–	–	–	–	–	–	–	–
MATRIX											
size in mm	*0.5-1.0*	–	*0.5-1.5*	*0.3-1.1*	*0.5-1.0*	*0.3-0.7*	*0.3-1.0*	*0.5-1.0*	*1.0-2.0*	*0.5-1.0*	*0.25-0.75*
Biotite	27	24	21	6	8	10	5	7	10	15	13
Muscovite	22	6	6	34	30	44	23	23	23	31	9
Plagioclase	tr	7	22	5	5	8	–	tr	12	tr	–
An	?	?	An_{36-38}	?	?	?	–	?	An_{28}	?	–
Kspar	–	–	5	–	–	–	–	–	–	–	–
Quartz	14	22	6	43	45	23	36	16	20	31	9
Hornblende	–	–	33	–	–	–	–	–	–	–	–
Andalusite	–	–	–	–	–	4	–	–	–	–	–
Chlorite	–	–	–	8	7	7	5	6	2	tr	–
Fibrolite	2	6	–	–	–	–	–	–	11	3	–
Sillimanite	5	3	–	–	–	–	–	–	3	8	–
Staurolite	–	–	–	–	–	–	–	–	4	–	–
Garnet	4	9	–	–	–	–	–	–	–	–	2
ACCESSORY											
Opaques	1	2	tr	2	tr	4	tr	2	2	tr	tr
Apatite	–	–	–	–	–	tr	–	–	–	–	1
Epidote	–	–	–	–	tr	–	2	–	–	–	–
Tourmaline	–	–	–	2	–	–	–	2	–	–	–
Zircon	–	–	–	–	–	tr	–	–	–	tr	tr
Chloritoid	–	–	–	–	1	–	–	–	–	–	–
TOTAL	100	100	100	100	100	100	100	100	100	100	100

Table 4.1 Thin section modes calculated using the point-count method with 100 points.

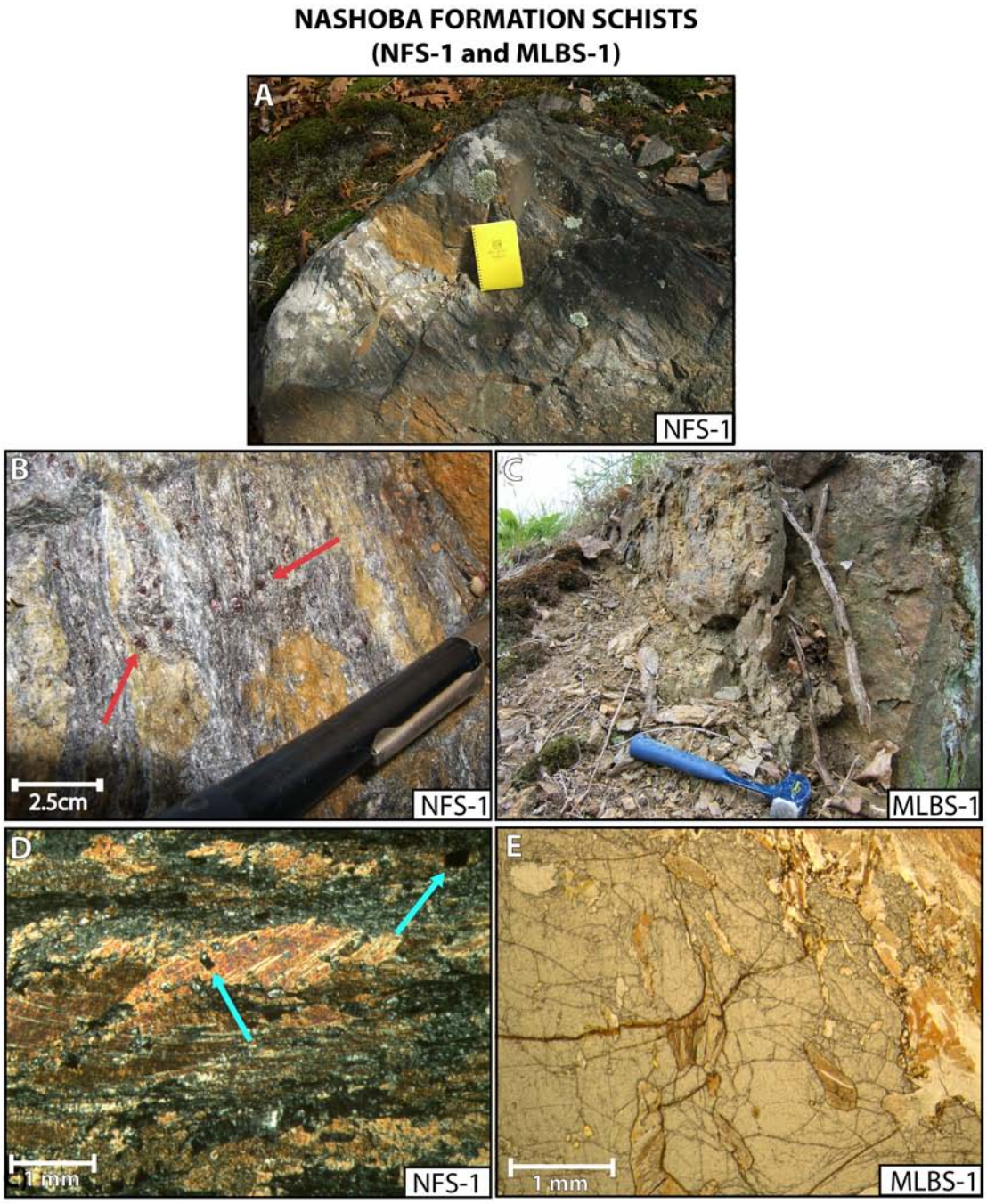

Figure 4.1 A) Unoriented photo taken by Andrew Kay of silvery sheen and rusty nature of NFS-1. **B)** Unoriented photo taken by Andrew Kay of garnet in NFS-1. **C)** Unoriented photo taken by MaryEllen Loan of the rusty brown coloring and friable nature of MLBS-1. **D)** Photomicrograph of unoriented thin section showing abundance of opaque minerals (arrow points to possible arsenopyrite) which likely formed during hydrothermal alteration (XPL). **E)** Photomicrograph of unoriented thin section of large porphyroblast of garnet (PPL).

II. Nashoba Formation amphibolite

The Nashoba Formation amphibolite (ER1 in Fig. 3.4) was sampled immediately east of the TBS. In the field it appears light to dark gray (Fig. 4.2A) with hornblende and biotite visible to the naked eye in hand sample. Large grains of hornblende reach a m aximum diameter of 3.0 mm. The main fabric is composed of K-spar, muscovite (var. sericite), quartz, biotite, plagioclase, and hornblende (Table 4.1; Fig. 4.2B & C). A large percentage of the plagioclase is altered to sericite (Fig. 4.2D), either by hydrothermal alteration or retrograde metamorphism. The plagioclase has an An_{36-38}, andesine, indicative of amphibolite facies metamorphism.

III. Northwest member of TBS

Two samples of the northwest member of the TBS were collected (ER4 and ER8; Fig. 3.4). It is a dark gray to rusty-orange phyllite with quartz bands that range in thickness from 10-50 cm (Fig. 4.3A; Fig. 4.3D). Rusty weathering is apparent in the field and in thin section and the rock is extremely friable in hand sample. Overall, the northwest member of the TBS is composed of biotite, plagioclase, chlorite, muscovite and quartz (Table 4.1). Shear bands composed of muscovite were observed in thin section (Fig. 4.3B). Only one sample showed any evidence of porphyroblasts, consisting of a few grains of andalusite that were ~5.0 mm in width (Table 4.1; Fig. 4.3C).

NASHOBA FORMATION AMPHIBOLITE
(ER1)

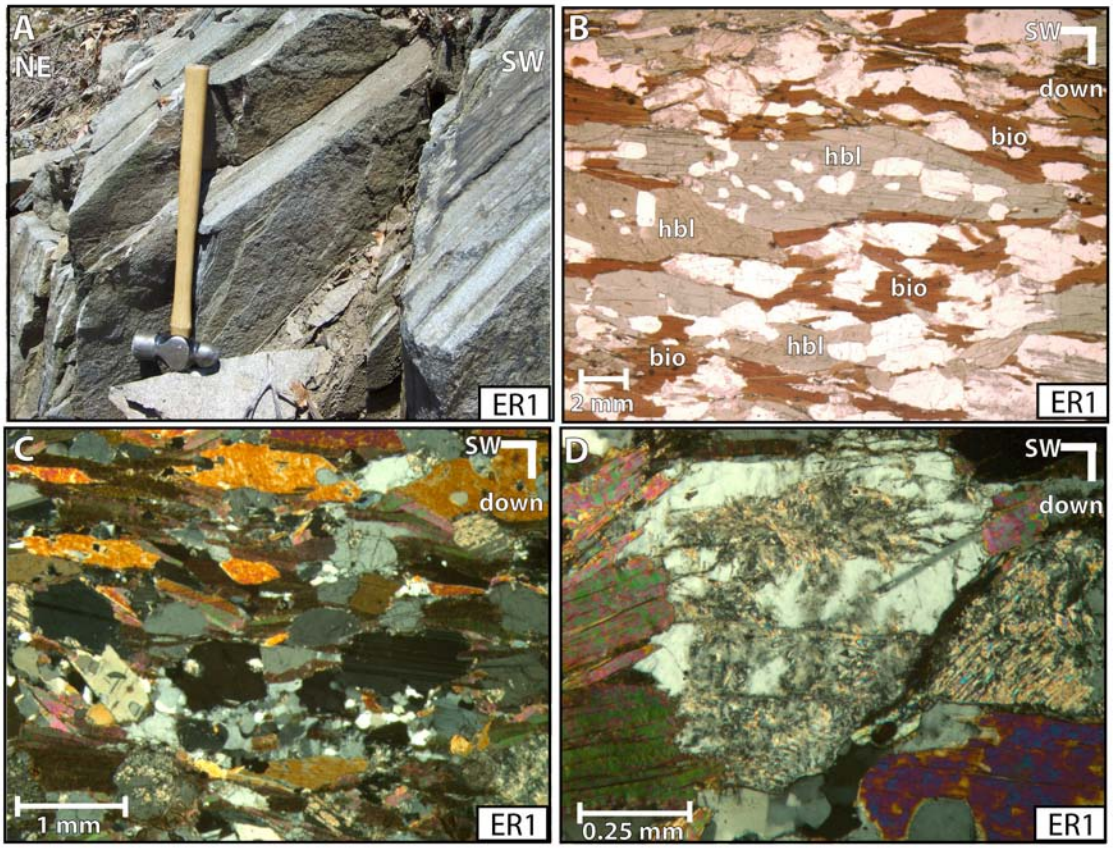

Figure 4.2 A) Photograph of the light to dark gray coloring of ER1. **B)** Photomicrograph of hornblende and biotite (PPL). **C)** Photomicrograph (XPL) of the main fabric. **D)** Photomicrograph of sericitization (XPL).

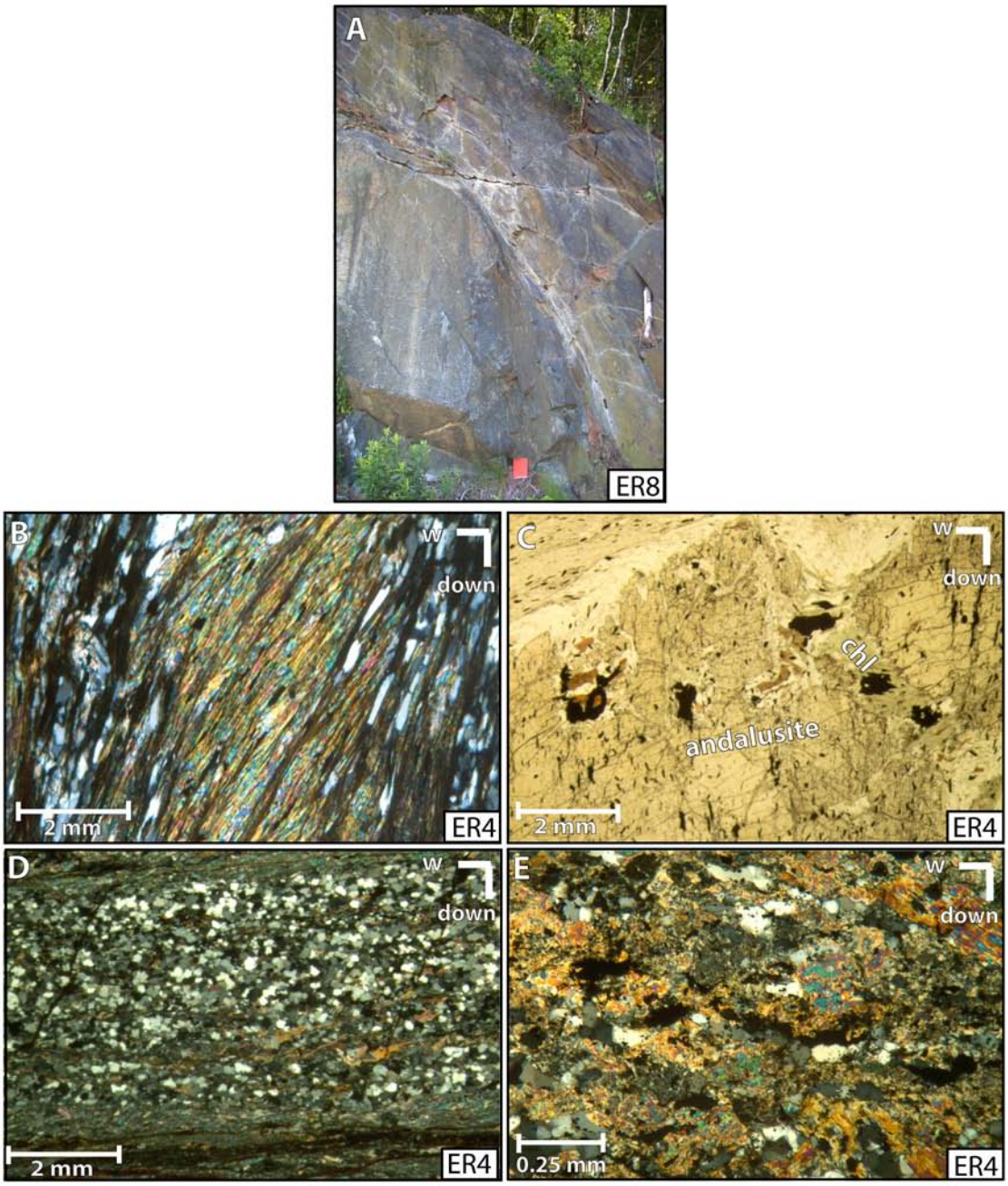

Figure 4.3 A) Field photograph of phyllitic member of TBS. **B)** Photomicrograph of muscovite forming normal west-northwest side down shear bands (XPL). **C)** Photomicrograph of andalusite weathering to chlorite (PPL) **D)** Photomicrograph of quartz-rich layer with faint normal shear sense (XPL). **E)** Photomicrograph of sericitization (XPL).

Sericitization is apparent in one of the thin sections (Fig. 4.3E). This sample exceeded biotite-grade metamorphism because andalusite is present. The samples are much finer-grained than the central member of TBS.

IV. Central member of TBS

One sample of the central member of the Tadmuck Brook Schist was collected (25.1; Fig. 3.4). This member is more schistose in nature than the northwest member (which is phyllitic) and displays brown to rusty-orange weathering in hand sample. It is less weathered than the northwest member. Large knots of resistant andalusite were observed to protrude from more easily weathered elements of the schist (Fig. 4.4A). It is composed largely of andalusite, chlorite, biotite, quartz, staurolite and muscovite (Table 4.1). Porphyroblasts of andalusite, quartz, biotite and staurolite are as large as 1.2 cm (Fig. 4.4B). Some of the biotite, of which at least two generations were observed, is being replaced by chlorite (Fig. 4.4 C). Localized randomly-oriented sericite is evidence of a possible late hydrothermal event (Fig. 4.4D).

CENTRAL MEMBER OF THE TADMUCK BROOK SCHIST
(25.1)

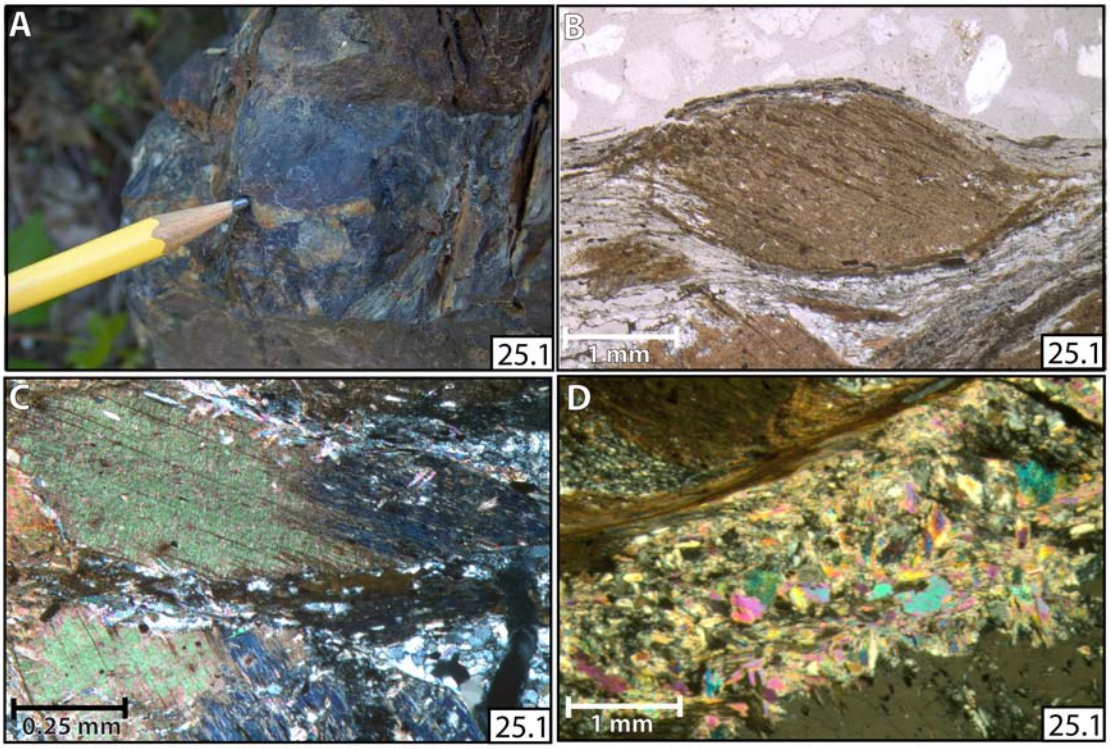

Figure 4.4 Photos and photomicrographs are unoriented **A)** Field photograph of andalusite knot. **B)** Photomicrograph of biotite porphyroblast (PPL). **C)** Photomicrograph of chlorite replacing biotite (XPL). **D)** Photomicrograph of hydrothermal alteration (XPL).

V. Southeast member of the TBS

Two samples (ER2 and ER3) of the southeast member of the Tadmuck Brook Schist were collected (Fig. 3.4). In the field the unit is dark orange to brown and very friable with rusty weathering (Fig. 4.5A). It has a silvery sheen due to the presence of fibrolite (Fig. 4.5B). Fresh samples were less friable and weathering coloration was more orange than brown. The samples are composed of staurolite, andalusite, sillimanite, fibrolite, quartz, biotite and muscovite (Table 4.1). Andalusite and staurolite were relict grains. Porphyroblasts of muscovite were observed up to 5.0 mm in diameter. Two generations of muscovite are evident: (1) an early generation of groundmass muscovite composing sinistral shear bands throughout the member (Fig. 4.5C), and (2) a later generation of muscovite porphyroblasts cross-cutting the main fabric (Fig. 4.5D & E). Quartz-rich layers reached thicknesses of 3-150 mm (Fig. 4.5F). Some plagioclase (An_{28}, oligoclase) shows evidence of sericitization (Fig. 4.5G).

VI. Ball Hill mylonite zone

One sample of an unnamed mylonitic biotite-quartz-plagioclase gneiss was collected from the Ball Hill mylonite zone on Smith Road in Northborough (ER20; Fig. 3.4). The outcrop varies in color from white to light gray and has been glacially polished (Fig. 4.6A). The sample is composed of garnet, muscovite, plagioclase, K-spar, biotite and quartz (Table 4.1). Sinistrally rotated

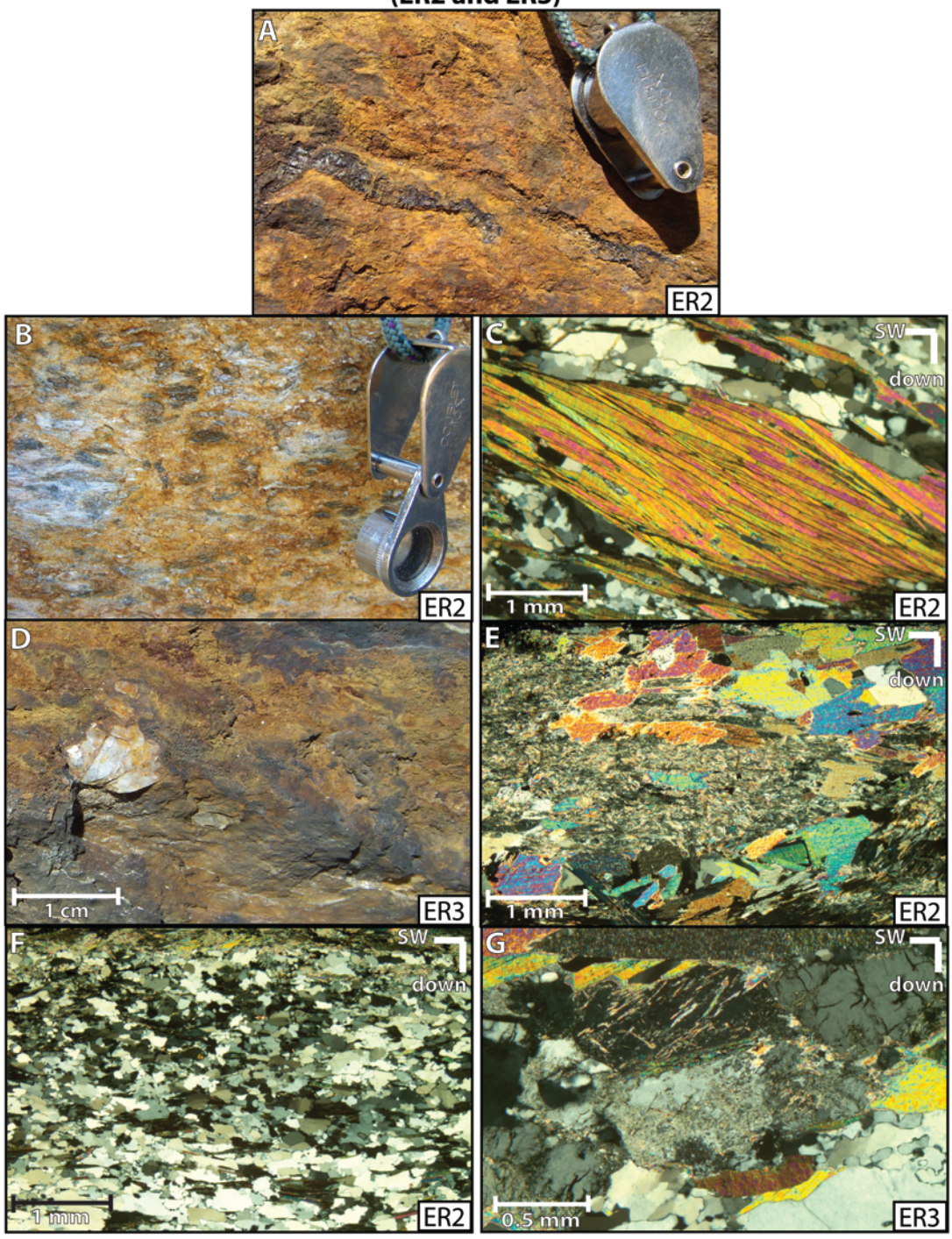

Figure 4.5 A) Horizontal field photograph showing rusty weathering. **B)** Horizontal field photograph of silvery sheen due to presence of fibrolite. **C)** Photomicrograph of sinistral shear bands composed of muscovite (XPL). **D)**Horizontal field photograph of late muscovite porphyroblasts. **E)** Photomicrograph of late muscovite (XPL). **F)** Photomicrograph of quartz-rich layers (XPL). **G)** Photomicrograph of sericitization(XPL).

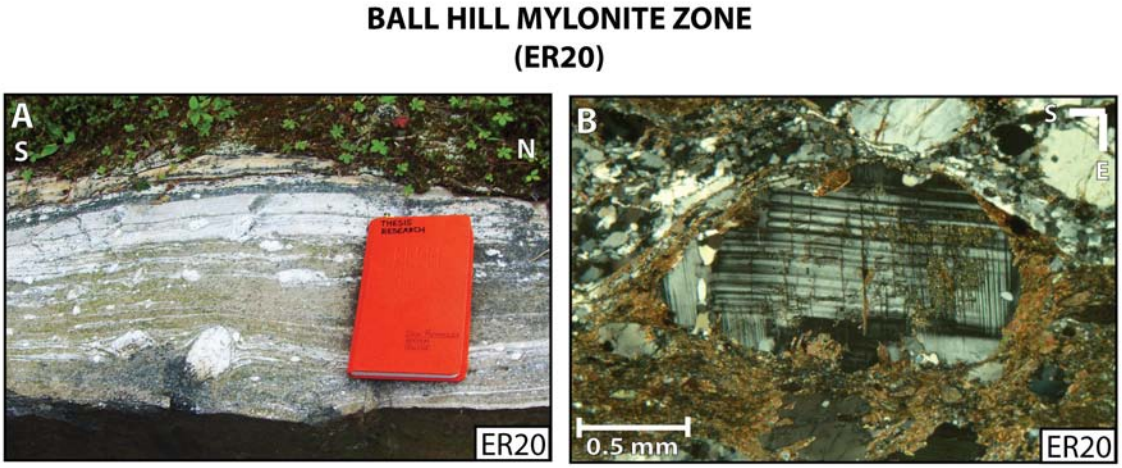

Figure 4.6 A) Field photograph (looking down) showing the glacially polished Ball Hill Mylonite. **B)** Photomicrograph (XPL) showing sericitization of a K-spar porphyroblast.

porphyroblasts of K-spar and plagioclase remain and are as large as 9.0 mm. Both feldspars have undergone sericitization (Fig. 4.6B).

VII. Interpretation of petrology

The observed mineral assemblages were compiled (Table 4.2) and plotted on a petrographic grid for metapelites (Fig. 4.7). Although all four assemblages could fit on one P-T-t path, they are interpreted as four separate events because of (1) overprinting textural relations of the mineral assemblages from this study, and (2) geochronology suggesting M_2, M_3, and M_4 were separate metamorphic events occurring over ~100 Myr (Stroud et al., 2009). This interpretation agrees with previous metamorphic studies done in the Nashoba terrane (Bober, 1990; Jerden, 1997; Markwort, 2007; Munn, 1987).

MINERAL ASSEMBLAGES

	Nashoba Fm. Schist	Nashoba Fm. Amphibolite	Northwest Member of TBS	Central Member of TBS	Southeast Member of TBS	Ball Hill Mylonite Zone
M_1	X	X	andalusite-biotite	andalusite-staurolite-biotite	andalusite-staurolite-biotite	X
M_2	fibrolite-biotite	biotite?	X	X	fibrolite-biotite (overprinting M_1)	X
M_3	sillimanite-biotite (overprinting M_2)	K-spar-biotite (overprinting M_2)	X	X	sillimanite-biotite (overprinting M_1 and M_2)	K-spar-biotite
M_4	muscovite (overprinting M_2 and M_3)	muscovite (overprinting M_2 and M_3)	chlorite-muscovite (overprinting M_1)	chlorite-muscovite (overprinting M_1)	chlorite-muscovite (overprinting M_1, M_2 and M_3)	muscovite (overprinting M_3)

Table 4.2 A summary of the distribution of metamorphic assemblages observed in thin sections in this study and by Jerden (1997), Markwort (2007) and Munn (1987). An "X" means that the mineral assemblage was not observed in that unit and that the event most likely did not affect it.

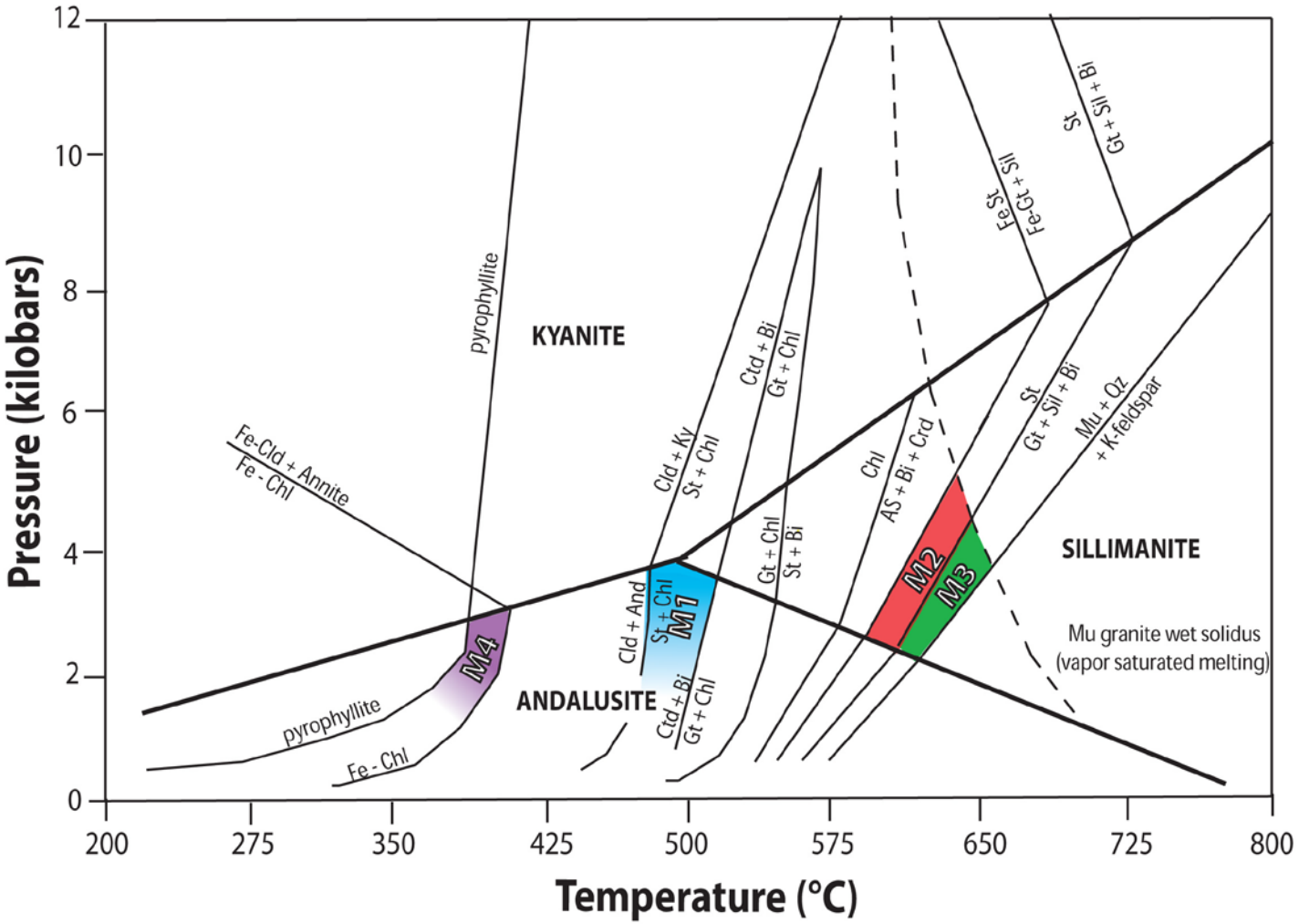

Fig 4.7 Petrographic grid (adapted from Spear and Cheney 1989). Colored boxes represent estimated pressure-temperature conditions for the four metamorphic events observed in the thin sections from this study and from the following studies: Bober (1990), Jerden (1997), Markwort (2007), and Munn (1987).

The M_1 mineral assemblage (biotite-andalusite and biotite-andalusite-staurolite) was observed in all members of the Tadmuck Brook Schist (TBS) (Table 4.2). M_1 is best preserved in the central member of the TBS because it is unaffected by pervasive overprinting seen in the southeast member of the TBS. M_1 was also observed by Jerden (1997) and Munn (1987) in the TBS. Whether M_1 affected the Ball Hill mylonite or the Nashoba Formation is unclear because andalusite and staurolite are not observed. The P-T conditions of this event in the study area are constrained by the absence of garnet and chloritoid. These constraints suggest the temperature ranged from 430-510 °C and the pressure was 1-3 kilobars (Fig. 4.7). It is the highest grade of metamorphism that the northwest and c entral members of TBS experienced as these units were not exposed to the high grade metamorphism of M_2 and M_3 (See metamorphic isograd; App. IIID). It is important to note that since Markwort (2007) and Stroud et al. (2009) considered the Tadmuck Brook Schist to be part of the Merrimack terrane they did not include M_1 among metamorphic events that affected the Nashoba terrane.

The M_2 mineral assemblage (M_1 of Markwort, 2007; Stroud et al., 2009) is biotite-fibrolite (Table 4.2). M_2 is observed in the southeast member of the TBS and the Nashoba Formation. This assemblage was also observed by Abu-Moustafa and Skehan (1976), Bober (1990), Jerden (1997), and Markwort (2007). In the southeast member of TBS the biotite ± fibrolite assemblage overprints the M_1 assemblage. The P-T conditions are constrained by the

presence of fibrolite and biotite and the absence of staurolite and K-spar. The petrological constraints suggest the temperature ranged from 600-650 °C and the pressure was 2-4 kilobars (Fig. 4.7). The abrupt dissipation of the M_2 mineral assemblage as the boundary between the southeast and central members of TBS is crossed (see metamorphic isograd; App. IIID) suggests M_2 was related to contact metamorphism. The thermal source of M_2 may have been located to the east of the TBS.

The M_3 mineral assemblage (M_2 of Markwort, 2007; Stroud et al., 2009) is K-spar-biotite (in rocks with an igneous protolith) and sillimanite-biotite (in metapelites). M_3 is observed in the southeast member of TBS, Ball Hill mylonite, and the Nashoba Formation. This metamorphic event is interpreted to have occurred after M_2 because sillimanite overgrows D_1 fabrics in some instances (postdates local deformation), while all fibrolite is sheared (see Chapter 6 for further discussion). The interpretation of sillimanite growth after fibrolite was also observed by Markwort (2007). Melting was not observed in any samples collected for this study, therefore the granite wet solidus was not surpassed. However, it is worth noting that partial melting did occur in the Nashoba Formation, east of the study area, suggesting that peak M_3 metamorphism reached higher temperatures there (Fig. 4.8; Jerden, 1997; Markwort, 2007; Munn, 1987). Petrological constraints suggest M_3 ranged from ~610-660 °C and ~2.5-4.5 kilobars (Fig. 4.7).

Figure 4.8 Melting in the Nashoba Formation. Outcrop was observed on Codman Hill Rd. in Boxborough, MA southeast of ER2 and ER3.

The M_4 mineral assemblage (M_3 of Markwort, 2007; Stroud et al., 2009) was muscovite-chlorite in all members of the TBS and muscovite in the Ball Hill mylonite zone and Nashoba Formation (Fig. 4.6). M_4 is constrained to 370-400 °C and 1.0-2.5 kilobars (Fig. 4.7) and is interpreted to be a retrograde event. It was also observed by Jerden (1997) and Munn (1987) in the TBS. This event seems to have occurred entirely post-deformation because muscovite and chlorite are randomly oriented and cut across the foliation throughout the field area. Geochronology suggests there may have been different events in the north

and south sections of the field area that led to this mineral growth (see Chapter 6).

B. STRUCTURAL GEOLOGY

I. Nashoba Formation schists

No structural mapping was performed in this study on the Nashoba Formation schists. The Nashoba Formation schist samples were collected by MaryEllen Loan a nd Andrew Kay during the summers of 2008 and 2009. Geologic mapping performed by Markwort (2007) showed the foliations of NFS-1 as dipping ~30º to the northwest and the lineations as plunging shallowly to the northeast. The main foliation of MLBS-1 is composed of biotite, muscovite, and quartz. The main foliation of NFS-1 is composed of biotite and quartz.

II. Nashoba Formation amphibolite

The foliation in the Nashoba Formation amphibolite dips 70-80° to the northwest (Fig. 4.9A; App. IIIA) and the amphibolite contains north-northeast sub-horizontal lineations which are composed of biotite (Fig. 4.9A; Fig. 4.10A; App.IIIB). The main foliation is composed of biotite and hornblende (Fig. 4.10B). A weak sinistral shear sense was observed in the field in discrete shear bands.

III. Northwest member of the TBS

In the field and in thin section a normal top-to-the-west shear sense was observed in the northwest member of the TBS (Fig. 4.10C). This was not observed elsewhere in this study. The foliation of the northwest member of the TBS dips 45-70° to the northwest (Fig. 4.9B; App. IIIA). This member has lineations composed of muscovite that plunge 40-60° to the west (App. IIIB). The main foliation is composed of muscovite, biotite, and quartz. Isoclinal folds were observed plunging shallowly to the northeast (Fig. 4.9B).

IV. Central member of the TBS

The foliation of the central member of the Tadmuck Brook Schist dips 30-85° with west to northwest dip directions (Fig. 4.9C; App. IIIA). The variation in foliations may be due to minor faults near where measurements were made. Lineations plunge 1-20° to the north (App. IIIB). The main S-C fabric is composed of muscovite and it has a sinistral shear sense. The axes of isoclinal folds were observed plunging shallowly to the northeast in the field.

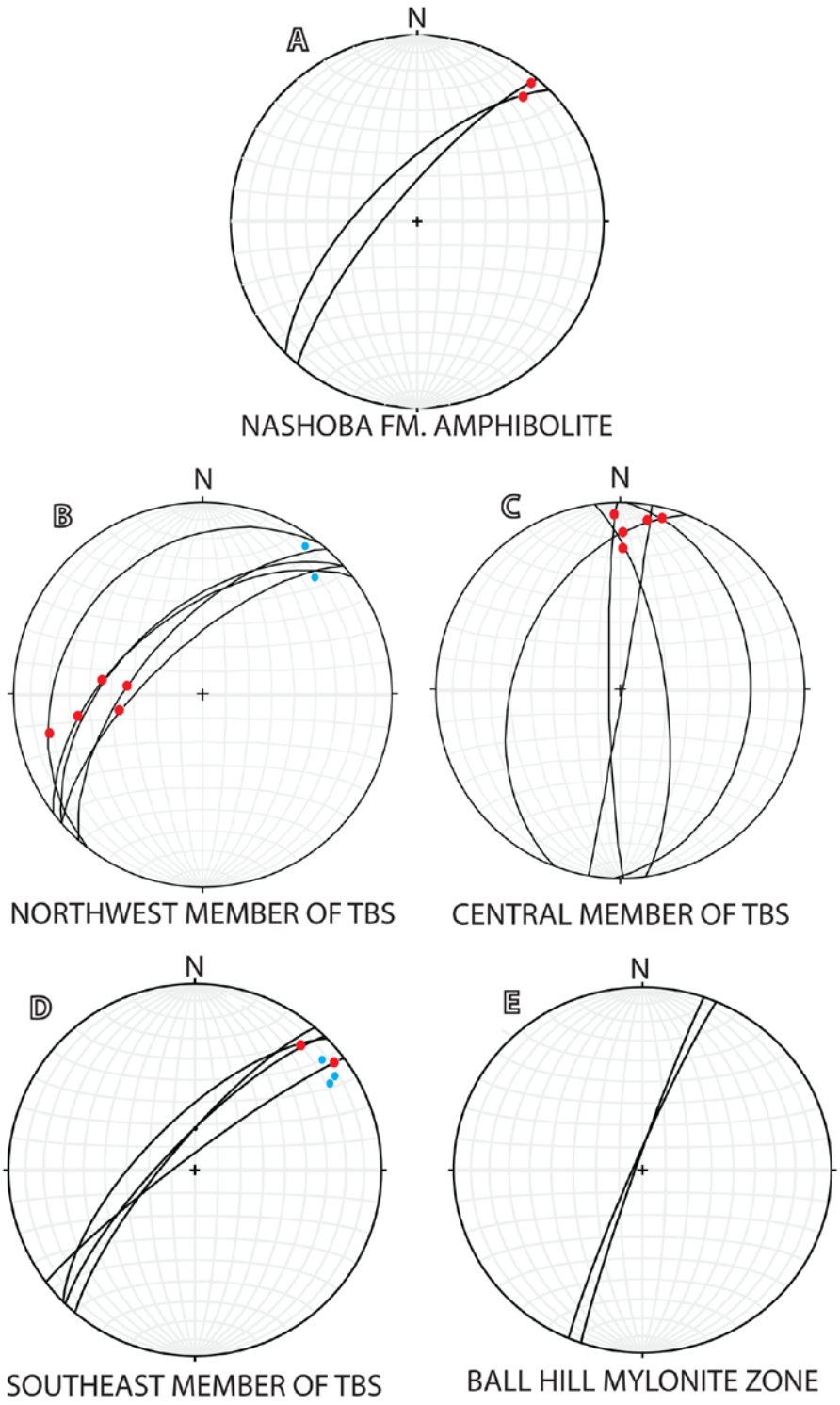

Figure 4.9 Equal area lower hemisphere projections of foliations (black great circles), lineations (red dots), and fold axes (blue dots).

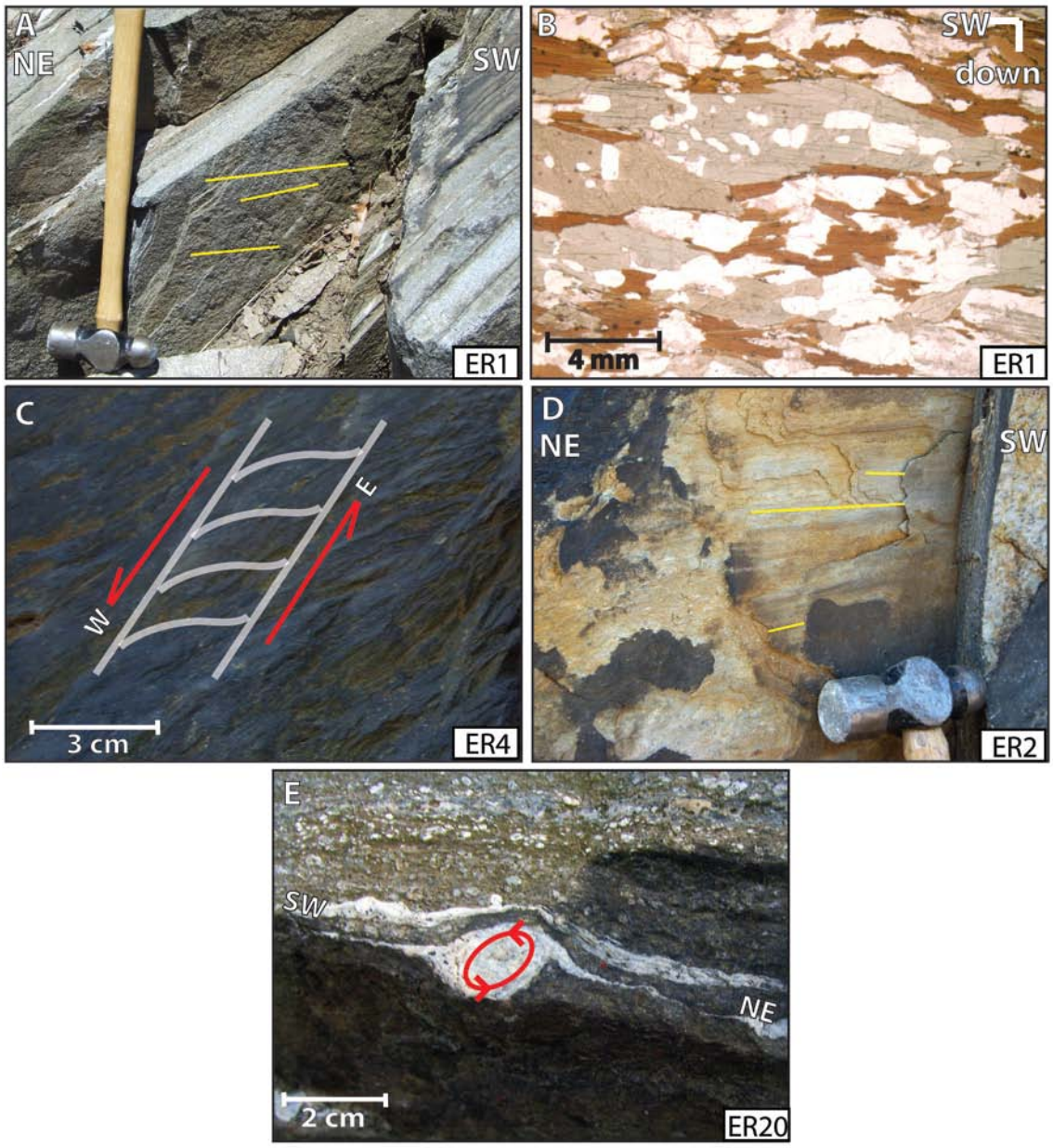

Figure 4.10 A) Horizontal field photograph of horizontal lineations in ER1. **B)** Photomicrograph of main foliation in ER1 (PPL). **C)** Horizontal field photograph of west-side-down normal shear sense in ER4. **D)** Horizontal field photograph of horizontal lineations in ER2. **E)** Field photograph of rotated delta clast (looking down) in ER20. The shear sense along the Ball Hill fault is sinistral.

V. Southeast member of the TBS

A sinistral shear sense was observed in mica fish (Fig. 4.5C) and the main S-C fabric in the southeast member of the TBS. The foliation dips 70-80° to the northwest and h as sub-horizontal lineations composed of muscovite and sillimanite that trend north-northeast (Fig. 4.9D; Fig. 4.10D; App. IIIA; App. IIIB). Isoclinal folds were observed plunging shallowly northeast.

VI. Ball Hill mylonite zone

The Ball Hill mylonite zone has foliations which dip 60-85° to the northwest (Fig. 4.9E; App. IIIA). Rotated delta clasts on the horizontal surface at sample ER20 showed an oblique sinistral shear sense (Fig. 4.10E; App. IIIC).

VII. Interpretation of deformation history

Structural observations from this study suggest that units in the field area were deformed by at least two major events. The origin of the observed isoclinal folds is unclear, but it is interpreted that they (1) were pre-existing and w ere modified during shearing or (2) formed during the shearing events described below.

The first major deformation event (D_1) tilted the foliation (S_1) so that it is now dipping 40-80° to the northwest. Because changes in lithology are subparallel to S_1 it is likely that S_1 is also subparallel to the original bedding plane (S_0). Observed shear zones and sinistral S-C fabric were entirely coplanar with

S_1. Therefore, it is interpreted that this sinistral shear also occurred penecontemporaneously with the formation of S_1, during D_1. The shear indicators for this high-grade shear event include (1) a sinistral S-C fabric (Fig. 4.5C) associated with subhorizontal lineations composed of biotite and biotite-sillimanite (App. IIIB; Fig. 4.10A & D), and (2) counter-clockwise rotated delta clasts in the Ball Hill mylonite zone (Fig. 4.10E). The sinistral shear event is observed in all units studied except the northwest member of TBS, where shearing may be overprinted by D_2.

The second deformation event (D_2) was only observed in the northwest member of the TBS, found in the footwall of the Clinton-Newbury fault. D_2 is characterized by a low-grade, normal top-to-the-west shear sense (App. IIIC). The shear sense indicators include a normal shear fabric (Fig. 4.10C) associated with west-plunging lineations composed of muscovite and minor biotite. The normal shear sense was previously observed along the Clinton-Newbury fault by Goldstein (1994) and Jerden (1997).

Chapter 5. $^{40}Ar/^{39}Ar$ GEOCHRONOLOGY DATA

Both inverse isochrons and age probability plots are provided for each sample, along with a graph of the total-fusion ages for easier reference of the relative errors of each data point. In the inverse isochron figures the purple line is the line for the age that is calculated assuming all non-radiogenic argon has atmospheric composition. The pink lines have been fit through the raw data. The ages in parts B-D of the figures were calculated assuming that all non-radiogenic Ar was of atmospheric composition. The probability diagrams do not include data that was removed due to excess or lost radiogenic argon.

A. $^{40}Ar/^{39}Ar$ Data

I. Nashoba Formation schist

Both biotite and muscovite were dated from MBLS-1, a schist from the Nashoba Formation.

<u>MBLS-1 – Muscovite</u>

One date was eliminated from the final analysis for MLBS-1 muscovite. Grain #10 had a 2σ error that was larger than the age itself (227 ± 456 Ma; Fig. 5.1A & 5.1B). The data intercepts with the value of atmospheric argon on the y-axis suggesting that these grains did not include any inherited argon. The inverse isochron gives an age of 257 ± 14 Ma with an acceptable MSWD of 0.49 (Fig. 5.1A).

MBLS-1 – Biotite

All dates were included in the final analyses for MLBS-1 biotite (Fig. 5.2B). The y-intercept of the inverse isochron suggests that there may be s ome inherited argon in these samples (Fig. 5.2A); however the range of possible ages on the x-axis (between the age corrected for atmospheric argon and that given by the samples) is very small. The inverse isochron gives an age of 305 ± 7 Ma. Although this sample has inherited argon and a high MSWD (17.11) it is included in the final analysis since there is a very small range in possible ages for this sample.

NSF-1 – Biotite

Date #9 was eliminated from the final analysis of NSF-1 biotite due to the fact that its age is much too old for this field area, possibly because of excess argon (Fig. 5.3B). The y-intercept of the inverse isochron suggests that there may be a large amount of inherited argon in this sample (Fig. 5.3A). Due to the fact that this sample has inherited argon and because it has a high MSWD (>100) it is not included in the final analysis in the discussion.

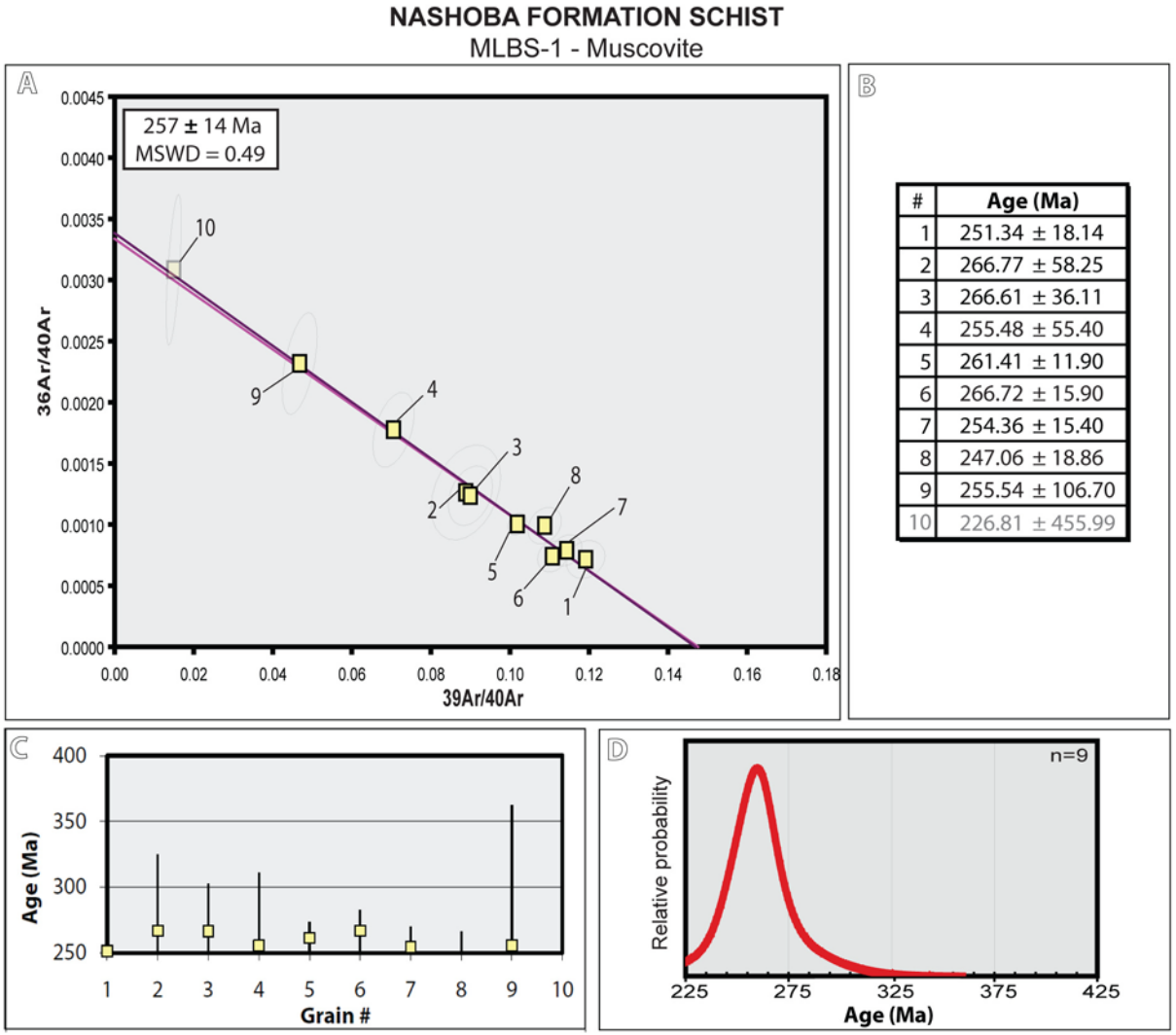

Figure 5.1 Muscovite from a Nashoba Formation Schist (MLBS-1). The ages in parts B-D of the figures were calculated assuming that all non-radiogenic Ar was of atmospheric composition. **A)** Inverse isochron diagram. The purple line is the line for the age that is calculated assuming all non-radiogenic argon has atmospheric composition. The pink lines have been fit through the raw data. **B)** Date #10 was eliminated from final analysis. **C)** Ages from total-fusion dating. **D)** Age probability chart.

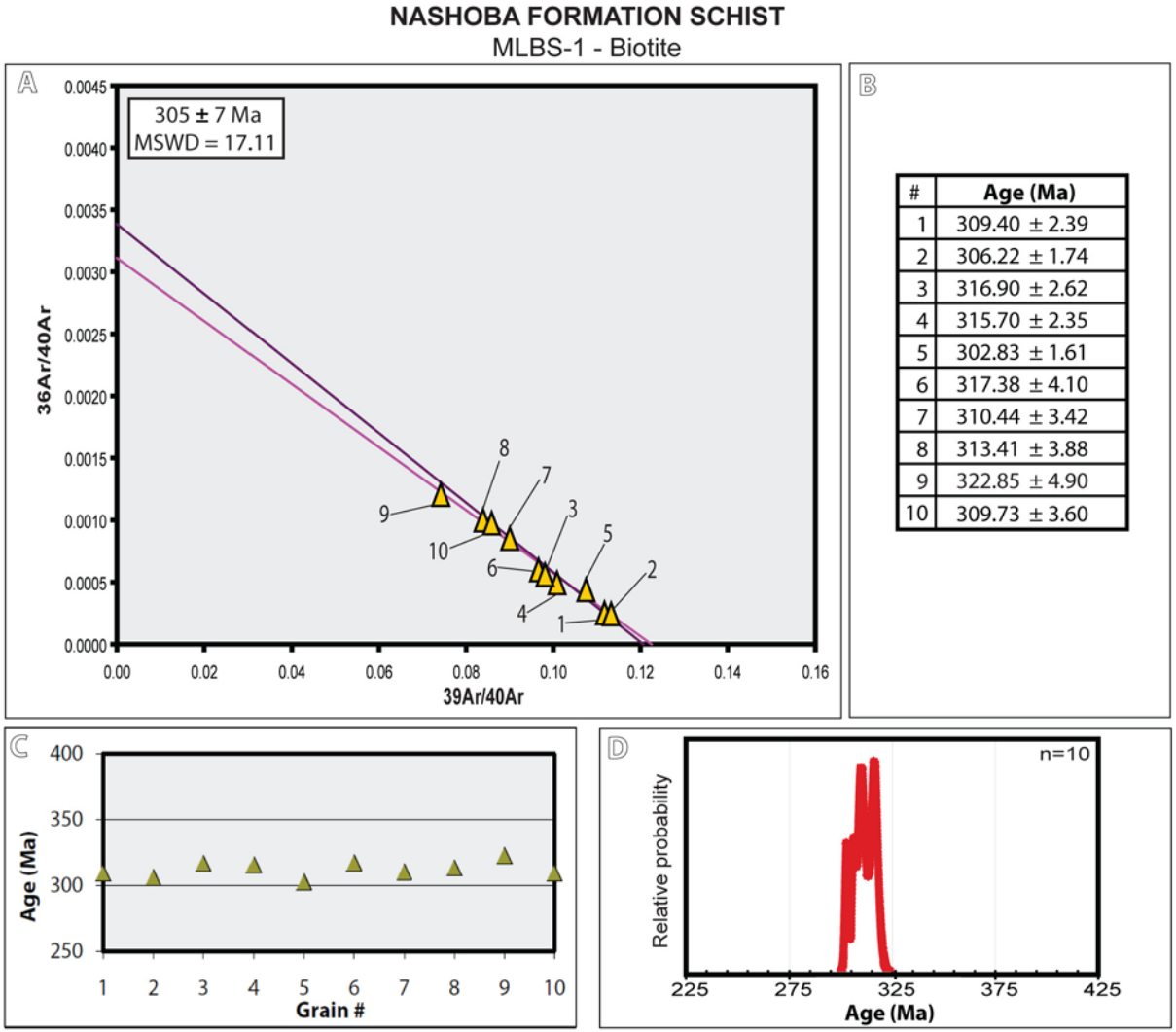

Figure 5.2 Biotite from the Nashoba Formation Schist (MLBS-1). The ages in parts B-D of the figures were calculated assuming that all non-radiogenic Ar was of atmospheric composition. **A)** Inverse isochron diagram. The purple line is the line for the age that is calculated assuming all non-radiogenic argon has atmospheric composition. The pink lines have been fit through the raw data. **B)** No ages were eliminated from the final analysis. **C)** Ages from total-fusion dating. **D)** Age probability chart.

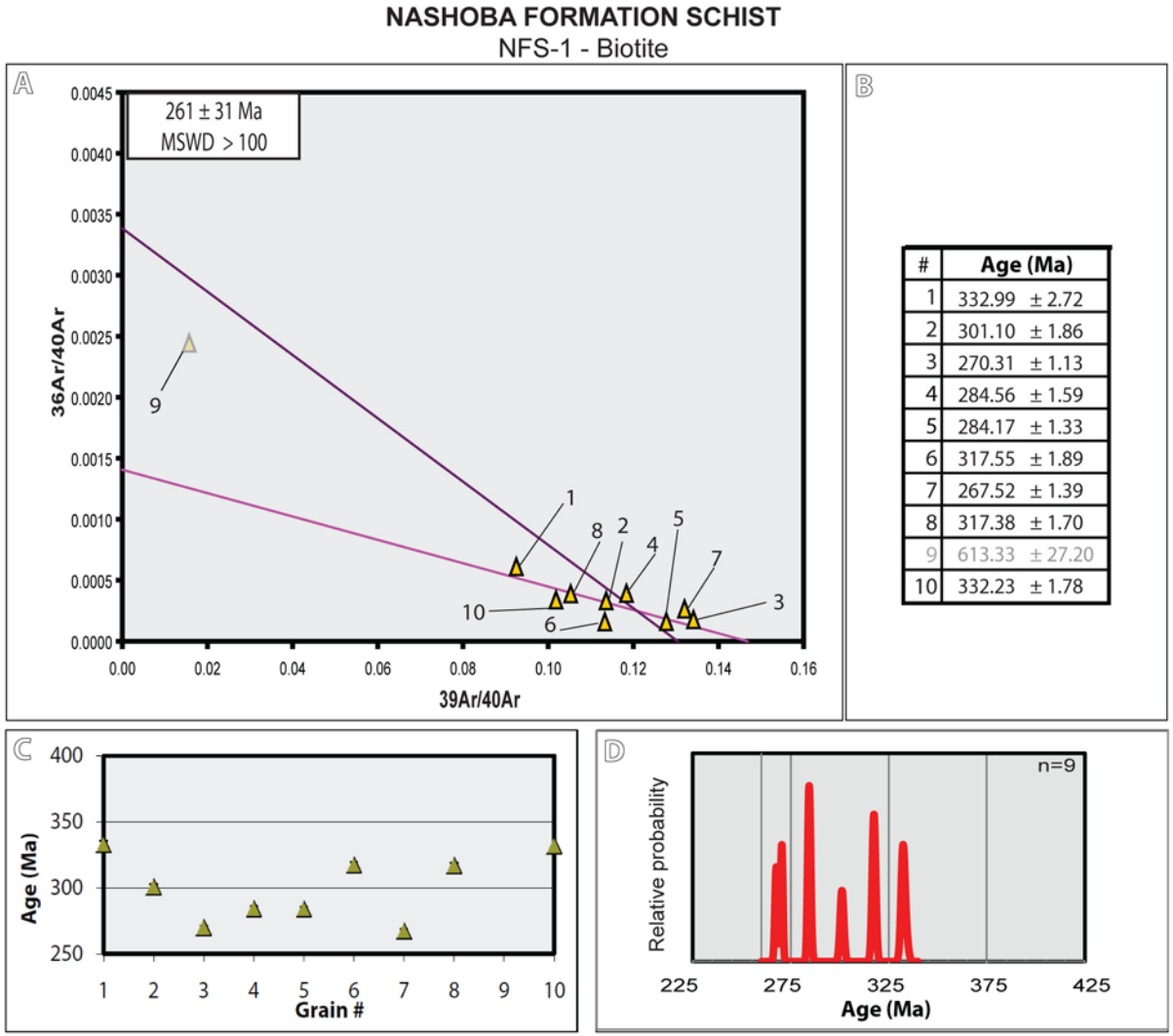

Figure 5.3 Biotite from a Nashoba Formation schist. The ages in parts B-D of the figures were calculated assuming that all non-radiogenic Ar was of atmospheric composition. **A)** Inverse isochron diagram. The purple line is the line for the age that is calculated assuming all non-radiogenic argon has atmospheric composition. The pink lines have been fit through the raw data. **B)** Date #9 was eliminated. **C)** Ages from total-fusion dating. **D)** Age probability chart.

II. Nashoba Formation amphibolite

Both biotite and hornblende were dated from the amphibolite at the western boundary of the Nashoba Formation.

ER1 – Hornblende

The hornblendes were first dated using the single grain total-fusion method, yielding an inverse isochron age of 432 ± 34 Ma (Fig. 5.4A); however, there were two grains (#6 and #7) that were found to be 465 Ma old and it was apparent on the inverse isochron diagram that they had inherited excess argon (Figure 5.4A). The four eliminated ages all have significantly high ^{38}Ar values when compared to the other 6 ages from this set (see full data in Appendix I). ^{38}Ar forms from the decay of ^{38}Cl, suggesting that chlorine is present in these grains, which is an issue because ^{36}Cl decays to ^{36}Ar quickly after irradiation (within months-years) and can result in errors of up to 5% in the calculated $^{40}Ar/^{39}Ar$ ages (McDougall and Harrison, 1999).

In order to better identify inherited argon the hornblende sample was then analyzed using the furnace step-heating method. Measurements were made at 19 steps which increased from 800 °C to 1350 °C. 10 of these steps yielded a plateau age (since they occur at high temperature and account for ~90% of the ^{39}Ar released) of 376 ± 9 Ma (Fig. 5.5).

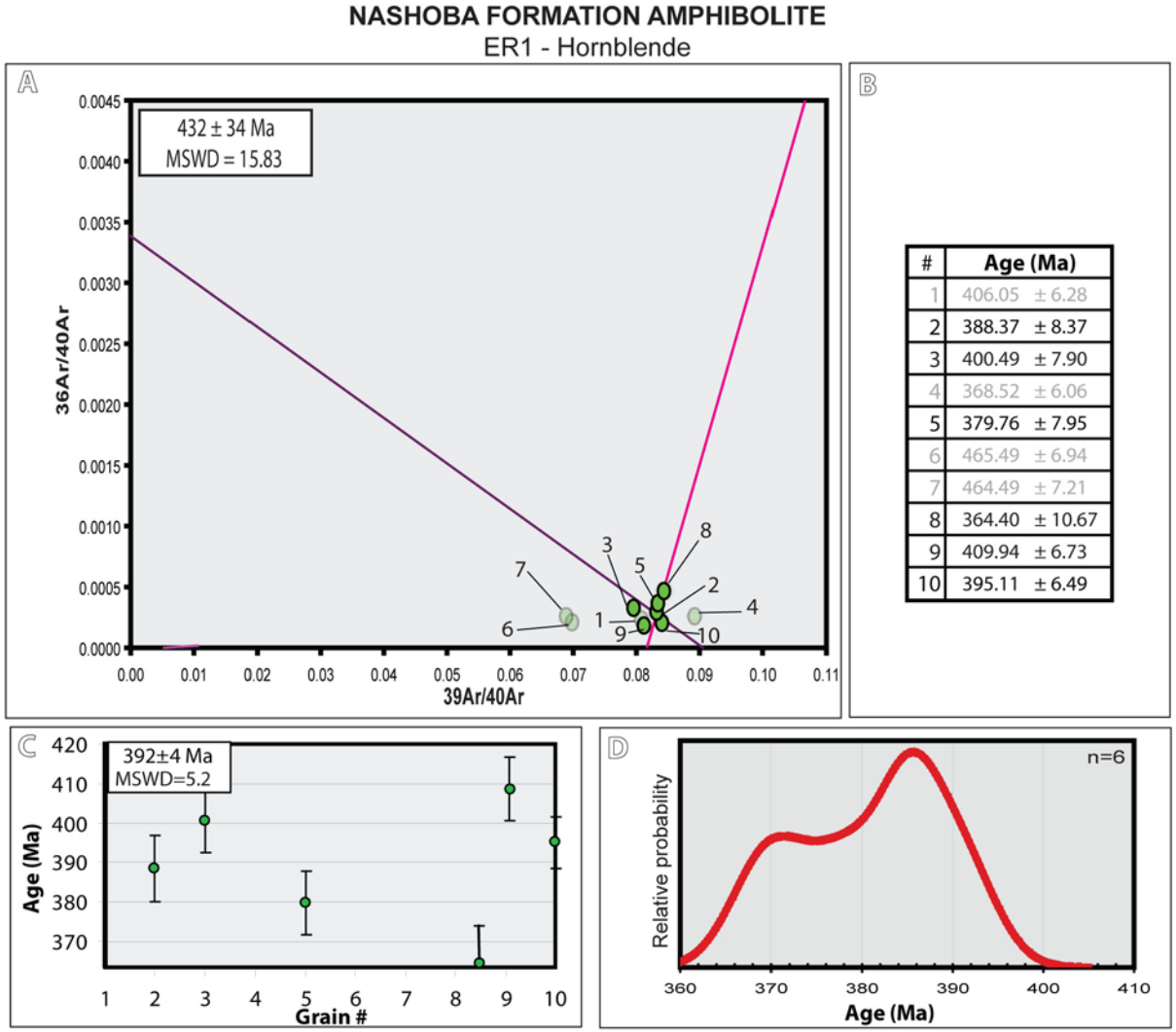

Figure 5.4 Hornblende from the amphibolite member of the Nashoba Formation. The ages in parts B-D of the figures were calculated assuming that all non-radiogenic Ar was of atmospheric composition. **A)** Inverse isochron diagram. The purple line is the line for the age that is calculated assuming all non-radiogenic argon has atmospheric composition. The pink lines have been fit through the raw data. **B)** Dates #1, #4, #6, and #7 were eliminated from final analysis. **C)** Ages from total-fusion dating. **D)** Age probability chart.

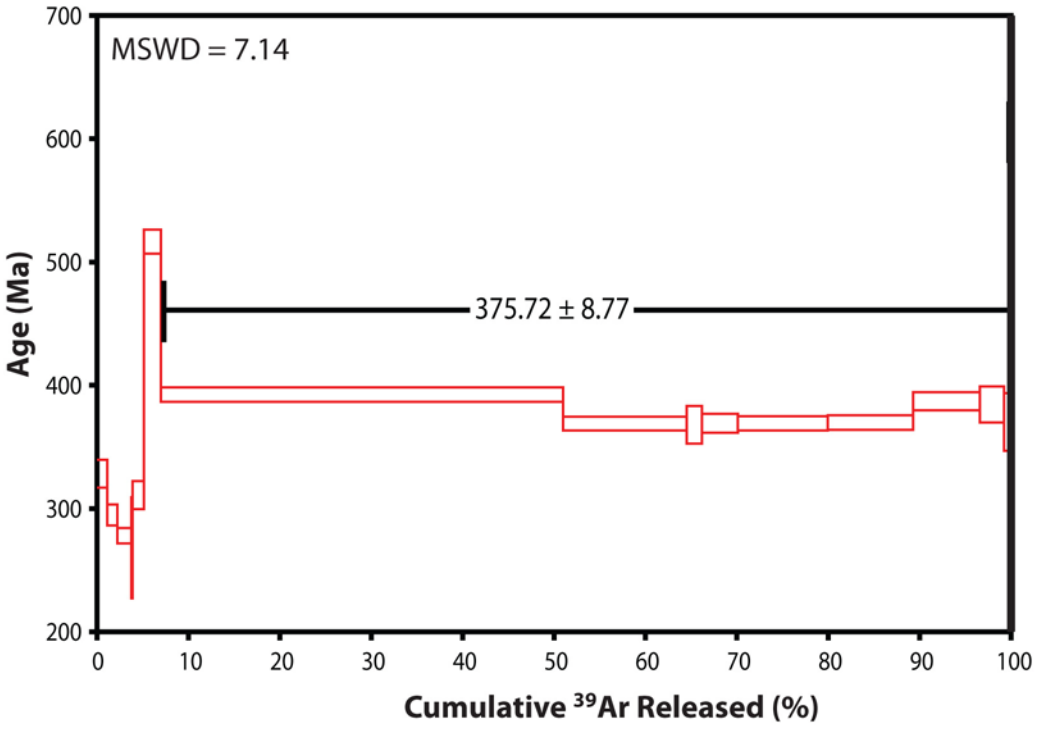

Figure 5.5 Ten grains of hornblende were dated using the furnace step-heating method after the single grain total fusion method yielded inconclusive results.

ER1 – Biotite

Two dates were eliminated from the final analysis (#4 and #8; Fig. 5.6B). These dates were eliminated for relatively low K/Ca ratios (compared to the eight other dates that contributed to this age; Appendix I), which is an issue because calcium can produce significant amounts of ^{36}Ar and ^{39}Ar. The other data intercepts the y-axis at the value of atmospheric argon on the inverse isochron, suggesting that there was no inherited argon (Fig. 5.6A). The inverse isochron gives an age of 330 ± 7 Ma with an acceptable MSWD of 0.26.

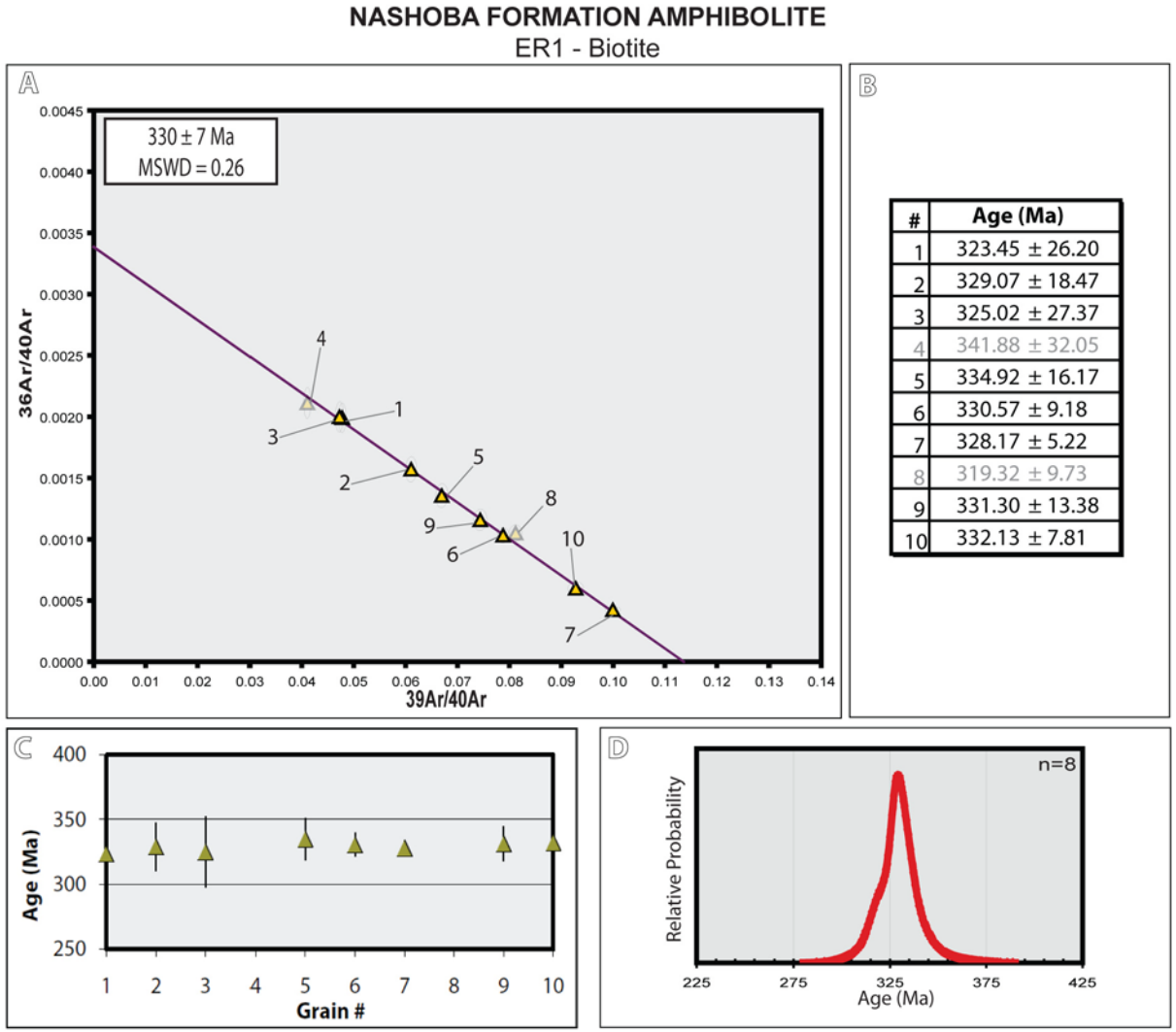

Figure 5.6 Biotite from the amphibolite member of the Nashoba Formation (ER1). The ages in parts B-D of the figures were calculated assuming that all non-radiogenic Ar was of atmospheric composition. **A)** Inverse isochron diagram. The purple line is the line for the age that is calculated assuming all non-radiogenic argon has atmospheric composition. The pink lines have been fit through the raw data. **B)** Dates #4 and #8 were eliminated from final analysis. **C)** Ages from total-fusion dating. **D)** Age probability chart.

III. Northwest member of the Tadmuck Brook Schist

ER4 – Muscovite

Grain #6 was eliminated due to the fact that it had a very large 2σ error (±455 Ma; Fig. 5.7B). The remaining 9 data points are all clustered near the x-axis of the inverse isochron. This suggests that there is little trapped/excess argon in this sample. The inverse isochron graph gave an age of 302 ± 5 Ma (Fig. 5.7A). Despite its high MSWD (27.82), this sample is included in further analysis in the discussion because the clustering of the data points near the x-axis suggests that there was little to no excess argon in the dated grains.

ER8 – Muscovite

All dated grains were included in the final analysis (Fig. 5.8B). The y-intercept of the inverse isochron graph is below the atmospheric argon composition, meaning that there may be some excess argon, however there are no data points close to the left side of the inverse isochron to ascertain this (Fig. 5.8A). The 10 data points are all clustered near the x-axis of the inverse isochron; therefore it is believed that this date is reliable. The inverse isochron graph of muscovite for ER8 gave an age of 267 ± 8 Ma (Fig. 5.8A). Despite its high MSWD (14.26), this sample is included in further analysis in the discussion.

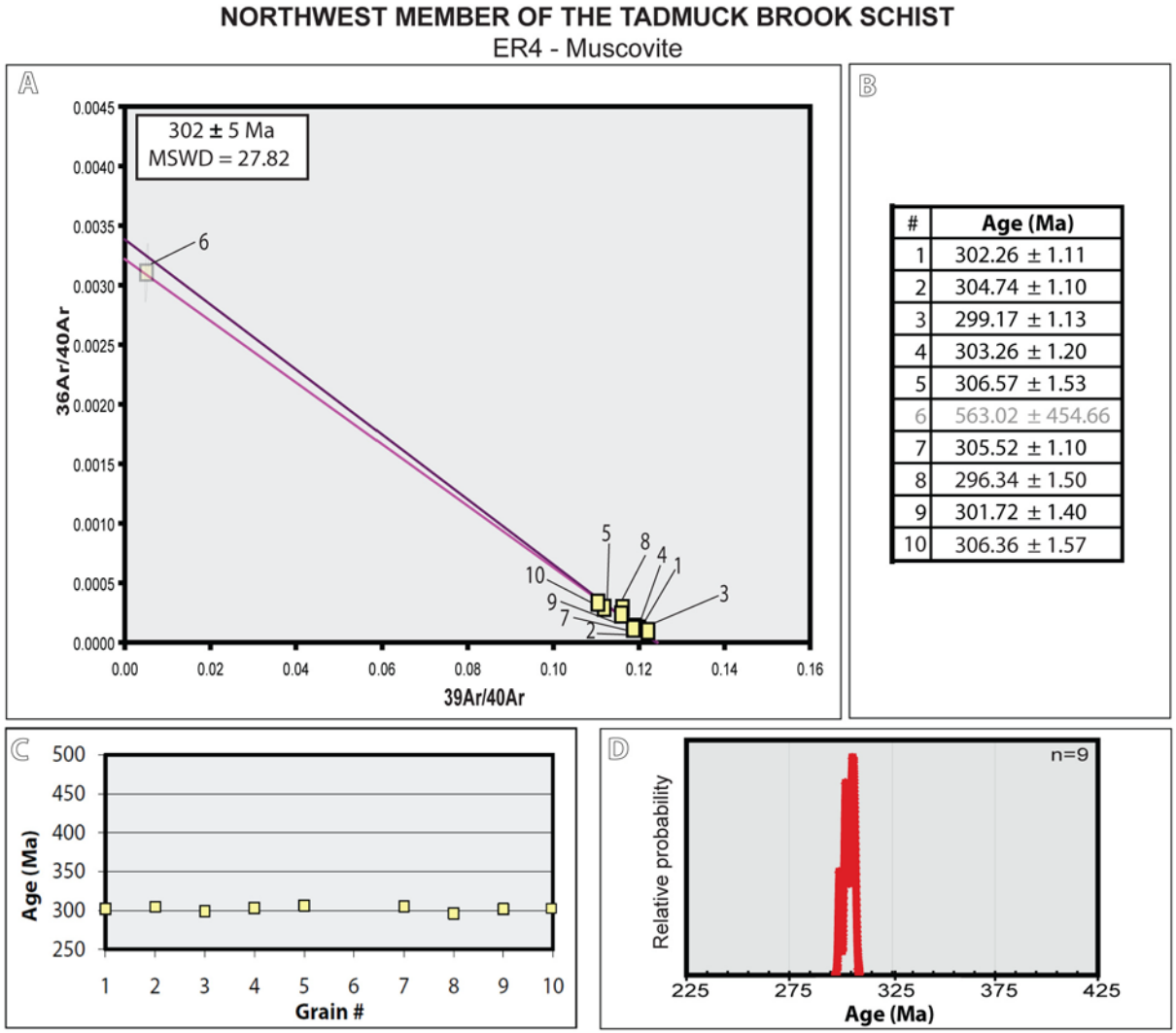

Figure 5.7 Muscovite from the Northwest Member of the TBS. The ages in parts B-D of the figures were calculated assuming that all non-radiogenic Ar was of atmospheric composition. **A)** Inverse isochron diagram. The purple line is the line for the age that is calculated assuming all non-radiogenic argon has atmospheric composition. The pink lines have been fit through the raw data. **B)** Date #6 was eliminated from final analysis. **C)** Ages from total-fusion dating. **D)** Age probability chart.

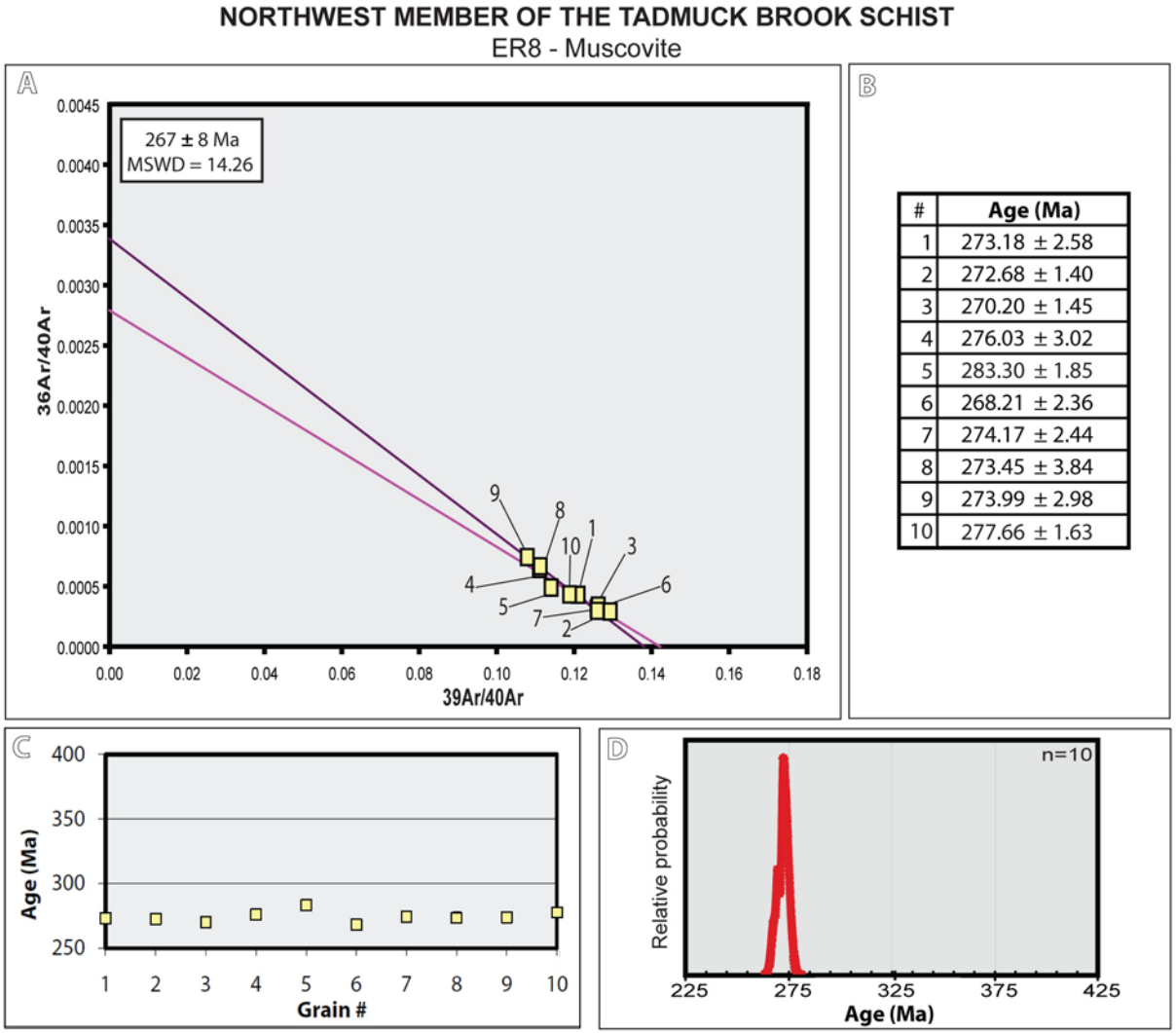

Figure 5.8 Muscovite from the Northwest Member of the TBS. The ages in parts B-D of the figures were calculated assuming that all non-radiogenic Ar was of atmospheric composition. **A)** Inverse isochron diagram. The purple line is the line for the age that is calculated assuming all non-radiogenic argon has atmospheric composition. The pink lines have been fit through the raw data. **B)** No dates were eliminated from final analysis. **C)** Ages from total-fusion dating. **D)** Age probability chart.

IV. Central member of the Tadmuck Brook Schist

25.1- Biotite

Date #2 was eliminated because it has an unexpectedly young age and has an error larger than the age itself (88 ± 335 Ma; Fig. 5.9B). On the inverse isochron graph the data intercepts the y-axis at the value of atmospheric argon (Fig. 5.9A), suggesting that there was no inherited argon. The inverse isochron gives an age of 268 ± 6 Ma with an acceptable MSWD of 0.64 (Fig. 5.9A).

25.1- Muscovite

No dates were eliminated from the final analysis (Fig. 5.10B). The y-intercept of the data on the inverse isochron diagram (Fig. 5.10A) is below the value of atmospheric argon suggesting that the sample had excess argon. The inverse isochron graph gave an age of 256 ± 5 Ma with an MSWD of 26.01 (Fig. 5.10A); however, there is a large amount of discrepancy between the x-axis intercepts of the line that passes through the data (272 Ma) and the line for the age that is calculated assuming all non-radiogenic argon has atmospheric composition (256 Ma). Because of this discrepancy, this age will not be used further in the discussion.

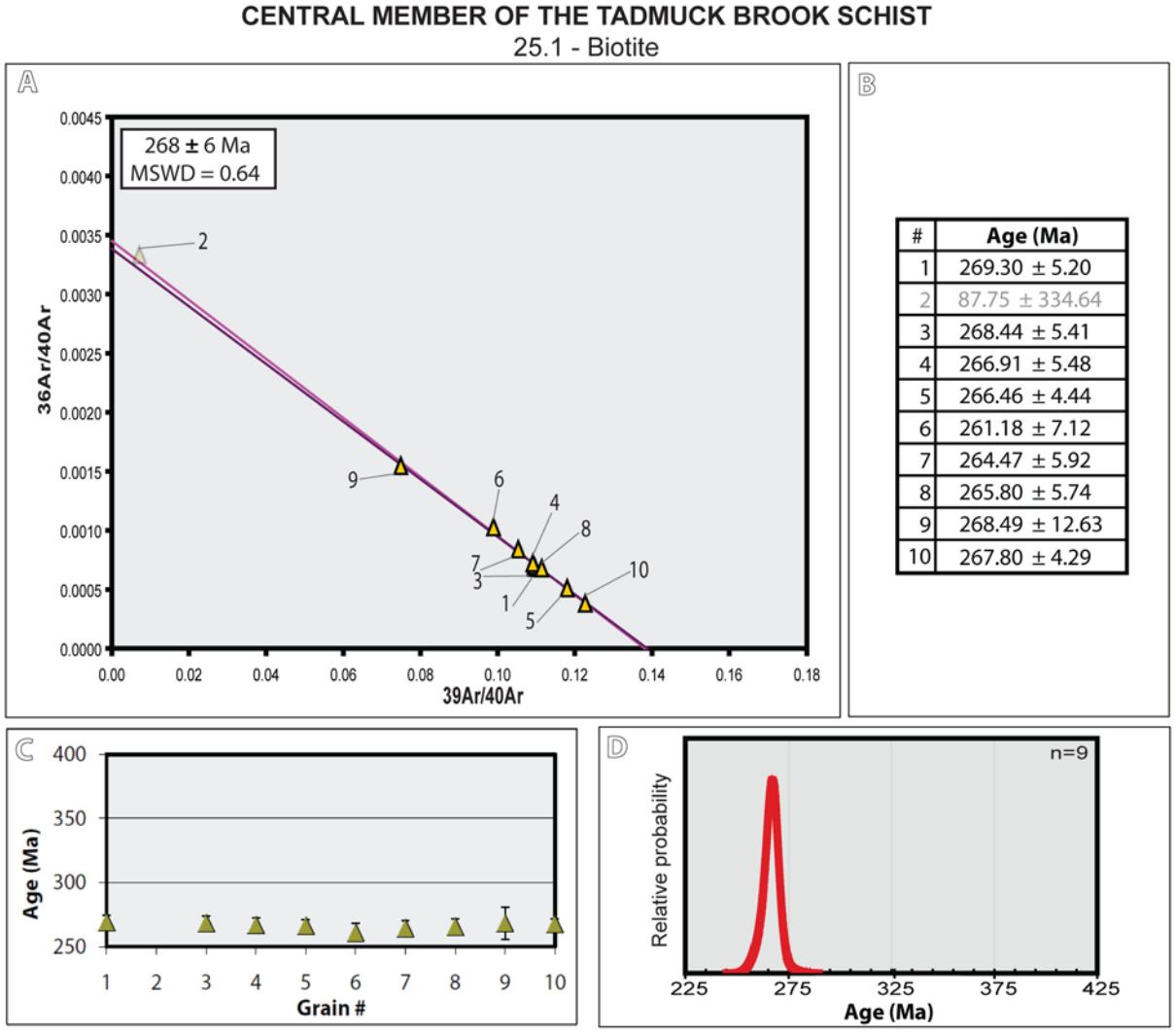

Figure 5.9 Biotite from the Central Member of the TBS (25.1). The ages in parts B-D of the figures were calculated assuming that all non-radiogenic Ar was of atmospheric composition. **A)** Inverse isochron diagram. The purple line is the line for the age that is calculated assuming all non-radiogenic argon has atmospheric composition. The pink lines have been fit through the raw data. **B)** Date #2 was eliminated from final analysis. **C)** Ages from total-fusion dating. **D)** Age probability chart.

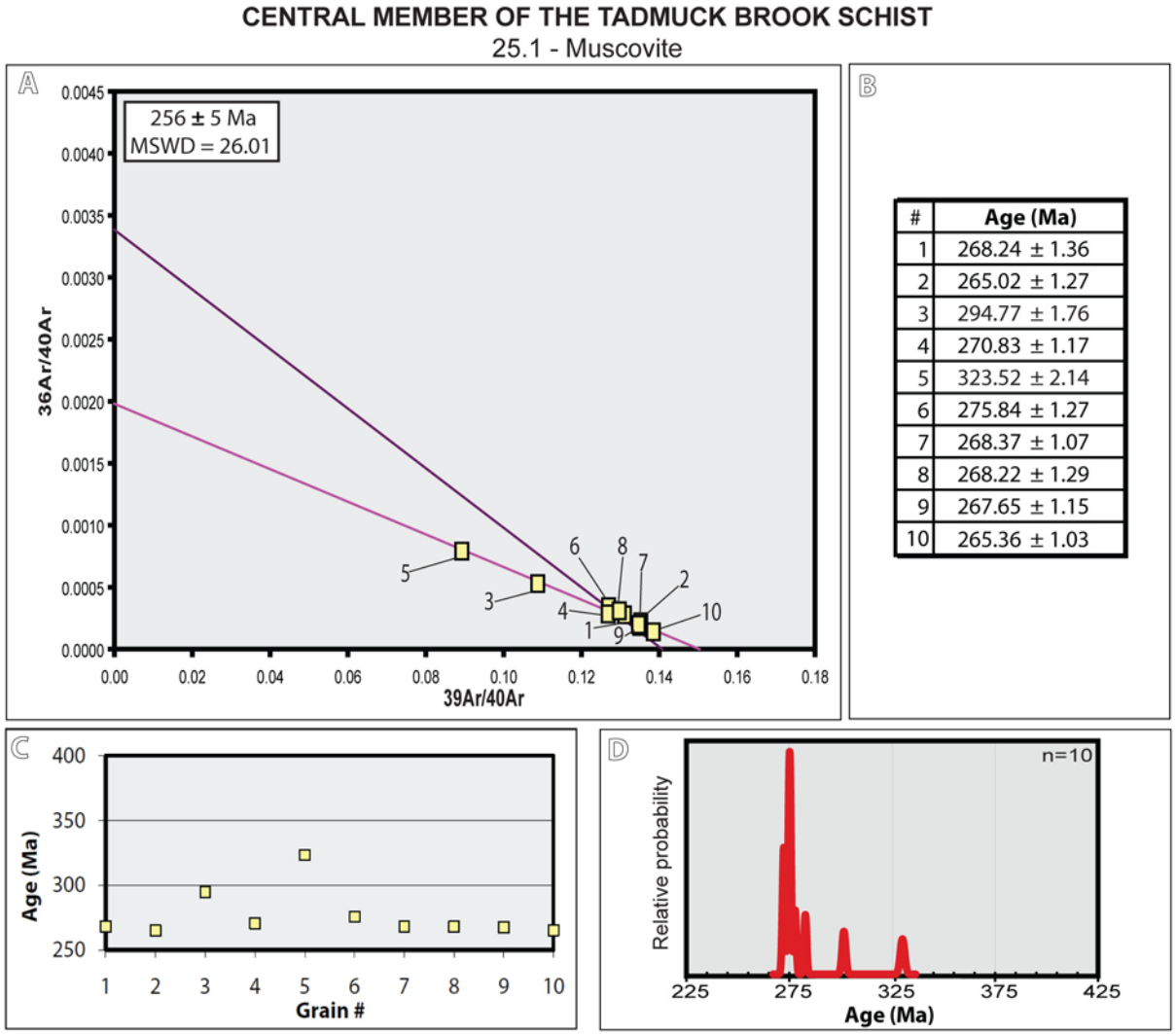

Figure 5.10 Muscovite from the Central Member of the TBS (25.1). The ages in parts B-D of the figures were calculated assuming that all non-radiogenic Ar was of atmospheric composition. **A)** Inverse isochron diagram. The purple line is the line for the age that is calculated assuming all non-radiogenic argon has atmospheric composition. The pink lines have been fit through the raw data. **B)** No dates were eliminated from final analysis. **C)** Ages from total-fusion dating. **D)** Age probability chart.

V. Southeast member of the Tadmuck Brook Schist

Muscovite was dated from two samples collected from the high grade member of the TBS. Both gave normal isochron ages of ~315 Ma.

ER2 – Muscovite

One date (#1) was eliminated from the final analysis due to the fact that it seemed to have lost a large amount of argon and gave a negative date (Fig. 5.11 B). The data plots on a line that intercepts the y-intercept only slightly above the value of atmospheric argon (Fig. 5.11A). The remaining 9 data points all cluster at the same point along the x-axis suggesting that there was a low component of non-radiogenic argon in these samples. The inverse isochron graph of muscovite for ER2 gave an age of 316 ± 6 Ma with an acceptable MSWD of 0.49 (Fig. 5.11A).

ER3 – Muscovite

Date #3 was eliminated from the final analysis due to the fact that it seemed to have excess argon and a relatively high ^{38}Ar (Fig. 5.12A; Appendix I). The data plots on a line that intercepts the y-intercept just slightly below the value of atmospheric argon (Fig. 5.12A). The inverse isochron graph of muscovite for ER3 gave an age of 314 ± 5 Ma with an MSWD of 0.47 (Fig. 5.12A).

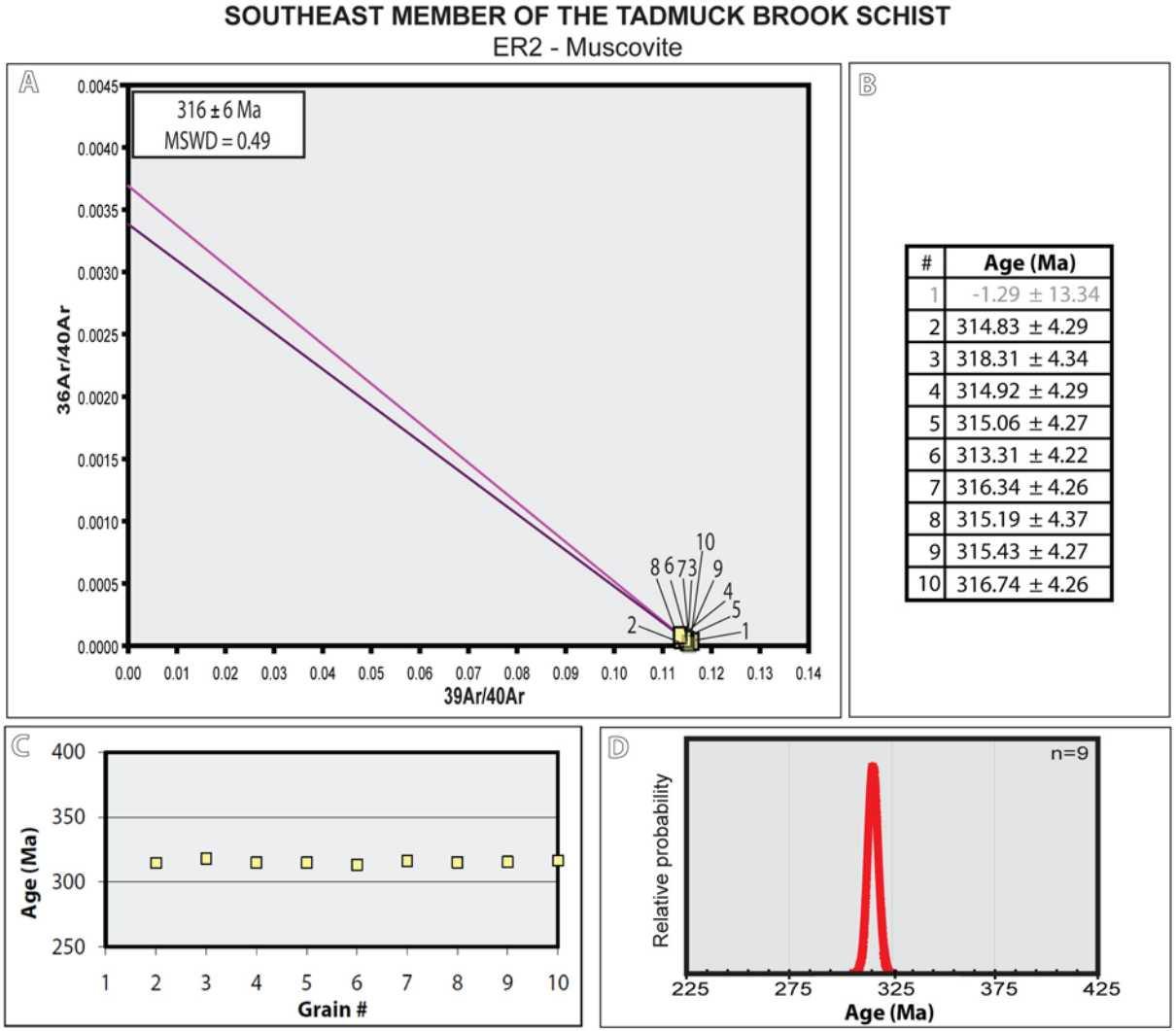

Figure 5.11 Muscovite from the Southeast Member of the Tadmuck Brook Schist. The ages in parts B-D of the figures were calculated assuming that all non-radiogenic Ar was of atmospheric composition. **A)** Inverse isochron diagram. The purple line is the line for the age that is calculated assuming all non-radiogenic argon has atmospheric composition. The pink lines have been fit through the raw data. **B)** Date #1 was eliminated from final analysis. **C)** Ages from total-fusion dating. **D)** Age probability chart.

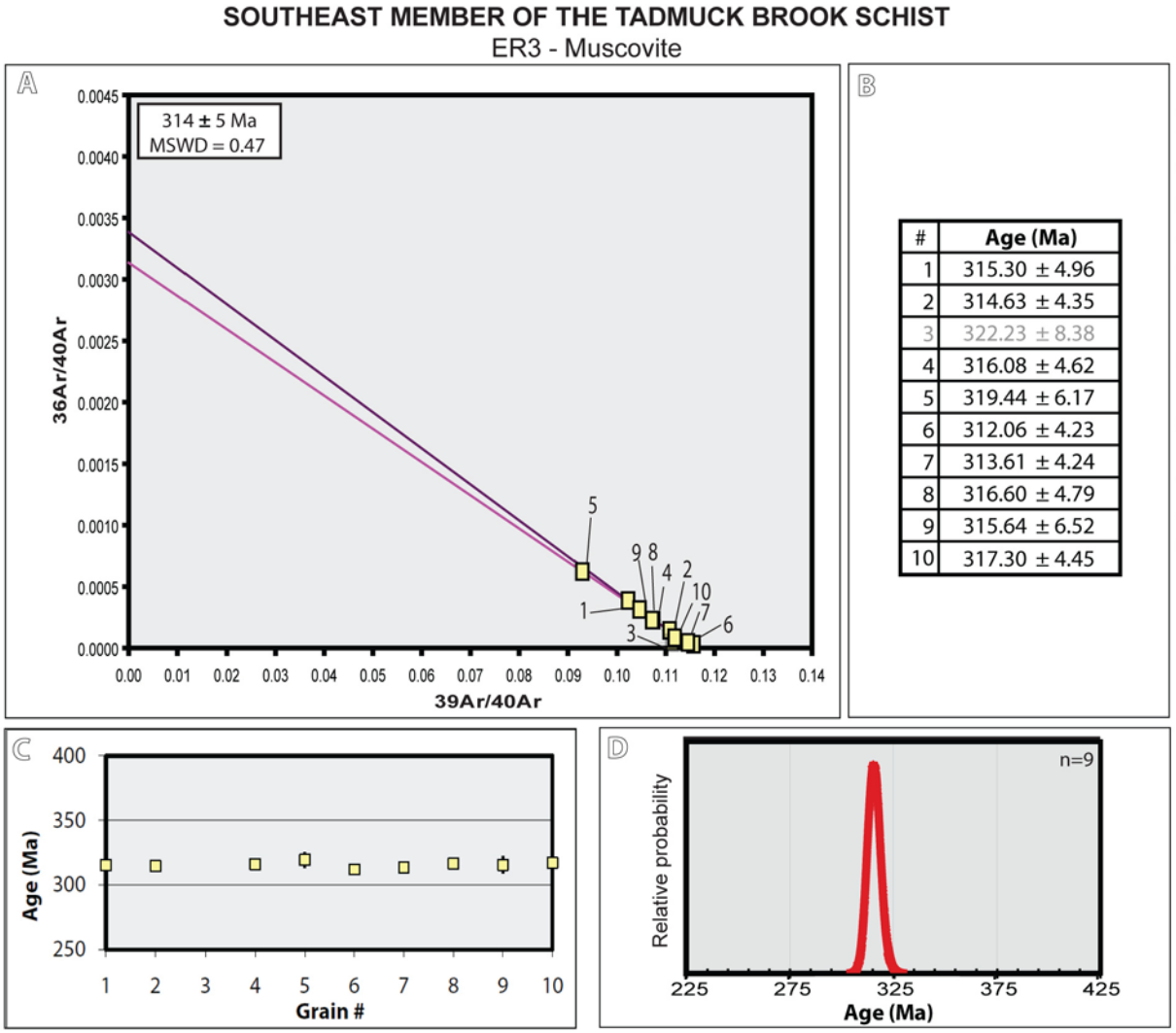

Figure 5.12 Muscovite from the Southeast Member of the TBS. The ages in parts B-D of the figures were calculated assuming that all non-radiogenic Ar was of atmospheric composition. **A)** Inverse isochron diagram. The purple line is the line for the age that is calculated assuming all non-radiogenic argon has atmospheric composition. The pink lines have been fit through the raw data. **B)** Date #3 was eliminated from final analysis. **C)** Ages from total-fusion dating. **D)** Age probability chart.

VI. Ball Hill mylonite zone

ER20 – Biotite

No ages were eliminated from the final analysis (Fig. 5.13B). The data plots on a line that intercepts the y-axis below the value of atmospheric argon, likely due to excess argon in some of the grains (Fig. 5.13A). The inverse isochron graph gave an age of 260 ± 7 Ma with an MSWD of 27.52 (Fig. 5.13A); however, there is a small age discrepancy between the line that passes through the raw data (267 Ma) and the line that assumes that all non-radiogenic argon has atmospheric composition (260 Ma). Because of the high MSWD, this age will not be used further in the discussion.

ER20 – Muscovite

No ages were eliminated from the final analysis (Fig. 5.14B). The data plots on a line that intercepts the y-axis above the value of atmospheric argon, most likely due to the fact that the data is clustered so closely together, which makes it difficult to get a constraint on the isochron (Fig. 5.14A). The inverse isochron graph of muscovite for ER20 gave an age of 294 ± 6 Ma with an acceptable MSWD of 3.50 (Fig. 5.14A). The 10 data points all cluster at the same point along the x-axis suggesting that there was no excess argon in these samples.

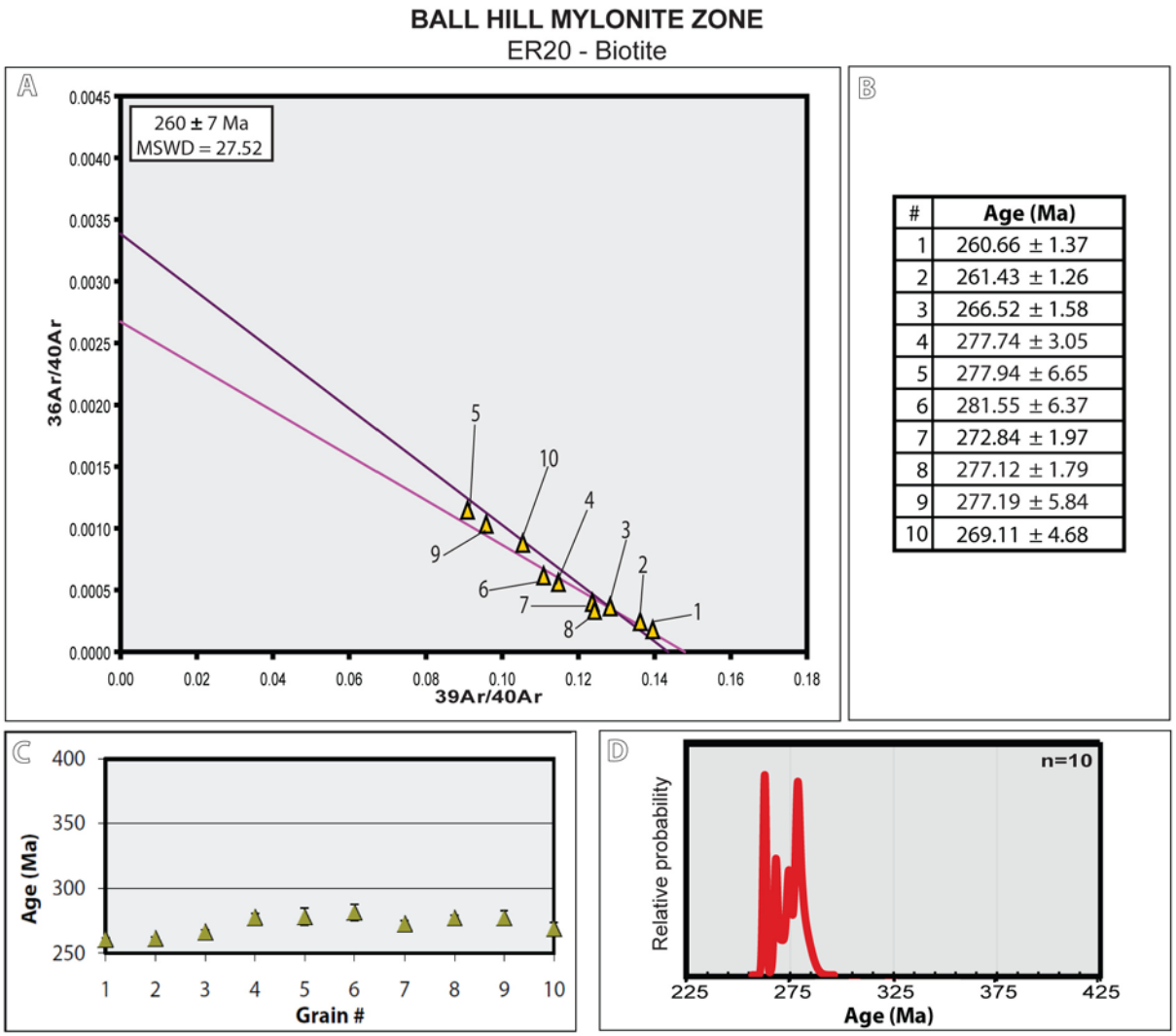

Figure 5.13 Biotite from the Ball Hill Mylonite Zone. The ages in parts B-D of the figures were calculated assuming that all non-radiogenic Ar was of atmospheric composition. **A)** Inverse isochron diagram. The purple line is the line for the age that is calculated assuming all non-radiogenic argon has atmospheric composition. The pink lines have been fit through the raw data. **B)** No dates were eliminated from final analysis. **C)** Ages from total-fusion dating. **D)** Age probability chart.

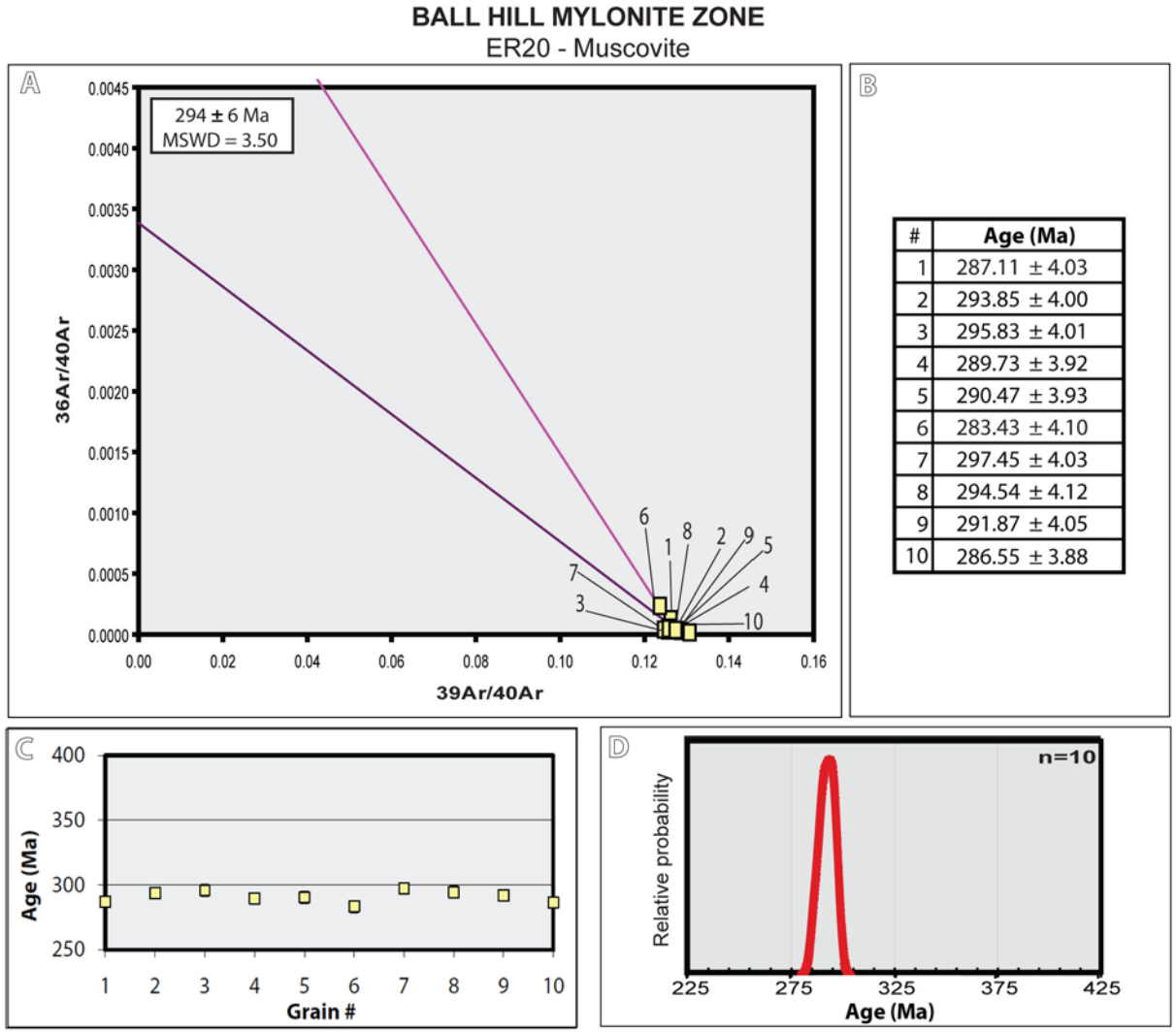

#	Age (Ma)
1	287.11 ± 4.03
2	293.85 ± 4.00
3	295.83 ± 4.01
4	289.73 ± 3.92
5	290.47 ± 3.93
6	283.43 ± 4.10
7	297.45 ± 4.03
8	294.54 ± 4.12
9	291.87 ± 4.05
10	286.55 ± 3.88

Figure 5.14 Muscovite from the Ball Hill Mylonite Zone. The ages in parts B-D of the figures were calculated assuming that all non-radiogenic Ar was of atmospheric composition. **A)** Inverse isochron diagram. The purple line is the line for the age that is calculated assuming all non-radiogenic argon has atmospheric composition. The pink lines have been fit through the raw data. **B)** No dates were eliminated from final analysis. **C)** Ages from total-fusion dating. **D)** Age probability chart.

Chapter 6. DISCUSSION

A. Final $^{40}Ar/^{39}Ar$ ages for study

Thirteen mineral separates were dated from nine different samples. Out of the thirteen dates obtained through $^{40}Ar/^{39}Ar$ dating, ten were suitable to be included in the final analysis (Fig. 6.1). The dates range from 376 ± 9 Ma to 257 ± 14 Ma. These dates have been divided into three different age populations (Table 6.1).

The oldest population (376-330 Ma) consists of the biotite and hornblende dates from the Nashoba Formation amphibolite. The assumption is made here that these two dates are related to cooling from the same event, for reasons described below. The remaining eight younger dates were plotted on a t-T graph (Fig. 6.2), revealing two additional discrete age populations: (1) ~300 Ma and (2) ~267 Ma.

I. Age population I: 376-330 Ma

Age population I was only observed in the Nashoba Formation amphibolite, located in the northern half of field area (Fig. 6.1; Table 6.1). The population includes a biotite date of 330 ± 7 Ma and an amphibolite date of 376 ± 9 Ma. Although the biotite date is nearly within error of age population II, very little biotite was observed cross-cutting the foliation in ER1 (Chapter 4), a texture more pervasive in the samples dating age population II.

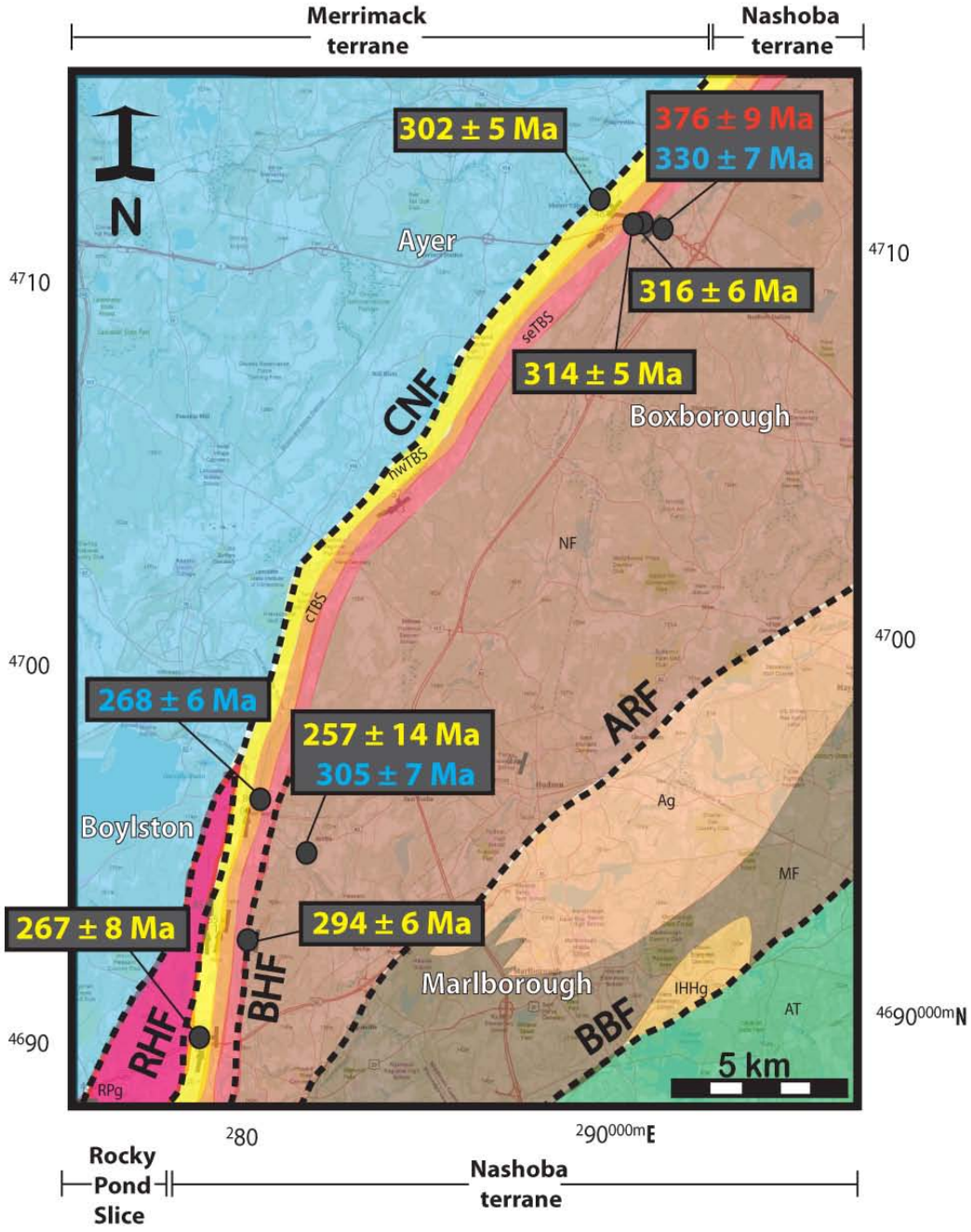

Figure 6.1 $^{40}Ar/^{39}Ar$ ages from this study with mineral closure temperatures. Approximate locations of units are based on maps by Jerden (1997), Kopera (2005), Kopera (2006), Kopera et al. (2006), Markwort (2007), and this study.

CNF = Clinton-Newbury Fault; RHF = Rattlesnake Hill Fault; BHF = Ball Hill Fault; ARF = Assabet River Fault; BBF = Bloody Bluff Fault

See next page for complete key.

KEY TO FIGURE 6.1

EXPLANATION OF LITHOLOGIC UNITS

Merrimack Terrane

MT Merrimack Terrane

Stratified Rocks of the Nashoba Terrane

Tadmuck Brook Schist

nwTBS NW member of TBS

cTBS Central member of TBS

seTBS SE member of TBS

NF Nashoba Formation

MF Marlboro Formation

Intrusive Rocks of the Nashoba Terrane

RPg Rocky Pond Granite

Ag Andover Granite

IHHg Indian Head Hill Granite

The Composite Avalon Terrane

AT Avalon Terrane

EXPLANATION OF MAP SYMBOLS

26 Strike and dip of dominant foliation

14 Trend and plunge of mineral lineation

ADDITIONAL SYMBOLS

Boylston Town location

Fault

EXPLANATION OF AGES

Hornblende age (~500 °C)

Muscovite age (~350 °C)

Biotite age (~300 °C)

	SAMPLE	MINERAL	AGE
Northwest member of TBS	ER4	Muscovite	302 ± 5 Ma
	ER8	Muscovite	267 ± 8 Ma
Central member of TBS	25.1	Biotite	268 ± 6 Ma
Southeast member of TBS	ER2	Muscovite	316 ± 6 Ma
	ER3	Muscovite	314 ± 5 Ma
Ball Hill mylonite zone	ER20	Muscovite	294 ± 6 Ma
Nashoba Fm. amphibolite	ER1	Biotite	330 ± 7 Ma
		Hornblende	376 ± 9 Ma
Nashoba Fm. schist	MLBS-1	Biotite	305 ± 7 Ma
		Muscovite	257 ± 14 Ma

Table 6.1 Summary of acceptable $^{40}Ar/^{39}Ar$ ages from this study.

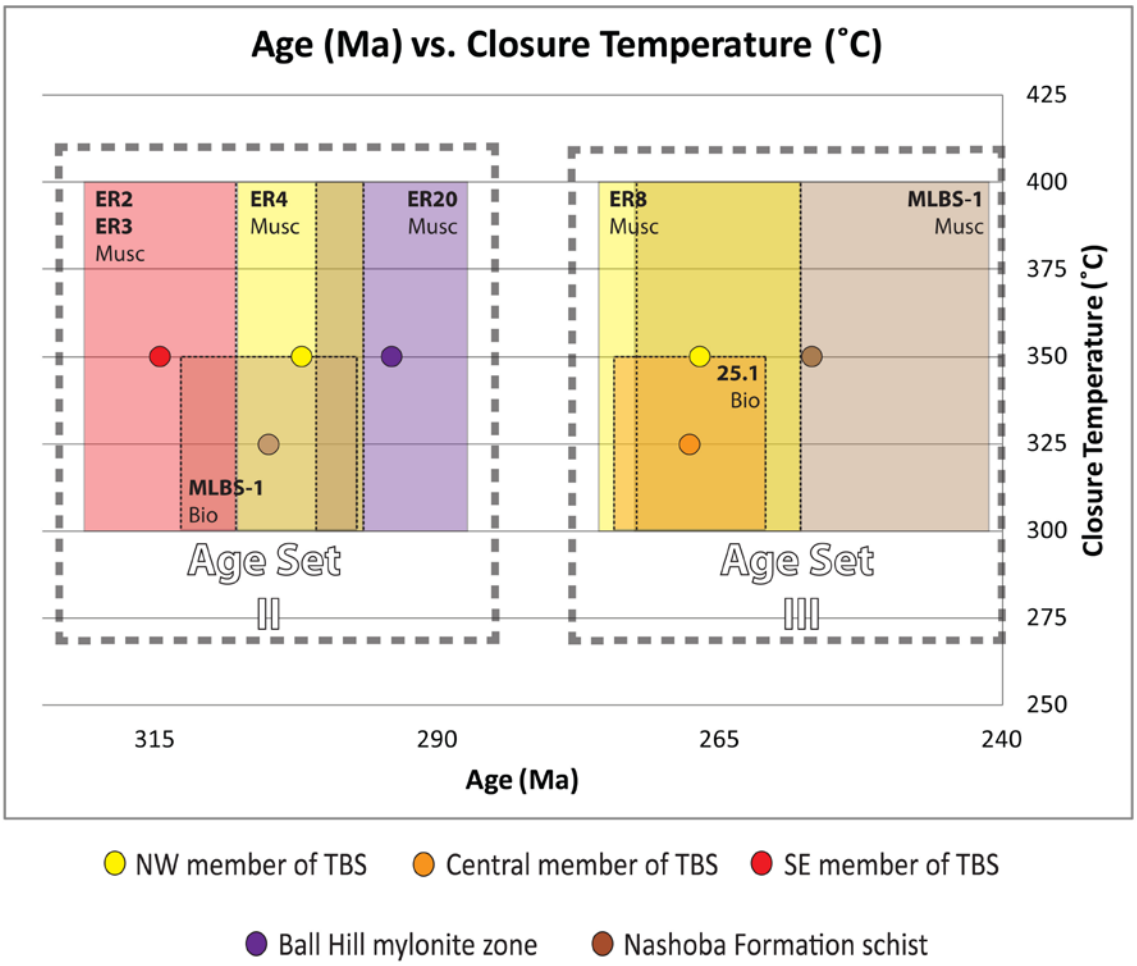

Figure 6.2 t-T graph of age (Ma) vs. closure temperature (˚C) for the youngest ages in this study. The box size for each sample represents the error (Ma) for the age and the error (in ˚C) of the closure temperature for the respective mineral. Two separate age sets are apparent.

Biotite in the Nashoba Formation amphibolite grew during M_2 and M_3. According to Stroud et al. (2009), M_3 (M_2 in their study) is related to a migmatization event in the Nashoba terrane. Based on observed mineral assemblages, M_3 reached a peak temperature of 610-660 °C in the study area (Fig. 4.7). This peak temperature would have reset any biotite ages related to M_2.

The biotite and hornblende ages were plotted on a t-T graph (Fig. 6.3) with the U/Pb monazite age of the migmatization event (Stroud et al., 2009). A cooling trend from the peak of metamorphism through the hornblende and biotite closure temperatures is observed (Fig. 6.3). This gives a cooling rate of ~8 °C/Myr for 390-376 Ma and ~4 °C/Ma for 376-330 Ma. These cooling rates are consistent with those from Wintsch et al. (1992) for the same time period in the Putnam terrane (3.5 °C/Myr; Fig. 1.1).

II. Age population II: ~300 Ma

The northwest member of the Tadmuck Brook Schist (TBS) was unaffected by the sillimanite-grade metamorphic events (M_2 and M_3). Therefore, it is unlikely that dates from this member represent cooling from M_3.

The muscovite-chlorite mineral assemblage (M_4) is predominant in the northwest member of TBS. Both samples from the northwest member of the TBS

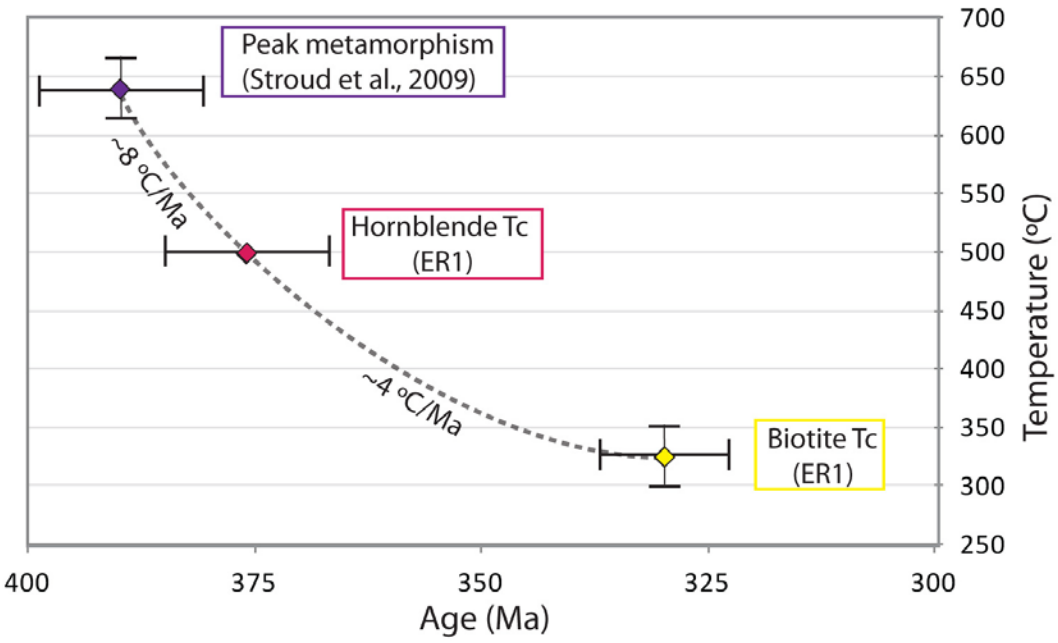

Figure 6.3 U/Pb Monazite ages from the Nashoba terrane (Stroud et al., 2009) and hornblende (closure temperature: ~500 ˚C) and biotite (closure temperature: 300-350 ˚C) $^{40}Ar/^{39}Ar$ ages from the Nashoba Formation amphibolite (this study). These ages are interpreted as showing the cooling rate from the Devonian-aged migmatization event in the Nashoba terrane.

examined for this study also have normal shear bands, composed of muscovite, with a west-side-down shear sense. Muscovite was dated in these samples.

Ductile shearing can occur at temperatures as low as ~350 °C (Passchier and Trouw, 1996). Because there is no evidence of late metamorphism above chlorite-muscovite grade in the northwest member of TBS, it is unlikely that ductile deformation occurred at temperatures much above 350 °C. The closure temperature of muscovite is 350 ± 50 °C, so the muscovite date of 302 ± 5 Ma (ER4) could represent either (1) new muscovite growth, or (2) resetting of $^{40}Ar/^{39}Ar$ age of muscovite only slightly above its closure temperature. Therefore,

this date is interpreted as the age of normal movement along the Clinton-Newbury fault.

Retrograde metamorphism (M_4) in the Nashoba terrane east of the TBS, was possibly related to discrete hydrothermal events that took place from 360-305 Ma at temperatures as low as 400 °C (Stroud et al., 2009). These localized events were strongest in areas adjacent to shear zones (Markwort, 2007). The Ball Hill mylonite zone (294 ± 6 Ma; ER20), Nashoba Formation schist (MLBS-1; 305 ± 7 Ma) and southeast member of the TBS (ER2 and ER3; 314 ± 5 Ma and 316 ± 6 Ma) are all significantly sheared. These samples contain minerals such as arsenopyrite and sericite, products of hydrothermal alteration. Therefore, these ages are interpreted as cooling ages from late hydrothermal events. It is also worth noting that a calc-silicate from the Nashoba Formation collected immediately adjacent to MLBS-1 yielded a few possible hydrothermal zircons (due to their appearance) and unexpectedly young ages of ~310 Ma (Loan, 2011). It is possible that this zircon age represents an actual age of hydrothermal alteration in the Nashoba terrane.

III. Age population III: ~267 Ma

Age population III (267 - 257 Ma) was observed in three samples: (1) muscovite in the northwest member of the TBS (ER8; 267 ± 8 Ma) (2) biotite in the central member of the TBS (25.1; 268 ± 6 Ma) (3) muscovite in the Nashoba Formation schist (MLBS-1; 257 ± 14 Ma). The samples were collected in the

southern half of the field area (Fig. 6.1). The first two were within 0.5 km of the Clinton-Newbury fault. Two possible explanations for these dates are: (1) a thermal pulse from the Alleghanian orogeny to the south, or (2) related to emplacement of the Rocky Pond Granite.

Zartman (1970) hypothesized that Permian K-Ar ages in New England are related to a thermal pulse from to the south (See Chapter 2-C). If this is true, late Permian to early Triassic ages should be seen south of the study area. However, Wintsch, et al., 1992 found $^{40}Ar/^{39}Ar$ ages of 352-331 Ma in the Putnam terrane west of the Clinton-Newbury fault (Fig. 1.1), suggesting age population III was a localized resetting event. Because there is a 20 k m gap between the northern and southern samples in this study it is difficult to discern how localized this Permian event was in the Nashoba terrane. Although the dates were discarded because they had high MSWDs, it is worth mentioning that the central member of TBS (25.1; muscovite) and the Ball Hill mylonite zone (ER20; biotite) also have ~267 Ma dates.

B. SYNTHESIS OF EVENTS

I. Ordovician through Silurian

A minimum age of deposition for the Tadmuck Brook Schist is given by U/Pb detrital zircon ages of 450-440 Ma from the Tadmuck Brook Schist and Nashoba Formation (Fig. 6.4; Loan, 2011). At this time the final stages of the Taconic orogeny were occurring as the leading edge of Ganderia was being accreted to Laurentia (van Staal et al., 2009).

M_1 (biotite-andalusite-staurolite and biotite-andalusite) assemblages were only observed in the Tadmuck Brook Schist. M_1 is interpreted as forming pre-tectonically or during the D_1 deformation, in agreement with previous studies of the TBS (Jerden, 1997). Jerden (1997) hypothesized that this mineral assemblage formed during nearly isobaric heating of the ambient crust, but at present the source of heating is unclear. Timing of M_1 is constrained by the deposition of the Tadmuck Brook Schist in the early Silurian (Loan, 2011) and M_2 in the late Silurian (~435-400 Ma; M_1 in Stroud et al., 2009).

M_2, defined by fibrolite-biotite, occurred ~435-400 Ma (M_1 in Stroud et al., 2009). Stroud et al. (2009) believe M_2 was related to a thermal overprint from I-type plutons emplaced within the Nashoba terrane. If so, it is likely that these plutons signal the start of subduction of the ocean slab between Ganderia and Avalon. M_2 must have occurred before D_1 because fibrolite has been sinistrally sheared in the southeastern member of TBS (Fig. 6.5).

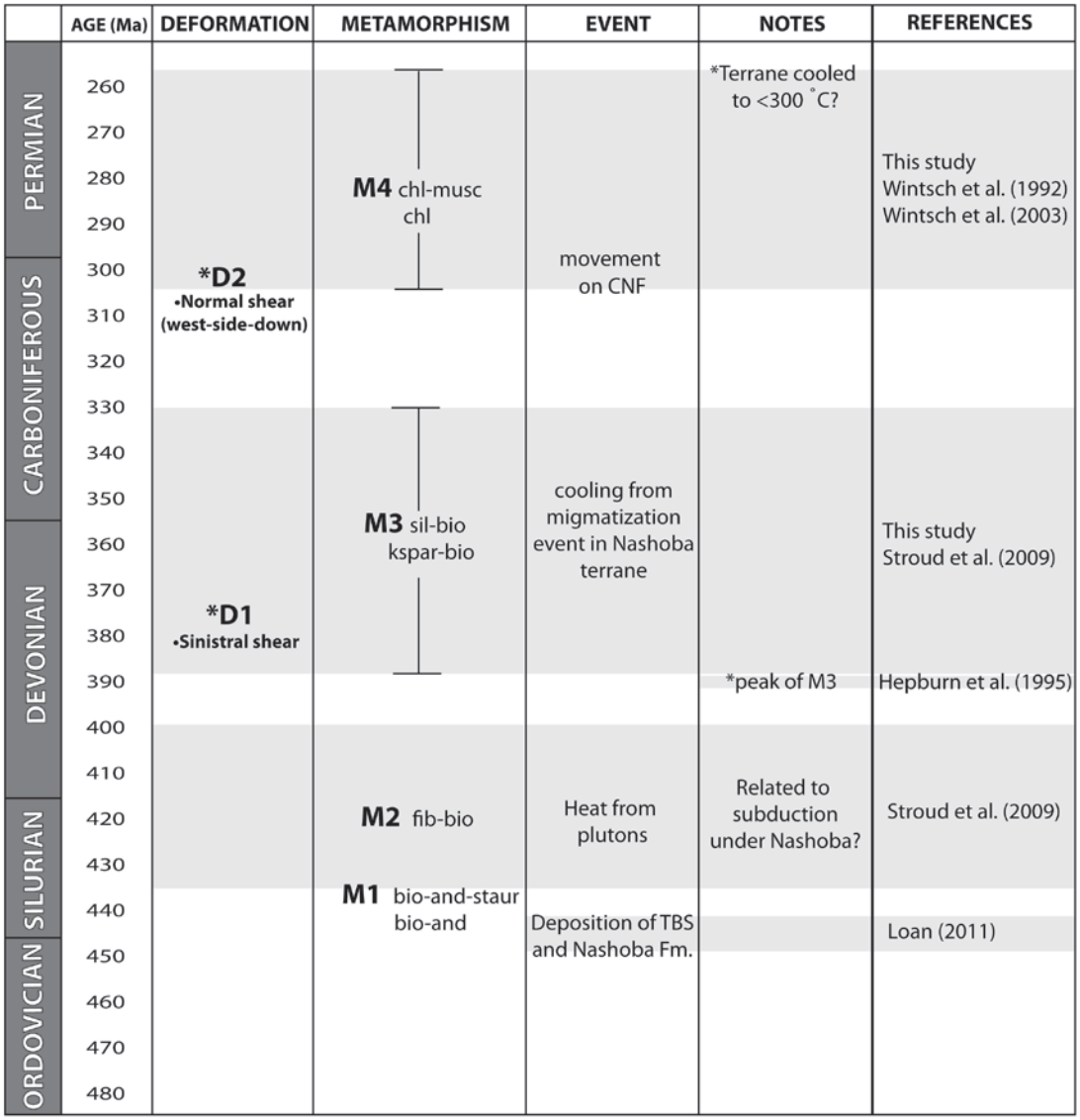

Figure 6.4 Possible metamorphic and deformation history for the Nashoba terrane. CNF = Clinton-Newbury fault; musc = muscovite; chl = chlorite; sil = sillimanite; bio = biotite; fib = fibrolite; kspar = potassium feldspar; staur = staurolite

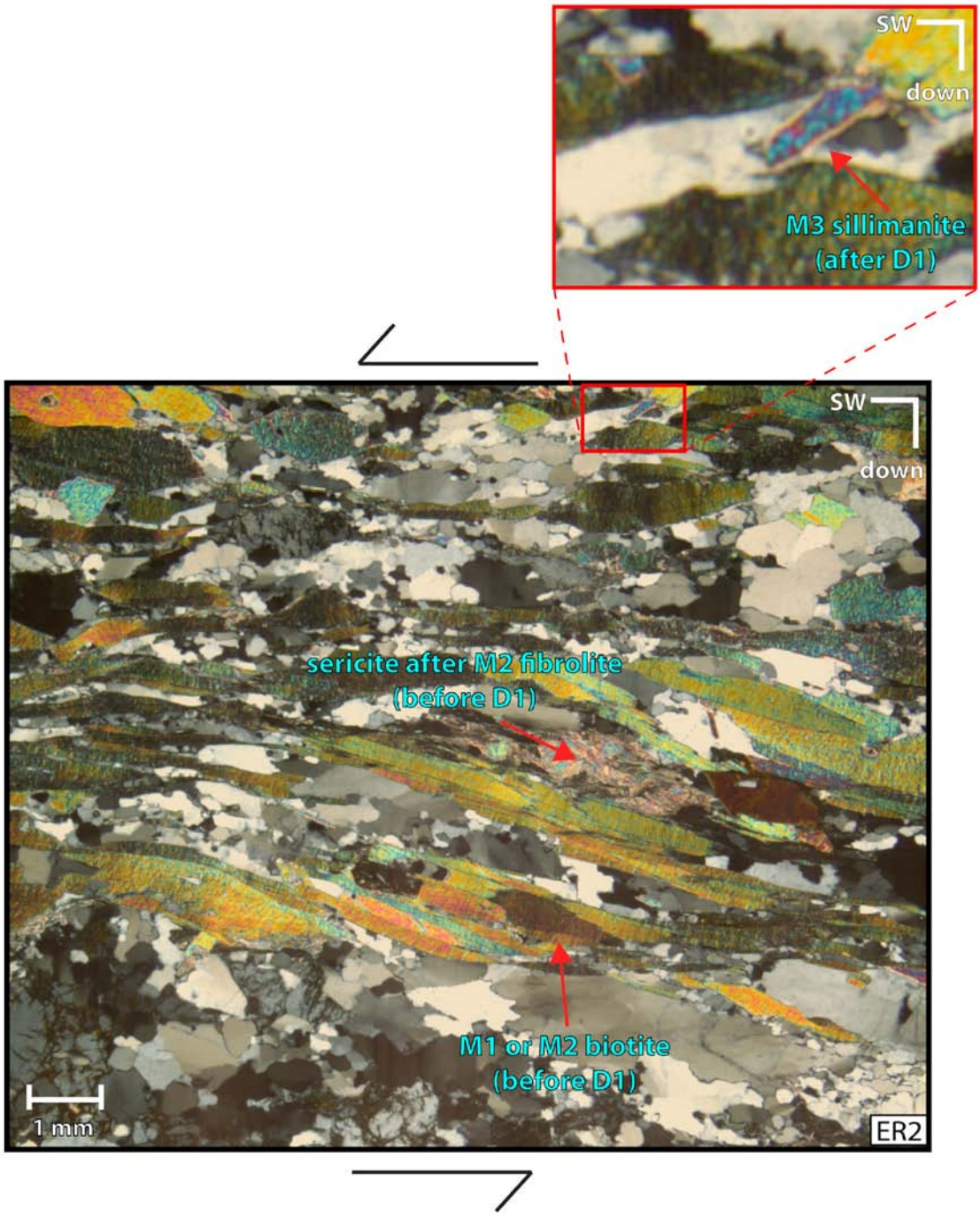

Figure 6.5 Photomicrograph of the Southeastern member of TBS showing the relationships of M1, M2, and M3 to D1. D1 is characterized by the formation of the main foliation and sinistral S-C fabric in this sample.

II. Devonian to Mississippian

D_1 sub-horizontal lineations are composed of the M_3 mineral assemblage (K-spar-biotite and sillimanite-biotite). D_1 ductile deformation began ~376 Ma (Markwort, 2007). M_3 metamorphism must have continued for a short period after D_1 because some M_3 sillimanite was observed cross-cutting the sinistrally sheared S-C fabric associated with D_1 in some thin sections (Fig. 6.5). The hornblende age from the Nashoba Formation amphibolite suggests that sillimanite would not be s table much later than 376 ± 9 Ma, which is approximately the time that ductile deformation was occurring, further strengthening the interpretation that although M_3 continued after D_1, it could not have been for a long period of time.

Peak M_3 conditions occurred ~395 Ma (Hepburn et al., 1995), producing associated anatexis believed to be related to the collision of Avalon with Nashoba (Stroud et al., 2009). M_3 was marked by widespread migmatization throughout the Nashoba terrane. This study suggests cooling from M_3 continued through ~330 Ma at ~325 ± 25 °C based on hornblende and biotite ages from the Nashoba amphibolite (Fig. 6.3). Calculated cooling rates from this event (slopes in Fig. 6.3; ~8 °C/Myr from 395-376 Ma; ~4 °C/Myr from 376-330 Ma) are similar to those observed by Wintsch et al. (1992) for the same time period in the Putnam terrane (south of the Nashoba terrane).

Previous $^{40}Ar/^{39}Ar$ hornblende ages from the eastern part of the Nashoba terrane (354-325 Ma; Hepburn et al., 1987b) are younger than the one

hornblende age from this study (~376 Ma). One possible explanation of this disagreement in ages is that the eastern part of the Nashoba terrane reached a higher peak temperature during M_3. Therefore, it took longer to cool to the hornblende closure temperature (~500 °C). This interpretation is supported by the fact that melting was not observed in the field area, but was elsewhere in the Nashoba Formation (Fig. 4.8), and previous metamorphic studies in the Nashoba terrane suggest higher P-T conditions during this migmatization event (Stroud et al., 2009).

III. Pennsylvanian through early Permian

This time period is characterized by at least two separate events ~300 Ma. The first event is related to discrete hydrothermal events seen in the southeast part of the field area. The second event is related to D_2 deformation (west-side-down normal movement) in the western part of the field area.

The normal movement on the Clinton-Newbury fault had been previously recognized by Goldstein (1994). This study suggests that normal movement occurred ~300 Ma. Because similar normal movement cross-cut the Carboniferous age rocks of the Narragansett Basin in the Avalon terrane (Fig. 1.1), Goldstein (1994) believed that normal movement on the Clinton-Newbury fault occurred after the Carboniferous, in general agreement with this study. There is evidence that fault reactivation in southeastern New England was also

occurring along the Bloody Bluff fault, Lake Char-Honey Hill fault, and Wekepeke fault at this time.

Bloody Bluff fault

It has been suggested that normal movement may have occurred along the southern part of the Bloody Bluff fault (Fig. 6.6) with top-to-the-south displacement during the Mesozoic (Goldstein and H epburn, 1999; Hepburn, 2008). This led to opening of the Carboniferous-aged Narragansett Basin, which constrains the timing of the normal movement along the Bloody Bluff fault (Fig. 1.1; Goldstein and Hepburn, 1999).

Normal movement was also observed on the Lake Char-Honey Hill fault system in Connecticut (Fig. 6.6; Goldstein, 1989). Normal movement here must have occurred after ~320 Ma because the normal shear sense cross-cuts a Pennsylvanian-aged gneissic fabric (Getty and Gromet, 1992).

Wekepeke fault

Samples from the Worcester Formation collected along the Wekepeke fault in the western part of the Merrimack were dated to~300 Ma (Attenoukon, 2009). The muscovite may have grown during fault reactivation.

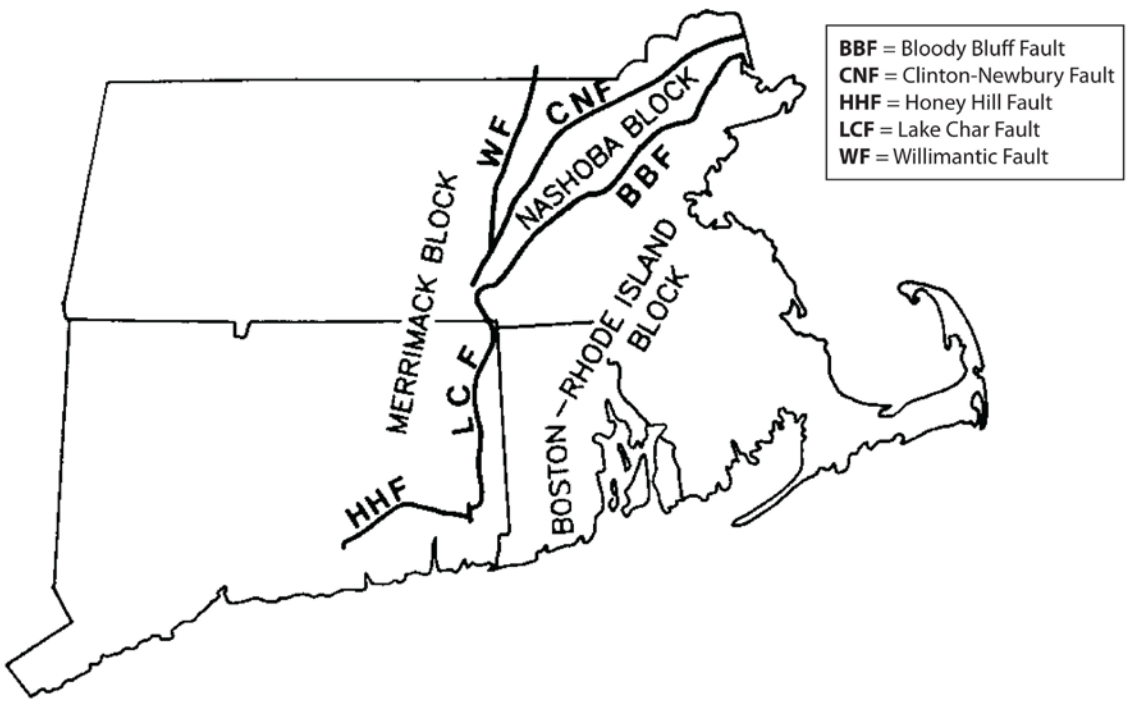

Figure 6.6 Shows the location of major faults in southern New England (Goldstein, 1989).

Orogenic collapse hypothesis

As noted previously, normal fault reactivation ~300 Ma was widespread in southeastern New England. It has previously been interpreted that late normal fault motion seen throughout southeastern New England could be related to orogenic collapse and not to widespread unrelated fault reactivation (Goldstein, 1994). Ages from this study from the northwest member of the Tadmuck Brook Schist, in the footwall of the Clinton-Newbury fault, constrain the age of normal movement to ~300 Ma, in agreement with the timing of orogenic collapse hypothesized by prior research (Goldstein, 1994).

IV. Late Permian

Age population III, ~267 Ma, is predominant in samples from the southwestern section of the field area. All of these samples are located within 2 km of the Rocky Pond Granite and most are immediately east of it. Because the samples from age population III are proximal to the Rocky Pond Granite, these ages may be related to emplacement of the granite. The granite has not been successfully dated, so all theories are purely speculative at this time, especially since similar peraluminous granites (i.e., Andover Granite; Fig. 2.1) formed as early as the Late Ordovician (Zartman and Naylor, 1984).

The Rocky Pond Granite is a peraluminous (S-type) granite that formed from partial melting of sediments (Zartman and Naylor, 1984). According to Winter (2001), S-type granites can form during orogenic collapse from decompression melting. The Rocky Pond Granite could have been emplaced during possible orogenic collapse at ~300 Ma. Water saturated granitic melt has a minimum melting temperature of ~650 °C. Assuming the Rocky Pond Granite was emplaced at the time of normal fault movement (~300 Ma), this gives a cooling rate of ~10 °C/Myr until the closure temperature of muscovite (350 ± 50 °C) was reached at ~267 Ma. Alternatively, as the Rocky Pond granite cooled it would have released water during crystallization. This fluid could have caused hydrothermal alteration of nearby units. It is possible that this hydrothermal alteration led to the resetting of ages ~267 Ma.

Chapter 7. CONCLUSIONS

1. Four metamorphic events affected the field area. They are characterized by the following mineral assemblages: M_1 (andalusite-biotite and andalusite-staurolite-biotite), M_2 (fibrolite-biotite), M_3 (K-spar-biotite and sillimanite-biotite), and M_4 (muscovite and chlorite-muscovite).

2. Two deformation events were identified. D_1 is characterized by the formation of a northwest-dipping foliation and a sinistral S-C fabric. D_2 is characterized by a west-side-down normal shear sense in the northwest member of the Tadmuck Brook Schist in the footwall of the Clinton-Newbury fault.

3. Three $^{40}Ar/^{39}Ar$ age populations were identified in a geochronology study of the Nashoba Formation, Tadmuck Brook Schist, and Ball Hill mylonite zone. The age populations are 376-330 Ma, 316-294 Ma, and 268-257 Ma.

4. Age population I was observed in the Nashoba Formation amphibolite (ER1) and includes a total-fusion age of biotite (330 ± 7 Ma) and furnace step-heating age of hornblende (376 ± 9 Ma). These ages may reflect cooling from a Devonian migmatization event (~395 Ma) in the Nashoba terrane defined by M_3 and D_1.

5. $^{40}Ar/^{39}Ar$ ages of muscovite from the northwest member of the Tadmuck Brook Schist (ER4; 302 ± 5 Ma), southeast member of the Tadmuck Brook Schist (ER2 and 3; 316 ± 6 Ma and 314 ± 5 Ma), and Ball Hill mylonite zone (ER20; 294 ± 6 Ma), as well as biotite from the Nashoba Formation schist (MLBS-1; 305 ± 7 Ma), make up age population II. This age in the northwest member of the Tadmuck Brook Schist may be related to normal movement on the Clinton-Newbury fault. The remaining samples may have experienced hydrothermal alteration ~300 Ma.

6. Age population III was observed in muscovite from the northwest member of the Tadmuck Brook Schist (ER8; 267 ± 8 Ma) and the Nashoba Formation schist (MLBS-1; 257 ± 14 Ma), as well as biotite from the central member of the Tadmuck Brook Schist (25.1; 268 ± 6 Ma). All of these samples were located in the southwest part of the field area. It is possible that these ages are related to emplacement of the Rocky Pond Granite, but this is purely speculative at this time.

7. By 257 Ma the field area had cooled to 300-350 °C, the youngest age in this study.

REFERENCES

Abu-Moustafa, A.A., and J.W. Skehan, 1976. Petrography and geochemistry of the Nashoba Formation, east-central Massachusetts in Lyons, P.C., and A.H. Brownlow, eds., Studies in New England geology: Geological Society of America Memoir 146. 31-70.

Aleinikoff, J. N., Wintsch, R. P., Tollo, R. P., Unruh, D. M., Fanning, C. M., and M.D. Schmitz, 2007. Ages and origins of rocks of the Killingworth dome, south-central Connecticut: Implications for the tectonic evolution of southern New England: American Journal of Science. Vol. 307. 63– 118.

Attenoukon, M.B., 2009. Ages and origins of metamorphic facies and the tectonics of southeastern New England.[Ph.D. Dissertation]. Indiana University.

Bell, K. and D. Alvord, 1976. Pre-Silurian Stratigraphy of northeastern Massachusetts. GSA Memoir 148.176-216.

Bober, R, 1990. Metamorphism of the Nashoba Terrane and the Tadmuck Brook Schist, East Central Massachusetts. [M.S. Thesis]. Boston College.

Castle, R.O., Dixon, H.R., Grew, E.S., Griscom, A., and I. Zietz, 1976. Structural dislocations in eastern Massachusetts: U.S. Geological Survey Bulletin 1410. 39.

Dodson, M.H., 1974. Closure temperature in cooling geochronological and petrological systems. Contributions to Mineralogy and Petrology. Vol. 40. 259-2774.

Getty, S. and L.P. Gromet, 1992. Evidence for extension at the Willimantic dome, Connecticut; implications for the late Paleozoic tectonic evolution of the New England Appalachians. American Journal of Science. Vol. 292. 398-420.

Goldsmith, R., 1991. Structural and metamorphic history of eastern Massachusetts, in Hatch, N.L., Jr., ed., The Bedrock Geology of Massachusetts: United States Geological Survey, Professional Paper. 1366 E-J. H1-H63.

Goldstein, A., 1989. Tectonic significance of multiple motions on terrane-bounding faults in the northern Appalachians. Geological Society of America Bulletin. Vol. 101. 927-938.

Goldstein, A., 1994. A shear zone origin for Alleghanian (Permian) multiple deformation in eastern Massachusetts. Tectonics. Vol. 13. 62-77.

Goldstein, A. and J.C. Hepburn, 1999. Possible correlations of the Norumbega fault system with faults in southeastern New England, in Ludman, A. and D.P. West, Jr., eds., Norumbega Fault System of the Northern Appalachians: Boulder, Colorado. Geological Society of America Special Paper 331. p. 73-83.

Grimes, S.W. and J.W. Skehan, 1995. Shear zones within the Bloody Fault Zone: Analysis and tectonic implications. Journal of Geodynamics. Vol. 19. No.¾. 213-230.

Hames, W. E., Tracy, R. J., Ratcliffe, N. M., and J.F. Sutter, 1991. Petrologic, structural, and geochronologic characteristics of the Acadian metamorphic overprint on the Taconide zone in part of southwestern New England. American Journal of Science. Vol. 291. 887-913.

Hatcher, R.D., Jr., 2010. The Appalachian orogen: A brief summary, *in* Tollo, R.P. Bartholomew, M.J., Hibbard, J.P., and P.M. Karabinos, eds., From Rodinia to Pangea: The Lithotectonic Record of the Appalachian Region. Geological Society of America. Memoir 206. 1–19

Hepburn, J.C., 2008. Mid-Paleozoic arc accretion on the eastern side of the Appalachian orogen, eastern Massachusetts and adjacent areas. Abstracts with Programs - Geological Society of America. Vol. 40. 2. 75.

Hepburn, J.C., Dunning, G.R., and R. Hon, 1995. Geochronology and regional tectonic implications of Silurian deformation in the Nashoba terrane, Southeastern New England, U.S.A. In: Hibbard, J.P., van Staal, C.R. and P.A. Cawood, eds., Current Perspectives in the Appalachian-Caledonian Orogen: Geological Association of Canada. Special Paper 41. 349-366.

Hepburn, J.C., Hill, M., and R. Hon, 1987a. The Avalonian and Nashoba terranes, eastern Massachusetts, U.S.A.: An overview. Maritime Sediments and Atlantic Geology. Vol. 23. 1-12.

Hepburn, J.C., Hon, R., Dunning, G.R., Baily, R.H., and K. Galli, 1993. The Avalon and Nashoba terranes (eastern margin of the Appalachian Orogen in southeastern New England, in Cheney, J.T. and J.C. Hepburn, eds., Field Trip Guidebook for the Northeastern United States: 1993 Boston GSA: Department of Geology and Geography. University of Massachusetts, Amherst, Massachusetts. Vol. 2. XI-X31.

Hepburn, J.C., Lux, D.R. and M. Hill, 1987b. $^{40}Ar/^{39}Ar$ Carboniferous cooling ages from the Nashoba Terrane, eastern Massachusetts. Abstracts with Programs - Geological Society of America. Vol. 19. No. 1. 18.

Hibbard, J.P., Van Staal, C.R., and D.W. Rankin, 2007. A comparative analysis of the pre-Silurian crustal building blocks of the northern and the southern Appalachian Orogen. American Journal of Science. Vol. 307. 23-45.

Jerden, J.L., 1997. Polyphase Metamorphism and Structure of the TBS, Eastern Massachusetts. [M.S. Thesis]. Boston College.

Jourdan, F. and P. R. Renne, 2007. Age calibration of the Fish Canyon sanidine $^{40}Ar/^{39}Ar$ dating standard using primary K–Ar standards. Geochimica et Cosmochimica. Vol. 71. 387–402.

Karabinos, P., Samson, S., Hepburn, J.C., and H.M. Stoll, 1998. Taconian orogeny in the New England Appalachians: Collision between Laurentia and the Shelburne Falls Arc. Geology. Vol. 26. No. 3.

Kay, A., Hepburn, J.C., and Y.D. Kuiper, 2011. Trace element and Sm-Nd isotopic geochemical characteristics of the Nashoba terrane, eastern Massachusetts. Abstracts with Programs – Geological Society of America. Vol. 43. 150.

Kay, A., Hepburn, J. C., Kuiper, Y. D., and J. Inglis, 2009. Nd isotopic constraints on the origin of the Nashoba Terrane, eastern Massachusetts. Abstracts with Programs - Geological Society of America. Vol. 41. 98.

Kopera J., 2005. Preliminary bedrock geologic map of the Hudson quadrangle. Massachusetts Geologic Survey (4th).

Kopera, J.P., 2006. Preliminary bedrock geologic map of the Ayer quadrangle, Massachusetts, Office of the Massachusetts State Geologist Open File Report 06-02. 1 sheet.

Kopera J., Hepburn J.C., and DiNitto R., 2006. Bedrock geologic map of the Marlborough quadrangle, Massachusetts. Office of the Massachusetts State Geologist Geologic Map 06-01.Scale 1:24,000. 1 sheet and digital product: Adobe PDF and ESRI ArcGIS database.

Kuiper, Y., 2002. The interpretation of inverse isochron diagrams in $^{40}Ar/^{39}Ar$ geochronology. Earth and Planetary Science Letters. Vol.203. No.1. 499-506.

Loan, M.L., 2011. New Constraints on the age of deposition and provenance of the metasedimentary rocks in the Nashoba terrane, SE New England. [M.S. Thesis] Boston College.

Markwort, R. J., 2007. Geology of the Shrewsbury Quadrangle, east-central Massachusetts. [M.S. Thesis]. Boston College.

Marrett, R. A., and R.W. Allmendinger, 1990. Kinematic analysis of fault-slip data. Journal of Structural Geology. Vol. 12. 973-986.

McDougall, I. and T. M Harrison, 1999. Geochronology and thermochronology by the $^{40}Ar/^{39}Ar$ method. Second edition. Oxford University Press, New York.

Moecher, D.P., 1999. Distribution, style, and intensity of Alleghanian metamorphism in south-central New England: Petrologic evidence from the Pelham and Willimantic Domes. The Journal of Geology. Vol. 107. No. 4. 449-471.

Mulch, A. and M.A. Cosca, 2004. Recrystallization or cooling ages: in situ UV-laser $^{40}Ar/^{39}Ar$ geochronology of muscovite in mylonitic rocks. Journal of the Geological Society, London. Vol. 161. 573-582.

Munn B.J., 1987. Bedrock geology at the western margin of the Nashoba block, east central Massachusetts [M.S. thesis]. Boston College.

Murphy, J. B. and A. S. Collins, 2008. 40Ar–39Ar white mica ages reveal Neoproterozoic/Paleozoic provenance and an Alleghanian overprint in coeval Upper Ordovician–Lower Devonian rocks of Meguma and Avalonia. Tectonophysics. Vol. 461. 265-276.

Osberg, P.H., Tull, J. F., Robinson, P., Hon, R., and J.R. Butler, 1989. The Geology of North America. Vol. F-2. The Appalachian-Ouachita Orogen in the United States. The Geological Society of America.

Passchier, C.W. and R.A.J. Trouw, 1996. Micotectonics. Springer-Verlag Berlin Heidelberg, New York.

Pollack, J. C., Wilton, D. H. C., van Staal, C. R., and K.D. Morrissey, 2007. U-Pb zircon geochronological constraints on the Late Ordovician-Early Silurian collision of Ganderia and Laurentia along the Dog Bay Line: The terminal Iapetan suture in the Newfoundland Appalachians: American Journal of Science. Vol. 307. 399–433.

Rankin, D.W., 1994. Continental margin of the eastern United States: Past and present, *in* Speen, R.C., ed., Phanerozoic Evolution of North American Continent-Ocean Transitions: Geological Society of America, DNAG Continental-Ocean Transect Volume. 129-218.

Rast, N., and J.W. Skehan, 1993. Mid-Paleozoic orogenesis in the North Atlantic: The Acadian Orogeny, In Roy, D.C. and J.W. Skehan, J.W., eds., The Acadian Orogeny: Recent Studies in New England, Maritime Canada and the Autochthonous Foreland. Geological Society of America. Special Paper 275. L-25.

Renne, P.R., C.C. Swisher, A.L. Deino, D.B. Karner, T.L. Owens, and D.J. DePaolo, 1998. Intercalibration of standards, absolute ages and uncertainties in $^{40}Ar/^{39}Ar$ dating. Chemical Geology. Vol. 145. 117–152.

Robinson, P. and R. Goldsmith, 1991. Stratigraphy of the Merrimack Belt, Central Massachusetts, in Hatch, N.L., Jr., ed., The Bedrock Geology of Massachusetts: United States Geological Survey. Professional Paper 1366 E-J. G1-G37.

Robinson, R., Tucker, R.D., Bradley, D., Berry, H.N. IV, and P.H. Osberg, 1998. Paleozoic orogens in New England, USA. GFF. Vol. 120. 119-148.

Samson, S.D. and J.E.C. Alexander, 1987. Calibration of the interlaboratory $^{40}Ar–^{39}Ar$ dating standard, MMhb–1. Chemical Geology. Vol. 66. 27–34.

Schoene, B. and S.A. Bowring, 2006. U–Pb systematics of the McClure Mountain syenite: thermochronological constraints on the age of the $^{40}Ar/^{39}Ar$ standard MMhb. Contributions to Mineralogy and Petrology. Vol. 151. 615–630

Skehan, J.W., 1997. Assembly and dispersal of supercontinents: The view from Avalon. Journal of Geodynamics. Vol. 23. No. ¾. 237-262.

Sorota, K.J., Hepburn, J.C., Kuiper, Y.D., and M.N. Tubrett, 2011. Age and origin of the Merrimack terrane, southeastern New England: A detrital zircon U-Pb geochronology study. Abstracts with Programs – Geological Society of America. Vol. 43. No. 5. 42.

Sorota, K.J., Hepburn, J.C., Kuiper, Y.D., and M.N. Tubrett, 2012. Detrital zircon study of the Merrimack terrane, MA and NH. Abstracts with Programs – Geological Society of America. Vol. 44. No. 2. 70.

Spear, F. and J.T. Cheney, 1989. A petrographic grid for pelitic schists in the system SiO_2-Al_2O_3-FeO-MgO-K_2O-H_2O. Contributions to Mineralogy and Petrology. Vol. 98. 507-517.

Spell, T.L. and I. McDougall, 2003. Characterization and calibration of $^{40}Ar/^{39}Ar$ dating standards. Chemical Geology. Vol 198. 189–211.

Stroud, M. M., 2007. Temporal and directional constraints on a major shear zone in eastern Massachusetts: Monazite dating of the Assabet River Fault Zone. [M.S. Thesis]. Boston College.

Stroud, M.M., Markwort, R.J., and J.C. Hepburn, 2009. Refining temporal constraints on metamorphism in the Nashoba terrane, southeastern New England, through monazite dating. Lithosphere. Vol. 1. No. 6. 337-342.

Thompson, M.D., Grunow, A.M., Barr, S.M., and C.E. White, 2010. Accretionary implications of paleomagnetic overprints in peri-Gondwanan terranes of southeastern New England and Cape Breton Island, Nova Scotia. Abstracts with Programs - Geological Society of America. Vol. 42. No. 1. 173.

van Staal, C. R., Whalen, J. B., Valverde-Vaquero, P., Barr, S., Zagorevski, A. and N. Rodgers, 2009. Pre-Carboniferous, episodic accretion-related, orogenesis along the Laurentian margin of the northern Appalachians: Geological Society, London, Special Publications. Vol. 327. 271-316.

Walsh, G.J., Aleinikoff, J.N., and M.J. Dorais, 2009. Tectonic history of the Avalon and Nashoba Terranes along the western flank of the Milford Antiform, Massachusetts. Abstracts with Programs - Geological Society of America. Vol. 41. No. 3. 98.

Walsh, G. J. and R. P. Wintsch, 2011. Origin of the Quinebaug-Marlboro Belt in Southeastern New England: Abstracts with Programs - Geological Society of America. Vol. 43. No. 1. 158.

Winter, J.D., 2001. An Introduction to Igneous and Metamorphic Petrology. Prentice Hall. Upper Saddle River, New Jersey.

Wintsch, R.P., Aleinikoff, J.N.,Walsh, G.J., Bothner, W.A., Hussey, II, A. M. and C.M. Fanning, 2007. Shrimp U-Pb evidence for a Late Silurian age of metasedimentary rocks in the Merrimack and Putnam-Nashoba terranes, eastern New England. American Journal of Science. Vol. 307. 119-167.

Wintsch, R. P., Kunk, M. J., Boyd, J. L., and Aleinikoff, J. N., 2003. P-T-t paths and differential Alleghanian loading and uplift of the Bronson Hill terrane, south-central New England: American Journal of Science. Vol. 303. 410-446.

Wintsch, R. P., Kunk, .M. J., Dorais, M. J., Attenoukon, M. B., McWilliams, C. K., Matthews, J. A., Walsh, G. J., and J.N. Aleinikoff, 2010. Dextral transpression and oblique crustal extrusion in the Alleghanian of eastern New England . Abstracts with Programs - Geological Society of America. Vol. 42. 173.

Wintsch, R.P. and J.F. Sutter, 1986. A tectonic model for the late Paleozoic of southeastern New England. Journal of Geology. Vol.94. No.4. 459-472.

Wintsch, R.P., Sutter, J.F., Kunk, M. J., Aleinikoff, J.N., and M.J. Donais, 1992. Contrasting P-T-t paths: Thermochronologic evidence for a late Paleozoic final assembly of the Avalon Composite Terrane in the New England Appalachians. Tectonics. Vol. 11. No. 3. 672-689.

Zartman, R.E., Hurley, P.M., Krueger, H.W., and B.J. Giletti, 1970. A Permian disturbance of K-Ar ages in New England – Its occurrence and cause. Geological Society of America Bulletin. Vol. 81. 3359-3373.

Zartman, R.E. and R.S. Naylor, 1984. Structural implications of some radiometric ages of igneous rocks in southeastern New England. Geological Society of America Bulletin. Vol.95. No.5. 522-539.

Zagorevski, A., van Staal, C.R., and V.J. McNicoll, 2007. Distinct Taconic, Salinic, and Acadian deformation along the Iapetus suture zone, Newfoundland Appalachians. Canadian Journal of Earth Science. Vol. 44**.** 1567-1585.

Zen, E-an, ed., Goldsmith, R., Ratcliffe, N.M., Robinson, P. and R.S. Stanley, compilers, 1983. Bedrock geologic map of Massachusetts: United States Geological Survey, 1:250,000.

APPENDIX I
$^{40}Ar/^{39}Ar$ Data

MLBS-1 **BIOTITE**

Grain #	36Ar(a)	37Ar(ca)	38Ar(cl)	39Ar(k)	40Ar(r)	Age ± 2σ (Ma)	40Ar(r) (%)	39Ar(k) (%)	K/Ca ± 2σ
1.00 W	0.002221	0.000273	0.004148	0.990649	8.207442	309.40 ± 2.39	92.28	7.16	1778.0 ± 9976.742
2.00 W	0.006839	0.061820	0.014058	3.184817	26.091163	306.22 ± 1.74	92.50	23.02	25.2 ± 0.832
3.00 W	0.006182	0.001884	0.004919	1.082375	9.204522	316.90 ± 2.62	83.19	7.82	281.6 ± 224.104
4.00 W	0.010737	0.028855	0.010173	2.193826	18.579269	315.70 ± 2.35	85.16	15.85	37.3 ± 3.026
5.00 W	0.014848	0.066290	0.013894	3.637801	29.444311	302.83 ± 1.61	86.75	26.29	26.9 ± 0.931
6.00 W	0.002998	0.000191	0.002067	0.483845	4.121383	317.38 ± 4.10	82.07	3.50	1240.0 ± 9719.806
7.00 W	0.005466	0.001033	0.002446	0.578289	4.808630	310.44 ± 3.42	74.66	4.18	274.4 ± 373.749
8.00 W	0.007267	0.000558	0.002457	0.609263	5.118960	313.41 ± 3.88	70.27	4.40	535.4 ± 1480.961
9.00 W	0.007054	0.000006	0.002478	0.434264	3.768799	322.85 ± 4.90	64.24	3.14	34299.9 ± 8848176.1
10.00 W	0.007291	0.000371	0.002933	0.642772	5.331624	309.73 ± 3.60	71.04	4.65	848.4 ± 3266.948
Σ	0.070904	0.153208	0.059574	13.837901	114.676103				J = 0.022581

MLBS-1 **MUSCOVITE**

Grain #	36Ar(a)	37Ar(ca)	38Ar(cl)	39Ar(k)	40Ar(r)	Age ± 2σ (Ma)	40Ar(r) (%)	39Ar(k) (%)	K/Ca ± 2σ
1.00 W	0.006203	0.017034	0.029903	1.034226	6.846852	251.34 ± 18.14	78.60	13.98	29.750 ± 5.548
2.00 W	0.004531	0.009136	0.012164	0.318770	2.249691	266.77 ± 58.25	62.52	4.31	17.096 ± 5.895
3.00 W	0.007075	0.007097	0.006520	0.514905	3.631570	266.61 ± 36.11	63.29	6.96	35.552 ± 15.716
4.00 W	0.008503	0.011507	0.007552	0.337904	2.276524	255.48 ± 55.40	47.43	4.57	14.389 ± 4.014
5.00 W	0.015555	0.040321	0.007564	1.578517	10.899746	261.41 ± 11.90	70.12	21.34	19.183 ± 1.696
6.00 W	0.007854	0.005737	0.005196	1.174784	8.289331	266.72 ± 15.90	77.87	15.89	100.332 ± 55.131
7.00 W	0.008412	0.004869	0.003025	1.219075	8.174423	254.36 ± 15.40	76.42	16.48	122.686 ± 79.358
8.00 W	0.009119	0.006167	0.002916	1.000116	6.500316	247.06 ± 18.86	70.46	13.52	79.461 ± 40.253
9.00 W	0.008687	0.001297	0.002150	0.175529	1.182844	255.54 ± 106.70	31.50	2.37	66.334 ± 159.312
10.00 W	0.008595	0.009911	0.002188	0.041699	0.247383	226.81 ± 455.99	8.87	0.56	2.062 ± 0.665
Σ	0.084533	0.113077	0.079178	7.395523	50.298681				J = 0.022581

NFS-1 **BIOTITE**

Grain #	36Ar(a)	37Ar(ca)	38Ar(cl)	39Ar(k)	40Ar(r)	Age ±2σ (Ma)	40Ar(r) (%)	39Ar(k) (%)	K/Ca ±2σ
1.00 W	0.003254	0.000893	0.039572	0.493857	4.375553	332.99 ± 2.72	81.75	1.57	271.108 ± 687.29
2.00 W	0.009237	0.082668	0.781398	3.162456	25.106386	301.10 ± 1.86	89.89	10.08	18.745 ± 0.686
3.00 W	0.007278	0.112269	1.515869	5.519701	38.996755	270.31 ± 1.13	94.39	17.60	24.091 ± 0.734
4.00 W	0.010117	0.067218	0.648110	3.053598	22.803122	284.56 ± 1.59	88.10	9.74	22.260 ± 1.071
5.00 W	0.006979	0.111233	1.653167	5.567541	41.515391	284.17 ± 1.33	94.90	17.75	24.526 ± 0.832
6.00 W	0.005192	0.067392	0.205897	3.725749	31.341421	317.55 ± 1.89	95.01	11.88	27.090 ± 1.143
7.00 W	0.010532	0.168716	0.595818	5.297840	37.013933	267.52 ± 1.39	91.88	16.89	15.386 ± 0.332
8.00 W	0.006259	0.034649	0.267118	1.698537	14.280082	317.38 ± 1.70	88.25	5.42	24.021 ± 1.767
9.00 W	0.006080	0.002136	0.003397	0.039119	0.692304	613.33 ± 27.20	27.80	0.12	8.973 ± 9.887
10.00 W	0.009310	0.068849	0.102754	2.801981	24.763935	332.23 ± 1.78	89.73	8.93	19.942 ± 0.881
Σ	0.074238	0.716023	5.813100	31.360378	240.888882				

J = 0.022879

ER-1 — **HORNBLENDE (SINGLE-GRAIN TOTAL-FUSION)**

Grain #	36Ar(a)	37Ar(ca)	38Ar(cl)	39Ar(k)	40Ar(r)	Age ± 2σ (Ma)	40Ar(r) (%)	39Ar(k) (%)	K/Ca ± 2σ
1.00 W	0.000864	2.545467	0.014439	0.300807	3.466841	406.05 ± 6.28	92.90	19.56	0.058 ± 0.003
2.00 W	0.000244	0.647576	0.003462	0.068472	0.750961	388.37 ± 8.37	91.01	4.45	0.052 ± 0.002
3.00 W	0.000334	0.875298	0.004448	0.080940	0.918598	400.49 ± 7.90	90.08	5.26	0.045 ± 0.002
4.00 W	0.000751	2.358720	0.011568	0.258588	2.675781	368.52 ± 6.06	92.08	16.81	0.054 ± 0.002
5.00 W	0.000288	0.716422	0.003563	0.065791	0.703826	379.76 ± 7.95	88.99	4.28	0.045 ± 0.002
6.00 W	0.000754	2.323740	0.016209	0.252465	3.393275	465.49 ± 6.94	93.63	16.42	0.053 ± 0.002
7.00 W	0.000764	2.005596	0.012366	0.203653	2.730490	464.49 ± 7.21	92.16	13.24	0.050 ± 0.002
8.00 W	0.000211	0.378851	0.001697	0.038205	0.390461	364.40 ± 10.67	86.01	2.48	0.049 ± 0.002
9.00 W	0.000294	1.356791	0.007257	0.130684	1.522264	409.94 ± 6.73	94.35	8.50	0.047 ± 0.002
10.00 W	0.000336	1.381112	0.006122	0.138371	1.546907	395.11 ± 6.49	93.73	9.00	0.049 ± 0.002
Σ	0.004840	14.589571	0.081130	1.537976	18.099404				

J = 0.0219015

ER-1 — **BIOTITE**

Grain #	36Ar(a)	37Ar(ca)	38Ar(cl)	39Ar(k)	40Ar(r)	Age ± 2σ (Ma)	40Ar(r) (%)	39Ar(k) (%)	K/Ca ± 2σ
1.00 W	0.003510	0.000145	0.000702	0.084183	0.725288	323.45 ± 26.20	41.09	6.46	285.053 ± 1038.0
2.00 W	0.001749	0.000305	0.000512	0.068022	0.597192	329.07 ± 18.47	53.50	5.22	109.397 ± 193.19
3.00 W	0.002661	0.000284	0.000536	0.062854	0.544404	325.02 ± 27.37	40.85	4.82	108.607 ± 213.26
4.00 W	0.002678	0.000485	0.000531	0.052028	0.476290	341.88 ± 32.05	37.52	3.99	52.523 ± 49.317
5.00 W	0.001023	0.000131	0.000505	0.050543	0.452372	334.92 ± 16.17	59.81	3.88	189.672 ± 622.54
6.00 W	0.002780	0.000543	0.001865	0.212279	1.872982	330.57 ± 9.18	69.34	16.28	191.455 ± 150.49
7.00 W	0.002118	0.000248	0.001210	0.499415	4.371349	328.17 ± 5.22	87.20	38.30	987.434 ± 2130.5
8.00 W	0.001469	0.000183	0.001069	0.113640	0.965439	319.32 ± 9.73	68.80	8.71	47.548 ± 35.036
9.00 W	0.000954	0.000631	0.000613	0.061274	0.541927	331.30 ± 13.38	65.63	4.70	303.985 ± 668.09
10.00 W	0.000644	0.000390	0.000899	0.099728	0.884457	332.13 ± 7.81	82.04	7.65	125.412 ± 157.99
Σ	0.019587	0.003083	0.008441	1.303967	11.431699				

J = 0.0227921

ER-1 **HORNBLENDE (FURNACE STEP-HEATING)**

Incremental Heating	36Ar(a)	37Ar(ca)	38Ar(cl)	39Ar(k)	40Ar(r)	Age ± 2σ (Ma)	40Ar(r) (%)	39Ar(k) (%)	K/Ca ± 2σ
800 °C	0.000913	0.030206	0.001393	0.059026	0.537734	328.21 ± 11.23	66.43	1.12	0.958 ± 0.056
850 °C	0.000497	0.047371	0.000900	0.058397	0.473244	294.75 ± 8.49	76.11	1.10	0.604 ± 0.031
900 °C	0.000449	0.095119	0.000874	0.080156	0.609434	277.87 ± 6.19	81.84	1.52	0.413 ± 0.020
900 °C	0.000175	0.014209	0.000001	0.007911	0.057888	268.17 ± 40.93	87.81	0.15	0.273 ± 0.024
950 °C	0.000263	0.207184	0.001779	0.064804	0.556497	310.91 ± 11.31	87.45	1.23	0.153 ± 0.007
1000 °C	0.000567	0.866046	0.007878	0.099236	1.502012	516.51 ± 9.75	89.80	1.88	0.056 ± 0.003
1050 °C	0.001609	22.380473	0.113225	2.324705	25.794100	392.45 ± 5.77	97.92	43.99	0.051 ± 0.002
1100 °C	0.000238	6.178045	0.029265	0.716051	7.415830	368.81 ± 5.59	98.76	13.55	0.057 ± 0.003
1100 °C	0.000094	0.862389	0.004032	0.087010	0.898811	367.95 ± 15.31	102.87	1.65	0.049 ± 0.002
1125 °C	0.000092	2.035793	0.009616	0.207835	2.155027	369.20 ± 7.69	100.97	3.93	0.050 ± 0.002
1150 °C	0.000008	5.122383	0.023580	0.520453	5.393789	369.03 ± 5.81	99.65	9.85	0.050 ± 0.002
1175 °C	0.000067	4.910873	0.022746	0.493641	5.128333	369.84 ± 5.88	99.32	9.34	0.049 ± 0.002
1200 °C	0.000032	3.682629	0.018062	0.384978	4.206481	387.07 ± 7.43	99.94	7.28	0.051 ± 0.002
1225 °C	0.000154	1.406840	0.006774	0.140883	1.528117	384.52 ± 14.57	102.75	2.67	0.049 ± 0.002
1250 °C	0.000066	0.269195	0.001220	0.027596	0.287092	370.31 ± 23.35	106.96	0.52	0.050 ± 0.002
1275 °C	0.000035	0.087534	0.000357	0.009235	0.105027	401.23 ± 63.27	90.81	0.17	0.052 ± 0.003
1300 °C	0.000024	0.027552	0.000162	0.002765	0.032084	408.56 ± 208.64	81.80	0.05	0.049 ± 0.004
1325 °C	0.000126	0.003284	0.000019	0.000307	0.000286	-37.11 ± 2422.51	0.77	0.01	0.046 ± 0.022
1350 °C	0.000169	0.001798	0.000019	0.000112	0.002795	788.03 ± 4396.27	5.29	0.00	0.030 ± 0.027
Σ	0.004352	48.228924	0.241901	5.285100	56.684009				

J = 0.0219015

ER4 **MUSCOVITE**

Grain #	36Ar(a)	37Ar(ca)	38Ar(cl)	39Ar(k)	40Ar(r)	Age ± 2σ (Ma)	40Ar(r) (%)	39Ar(k) (%)	K/Ca ± 2σ
1.00 W	0.004820	0.085328	0.003974	5.040556	40.563579	302.26 ± 1.11	96.26	13.34	28.945 ± 0.785
2.00 W	0.004748	0.083638	0.002259	4.543419	36.888861	304.74 ± 1.10	95.99	12.02	26.618 ± 0.878
3.00 W	0.004802	0.109811	0.015327	6.199948	49.339838	299.17 ± 1.13	96.85	16.40	27.665 ± 0.911
4.00 W	0.005593	0.114776	0.003227	5.151623	41.605860	303.26 ± 1.20	95.84	13.63	21.993 ± 0.938
5.00 W	0.007103	0.055830	0.001762	2.733649	22.340254	306.57 ± 1.53	91.11	7.23	23.992 ± 1.081
6.00 W	0.002482	0.000254	0.000115	0.004076	0.065873	563.02 ± 454.66	8.24	0.01	7.876 ± 36.166
7.00 W	0.005067	0.071520	0.004493	5.279669	42.986354	305.52 ± 1.10	96.29	13.97	36.172 ± 1.520
8.00 W	0.007560	0.055766	0.003509	3.061044	24.110125	296.34 ± 1.50	91.20	8.10	26.897 ± 0.994
9.00 W	0.006073	0.052689	0.003443	3.020401	24.259388	301.72 ± 1.40	92.79	7.99	28.089 ± 1.180
10.00 W	0.008328	0.048282	0.002939	2.759170	22.531642	306.36 ± 1.57	89.85	7.30	28.002 ± 1.055
Σ	0.056576	0.677388	0.041048	37.793556	304.691774				J = 0.022665

ER8 **MUSCOVITE**

Grain #	36Ar(a)	37Ar(ca)	38Ar(cl)	39Ar(k)	40Ar(r)	Age ± 2σ (Ma)	40Ar(r) (%)	39Ar(k) (%)	K/Ca ± 2σ
1.00 W	0.003870	0.027359	0.022584	1.093001	7.884184	273.18 ± 2.58	87.02	6.48	19.576 ± 1.510
2.00 W	0.008886	0.056528	0.020479	3.534411	25.444104	272.68 ± 1.40	90.30	20.95	30.637 ± 1.424
3.00 W	0.007417	0.098328	0.010186	2.762121	19.690069	270.20 ± 1.45	89.64	16.37	13.765 ± 0.369
4.00 W	0.005621	0.000986	0.002065	0.971111	7.083786	276.03 ± 3.02	80.73	5.76	482.695 ± 1033.9
5.00 W	0.008554	0.033401	0.010344	1.997424	14.984617	283.30 ± 1.85	85.27	11.84	29.302 ± 2.275
6.00 W	0.002650	0.010424	0.003873	1.183983	8.373352	268.21 ± 2.36	91.09	7.02	55.657 ± 11.635
7.00 W	0.002852	0.005429	0.017900	1.216773	8.811192	274.17 ± 2.44	90.92	7.21	109.822 ± 44.139
8.00 W	0.004411	0.002452	0.001373	0.737319	5.324222	273.45 ± 3.84	80.06	4.37	147.362 ± 122.94
9.00 W	0.007100	0.006015	0.010518	1.033238	7.476933	273.99 ± 2.98	77.84	6.12	84.170 ± 28.899
10.00 W	0.008518	0.046918	0.011240	2.342915	17.199437	277.66 ± 1.63	86.92	13.89	24.469 ± 1.361
Σ	0.059880	0.285868	0.110561	16.872297	122.271897				J = 0.022665

25.1 **MUSCOVITE**

Grain #	36Ar(a)	37Ar(ca)	38Ar(cl)	39Ar(k)	40Ar(r)	Age ± 2σ (Ma)	40Ar(r) (%)	39Ar(k) (%)	K/Ca ± 2σ
1.00 W	0.004870	0.035378	0.000782	2.314278	16.215789	268.24 ± 1.36	91.49	7.09	32.054 ± 1.380
2.00 W	0.005926	0.068733	0.003872	3.658806	25.305275	265.02 ± 1.27	93.15	11.21	26.084 ± 0.910
3.00 W	0.008093	0.029721	0.000167	1.668299	12.942643	294.77 ± 1.76	84.13	5.11	27.505 ± 1.440
4.00 W	0.009168	0.061144	0.002058	3.401635	24.081892	270.83 ± 1.17	89.55	10.42	27.260 ± 1.023
5.00 W	0.007117	0.002045	0.008040	0.804241	6.904262	323.52 ± 2.14	76.45	2.46	192.689 ± 132.2
6.00 W	0.008423	0.110061	0.000884	3.768080	27.208821	275.84 ± 1.27	91.27	11.54	16.776 ± 0.415
7.00 W	0.005166	0.072994	0.003829	3.847559	26.972586	268.37 ± 1.07	94.26	11.78	25.828 ± 0.857
8.00 W	0.007454	0.052347	0.002388	3.143053	22.020704	268.22 ± 1.29	90.55	9.63	29.421 ± 1.240
9.00 W	0.006184	0.057795	0.001819	4.211197	29.436758	267.65 ± 1.15	93.77	12.90	35.704 ± 1.639
10.00 W	0.005826	0.087557	0.003435	5.835716	40.417848	265.36 ± 1.03	95.52	17.87	32.659 ± 1.294
Σ	0.068227	0.577775	0.026941	32.652865	231.506578				J = 0.022879

25.1 **BIOTITE**

Grain #	36Ar(a)	37Ar(ca)	38Ar(cl)	39Ar(k)	40Ar(r)	Age ± 2σ (Ma)	40Ar(r) (%)	39Ar(k) (%)	K/Ca ± 2σ
1.00 W	0.013238	0.005498	0.122754	2.128540	15.491444	269.30 ± 5.20	79.56	18.42	189.695 ± 26.851
2.00 W	0.001538	0.000026	0.000145	0.003309	0.007455	87.75 ± 334.64	1.61	0.03	62.362 ± 1304.09
3.00 W	0.020960	0.025078	0.117138	3.289017	23.855533	268.44 ± 5.41	79.11	28.47	64.264 ± 3.824
4.00 W	0.002784	0.000246	0.012093	0.420806	3.033377	266.91 ± 5.48	78.39	3.64	839.715 ± 1599.6
5.00 W	0.008255	0.007054	0.072895	1.910424	13.746231	266.46 ± 4.44	84.61	16.54	132.701 ± 13.899
6.00 W	0.005480	0.000577	0.015537	0.528394	3.721082	261.18 ± 7.12	69.46	4.57	448.834 ± 326.76
7.00 W	0.013486	0.007432	0.050520	1.692097	12.077372	264.47 ± 5.92	74.94	14.65	111.568 ± 10.903
8.00 W	0.001548	0.000094	0.006383	0.254270	1.824720	265.80 ± 5.74	79.68	2.20	1325.458 ± 5097.9
9.00 W	0.016171	0.000248	0.004080	0.784060	5.687960	268.49 ± 12.63	54.22	6.79	1551.711 ± 3322.2
10.00 W	0.001676	0.000160	0.028984	0.541005	3.913738	267.80 ± 4.29	88.42	4.68	1651.768 ± 6515.0
Σ	0.085877	0.043395	0.430525	11.553369	83.373682				J = 0.0221202

ER2 **MUSCOVITE**

Grain #	36Ar(a)	37Ar(ca)	38Ar(cl)	39Ar(k)	40Ar(r)	Age ± 2σ (Ma)	40Ar(r) (%)	39Ar(k) (%)	K/Ca ± 2σ
1.00 W	0.028506	0.445853	0.024910	1.461583	0.047101	-1.29 ± 13.34	0.56	18.37	1.606 ± 0.073
2.00 W	0.000172	0.000132	0.000050	0.436070	3.783906	318.31 ± 4.34	98.32	5.48	1616.856 ± 4079.2
3.00 W	0.000189	0.000374	0.000008	0.491026	4.211393	314.92 ± 4.29	98.33	6.17	644.067 ± 466.29
4.00 W	0.000159	0.000482	0.000082	0.614013	5.268667	315.06 ± 4.27	98.76	7.72	624.345 ± 490.76
5.00 W	0.000348	0.003584	0.000018	1.192870	10.173739	313.31 ± 4.22	98.64	14.99	163.089 ± 17.551
6.00 W	0.000238	0.000102	0.000065	0.909624	7.839984	316.34 ± 4.26	98.75	11.43	4352.801 ± 12149.6
7.00 W	0.000151	0.000037	0.000135	0.320673	2.752863	315.19 ± 4.37	98.05	4.03	4205.893 ± 33861.5
8.00 W	0.000697	0.000320	0.000206	0.956868	8.221261	315.43 ± 4.27	97.21	12.03	1462.984 ± 1218.5
9.00 W	0.000116	0.000328	0.000144	1.007487	8.695188	316.74 ± 4.26	99.25	12.66	1503.562 ± 1630.9
10.00 W	0.000221	0.000107	0.000122	0.566524	4.857343	314.83 ± 4.29	98.32	7.12	2603.905 ± 6636.0
Σ	0.030797	0.449321	0.024531	7.956738	55.757243				J = 0.0222374

ER3 **MUSCOVITE**

Grain #	36Ar(a)	37Ar(ca)	38Ar(cl)	39Ar(k)	40Ar(r)	Age ± 2σ (Ma)	40Ar(r) (%)	39Ar(k) (%)	K/Ca ± 2σ
1.00 W	0.001580	0.000019	0.000055	0.418566	3.626500	315.30 ± 4.96	88.31	3.98	10648.8 ± 250235.9
2.00 W	0.001141	0.000430	0.000271	0.878244	7.591461	314.63 ± 4.35	95.41	8.35	999.787 ± 980.445
3.00 W	0.001416	0.010949	0.008967	3.704653	32.867141	322.23 ± 8.38	98.39	35.24	165.788 ± 14.368
4.00 W	0.000963	0.000388	0.000103	0.457023	3.970390	316.08 ± 4.62	93.00	4.35	577.163 ± 648.8
5.00 W	0.001912	0.000189	0.000189	0.285380	2.507934	319.44 ± 6.17	81.37	2.71	738.689 ± 1823.3
6.00 W	0.000506	0.005190	0.000455	1.968194	16.861407	312.06 ± 4.23	98.76	18.72	185.836 ± 19.814
7.00 W	0.000735	0.005472	0.003022	1.832809	15.786524	313.61 ± 4.24	98.29	17.44	164.130 ± 23.763
8.00 W	0.000702	0.000109	0.000170	0.331023	2.880871	316.60 ± 4.79	92.97	3.15	1494.820 ± 6350.3
9.00 W	0.000404	0.000180	0.000102	0.134617	1.167683	315.64 ± 6.52	90.43	1.28	366.199 ± 915.1
10.00 W	0.000373	0.000195	0.000027	0.501292	4.373313	317.30 ± 4.45	97.20	4.77	1256.902 ± 2804.6
Σ	0.009731	0.021068	0.013102	10.511802	91.633225				J = 0.0220421

ER20 **MUSCOVITE**

Grain #	36Ar(a)	37Ar(ca)	38Ar(cl)	39Ar(k)	40Ar(r)	Age ± 2σ (Ma)	40Ar(r) (%)	39Ar(k) (%)	K/Ca ± 2σ
1.00 W	0.000350	0.000010	0.000360	0.355122	2.710089	287.11 ± 4.03	95.95	3.40	18286.1 ±78725.5
2.00 W	0.000297	0.000337	0.001992	0.682082	5.337768	293.85 ± 4.00	97.99	6.52	992.183 ± 1148.4
3.00 W	0.000512	0.004943	0.002253	1.969209	15.522757	295.83 ± 4.01	98.64	18.83	195.193 ± 20.112
4.00 W	0.000511	0.004367	0.000973	2.317360	17.859929	289.73 ± 3.92	98.76	22.16	259.995 ± 38.675
5.00 W	0.000541	0.004690	0.001684	1.964973	15.185747	290.47 ± 3.93	98.56	18.79	205.289 ± 27.077
6.00 W	0.000537	0.000104	0.001875	0.283377	2.132641	283.43 ± 4.10	92.71	2.71	1336.978 ± 5339.3
7.00 W	0.000334	0.000101	0.001818	1.044632	8.283509	297.45 ± 4.03	98.44	9.99	5055.367 ± 21757.3
8.00 W	0.000091	0.000299	0.000101	0.253090	1.985619	294.54 ± 4.12	98.27	2.42	414.706 ± 595.6
9.00 W	0.000068	0.000055	0.000135	0.247311	1.921236	291.87 ± 4.05	98.56	2.37	2222.217 ± 16705.9
10.00 W	0.000155	0.000930	0.000089	1.338801	10.195642	286.55 ± 3.88	99.14	12.80	705.516 ± 321.97
Σ	0.003396	0.014247	0.011280	10.455957	81.134938				J = 0.0226046

ER20 **BIOTITE**

Grain #	36Ar(a)	37Ar(ca)	38Ar(cl)	39Ar(k)	40Ar(r)	Age ± 2σ (Ma)	40Ar(r) (%)	39Ar(k) (%)	K/Ca ± 2σ
1.00 W	0.005323	0.082620	0.238440	4.201735	28.546974	260.66 ± 1.37	94.38	23.53	24.920 ± 0.717
2.00 W	0.006917	0.083698	0.173294	3.882576	26.461996	261.43 ± 1.26	92.45	21.74	22.730 ± 0.758
3.00 W	0.007970	0.090735	0.027146	2.819255	19.617659	266.52 ± 1.58	88.94	15.79	15.225 ± 0.567
4.00 W	0.004665	0.011333	0.037193	0.957469	6.965242	277.74 ± 3.05	83.19	5.36	41.396 ± 4.862
5.00 W	0.004994	0.008795	0.016853	0.396511	2.886663	277.94 ± 6.65	65.99	2.22	22.092 ± 3.457
6.00 W	0.002266	0.000786	0.016485	0.408862	3.018298	281.55 ± 6.37	81.57	2.29	254.920 ± 384.21
7.00 W	0.005814	0.050742	0.080924	1.801639	12.857192	272.84 ± 1.97	87.89	10.09	17.398 ± 0.542
8.00 W	0.006300	0.037140	0.045123	2.347632	17.036547	277.12 ± 1.79	89.81	13.15	30.973 ± 1.476
9.00 W	0.004915	0.003313	0.017360	0.456575	3.314263	277.19 ± 5.84	69.33	2.56	67.538 ± 22.677
10.00 W	0.004870	0.008923	0.024331	0.585861	4.119357	269.11 ± 4.68	73.87	3.28	32.172 ± 4.364
Σ	0.054035	0.378085	0.677148	17.858114	124.824191				J = 0.022879

APPENDIX II
Sample locations

MLBS-1 NASHOBA FORMATION SCHIST

42.380556° N, 71.645278° W

Collected from an outcrop in the spillway of a flood control dam off of Linden St. in Berlin, Ma.

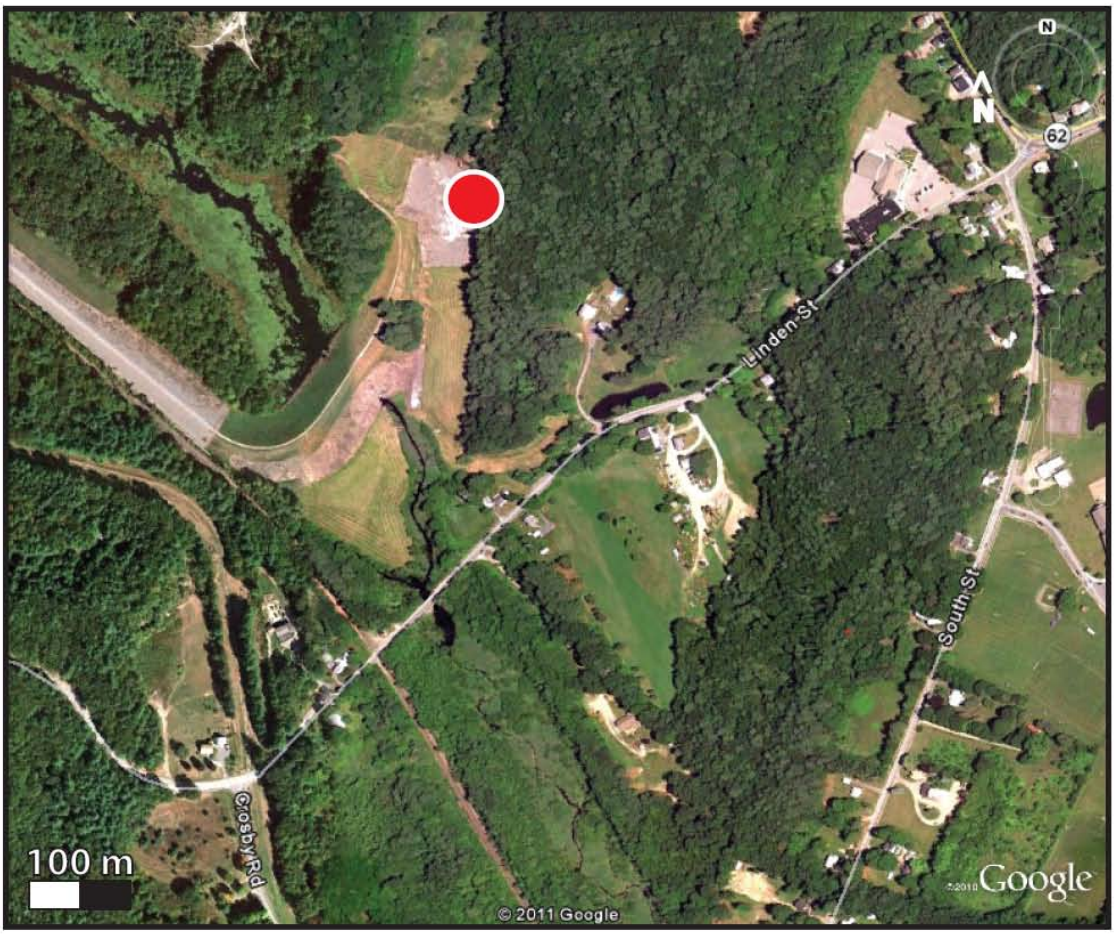

NFS-1 NASHOBA FORMATION SCHIST

42.34019 N°, 71.66360° W
Collected from an outcrop on Green St ~600m north of I-290 in Northborough, Ma.

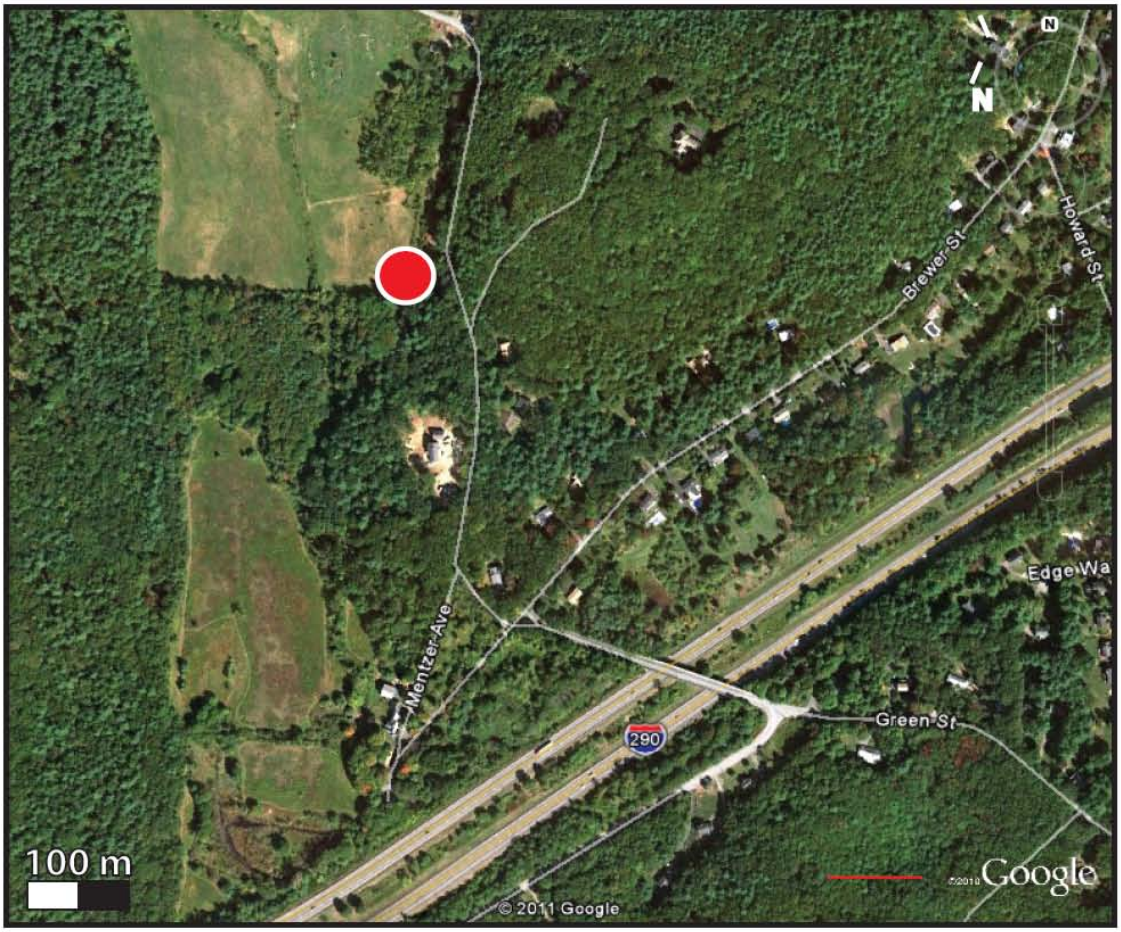

ER1 NASHOBA FORMATION AMPHIBOLITE

42.526111° N, 71.519444° W
Collected from an outcrop on Route 2 ~250 m southeast of Whitcomb Ave in Littleton, MA.

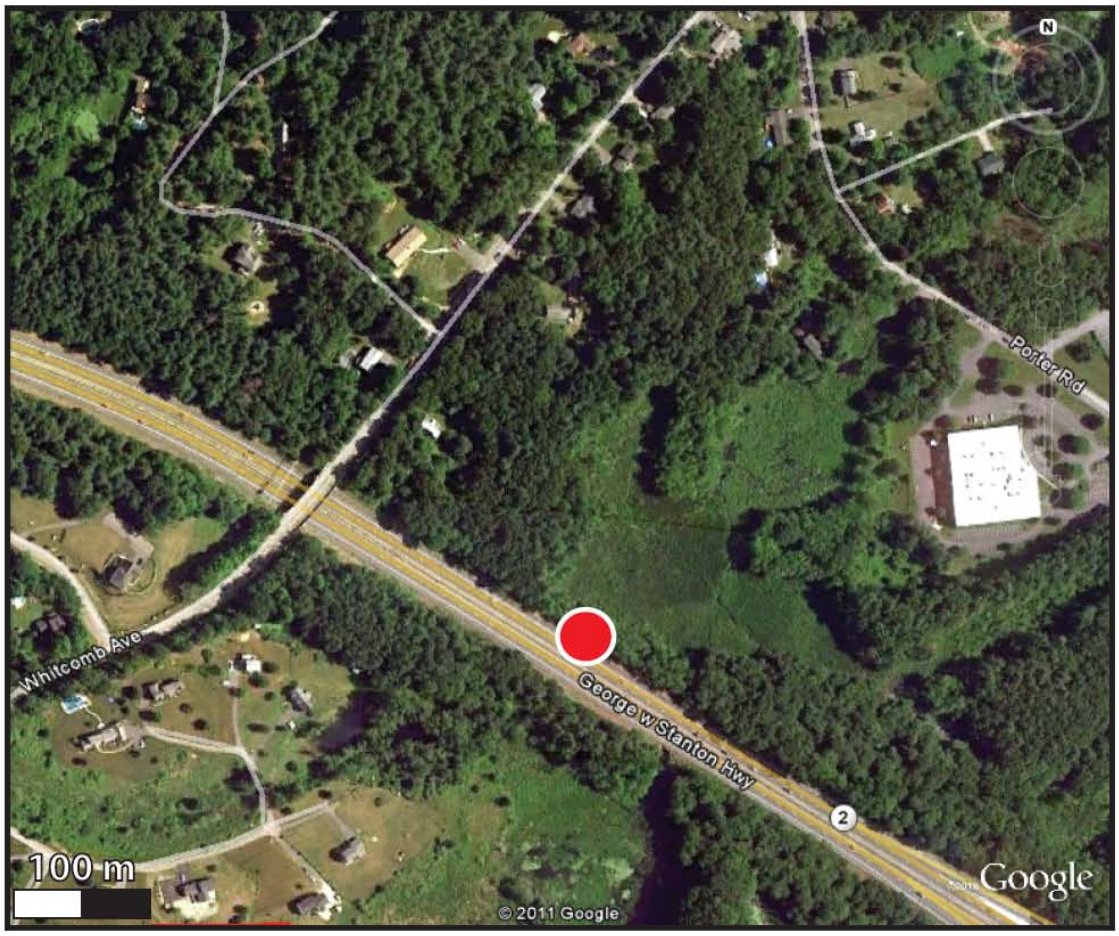

ER2 SOUTHEAST MEMBER OF TADMUCK BROOK SCHIST

42.527778° N, 71.523056° W
Collected from an outcrop on Route 2 ~100 m northwest of Whitcomb Ave in Littleton, MA.

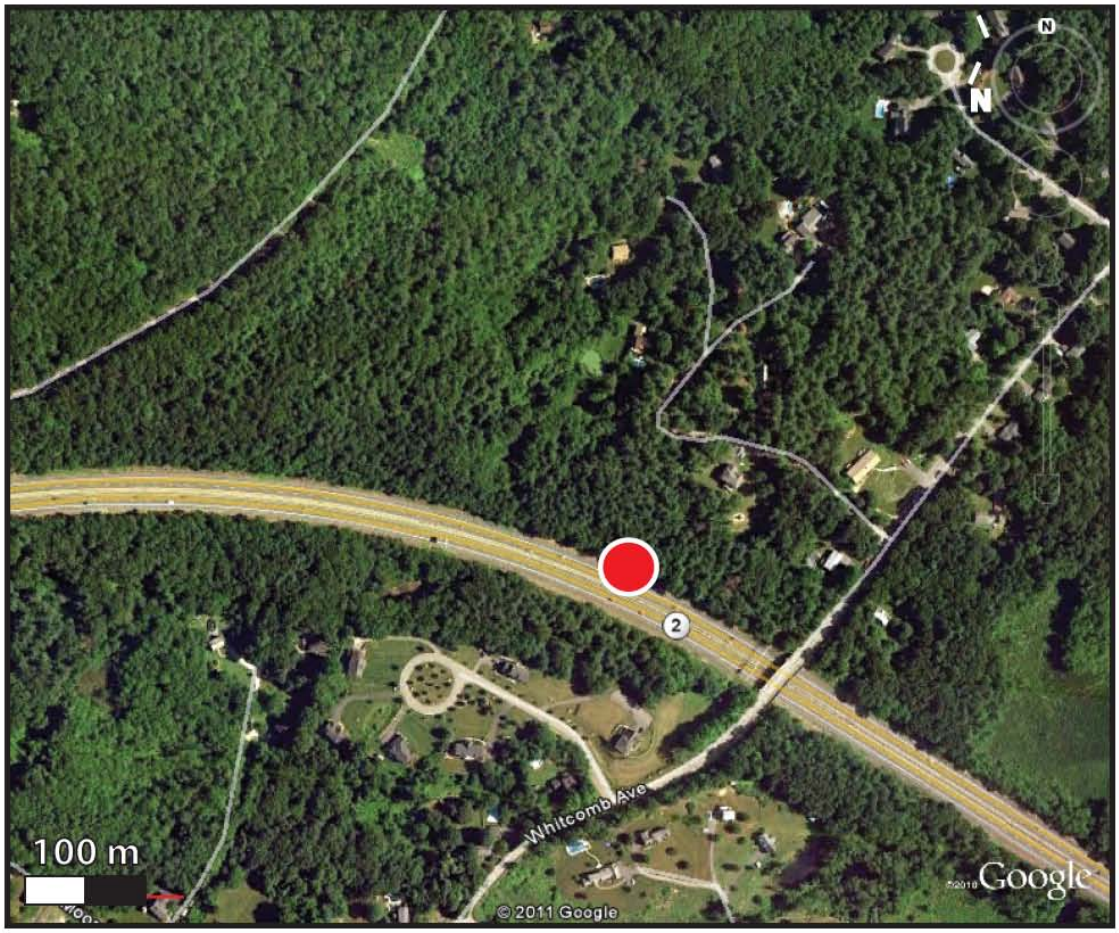

ER3 SOUTHEAST MEMBER OF TADMUCK BROOK SCHIST

42.528056° N, 71.5250° W
Collected from an outcrop on Route 2 ~300 m northwest of Whitcomb Ave in Littleton, MA.

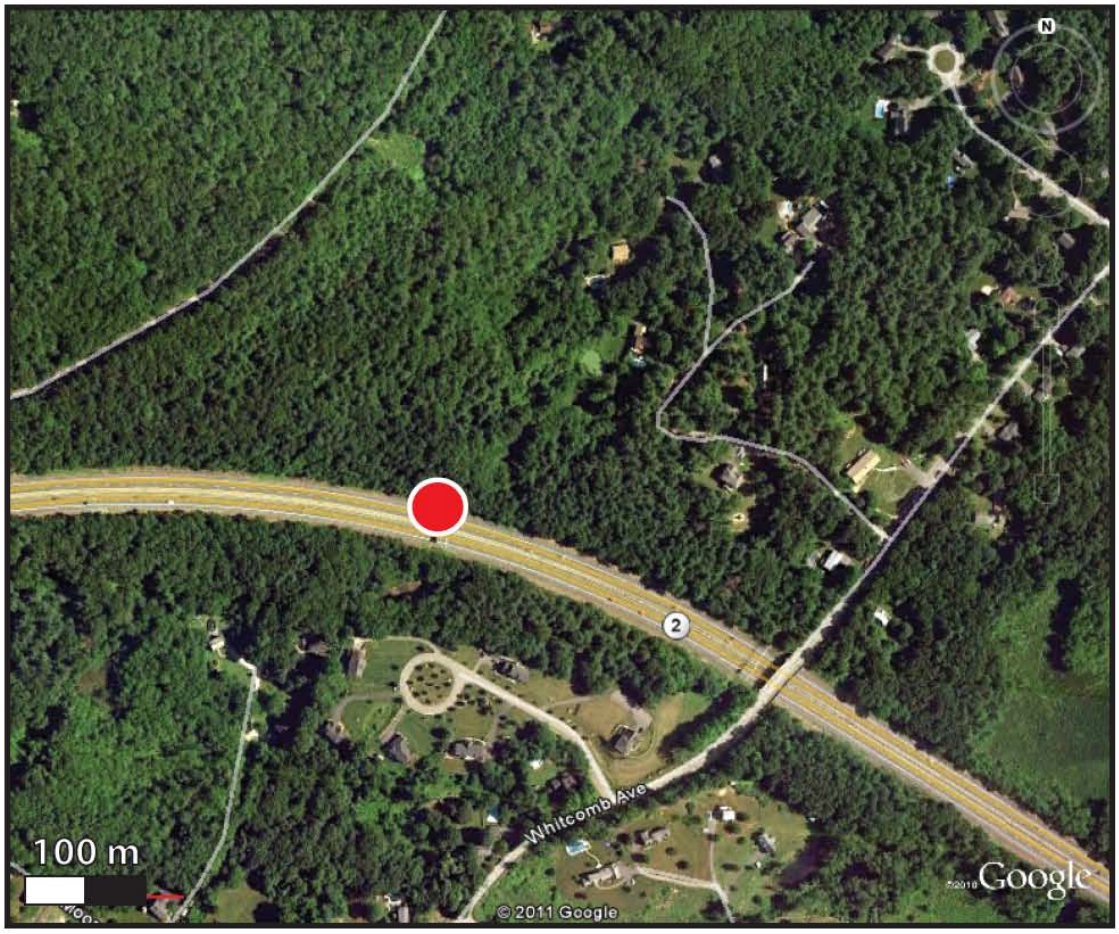

25.1 CENTRAL MEMBER OF TADMUCK BROOK SCHIST

42.388056° N, 71.662222° W
Collected from an outcrop on Route 62 near Lincoln Rd in West Berlin, MA.

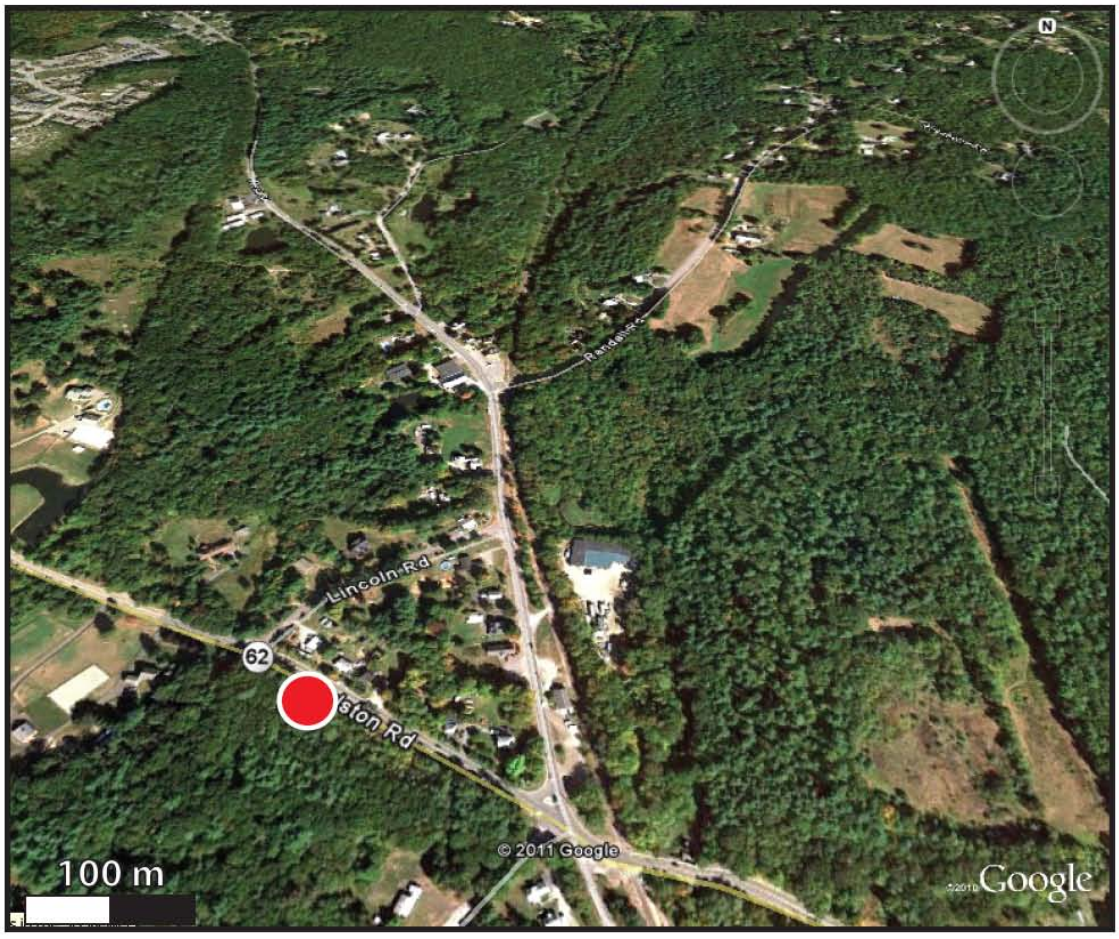

ER4 NORTHWEST MEMBER OF THE TADMUCK BROOK SCHIST

42.532222° N, 71.536111° W
Collected from an outcrop on Littleton Rd in Harvard, MA (just over the border from Littleton, MA).

ER8 NORTHWEST MEMBER OF TADMUCK BROOK SCHIST

42.331944° N, 71.675556° W
Collected from an outcrop on the east bound side of Route 290 at exit 24 in Northborough, MA.

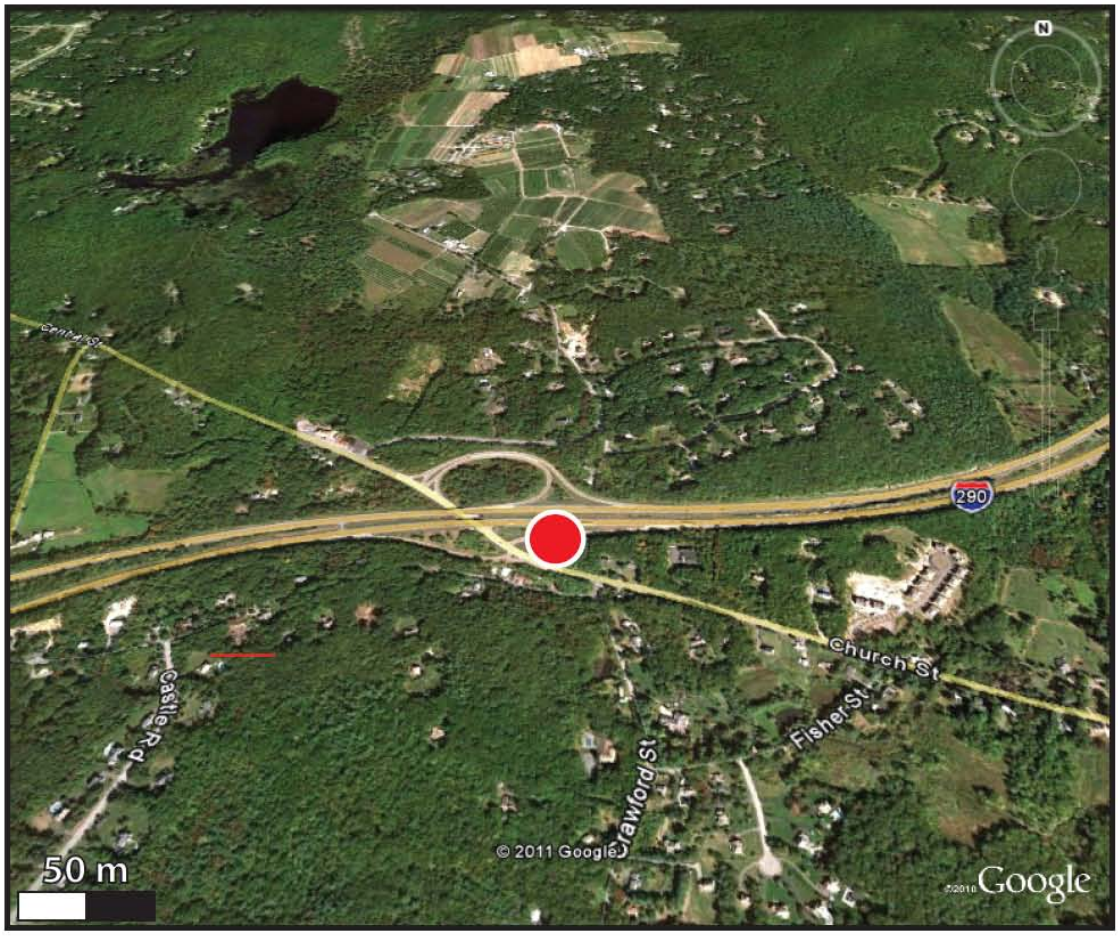

ER20 **BALL HILL MYLONITE**

42.359167° N, 71.671667° W
Collected from an outcrop in front of 19 Smith Road in Northborough, MA.

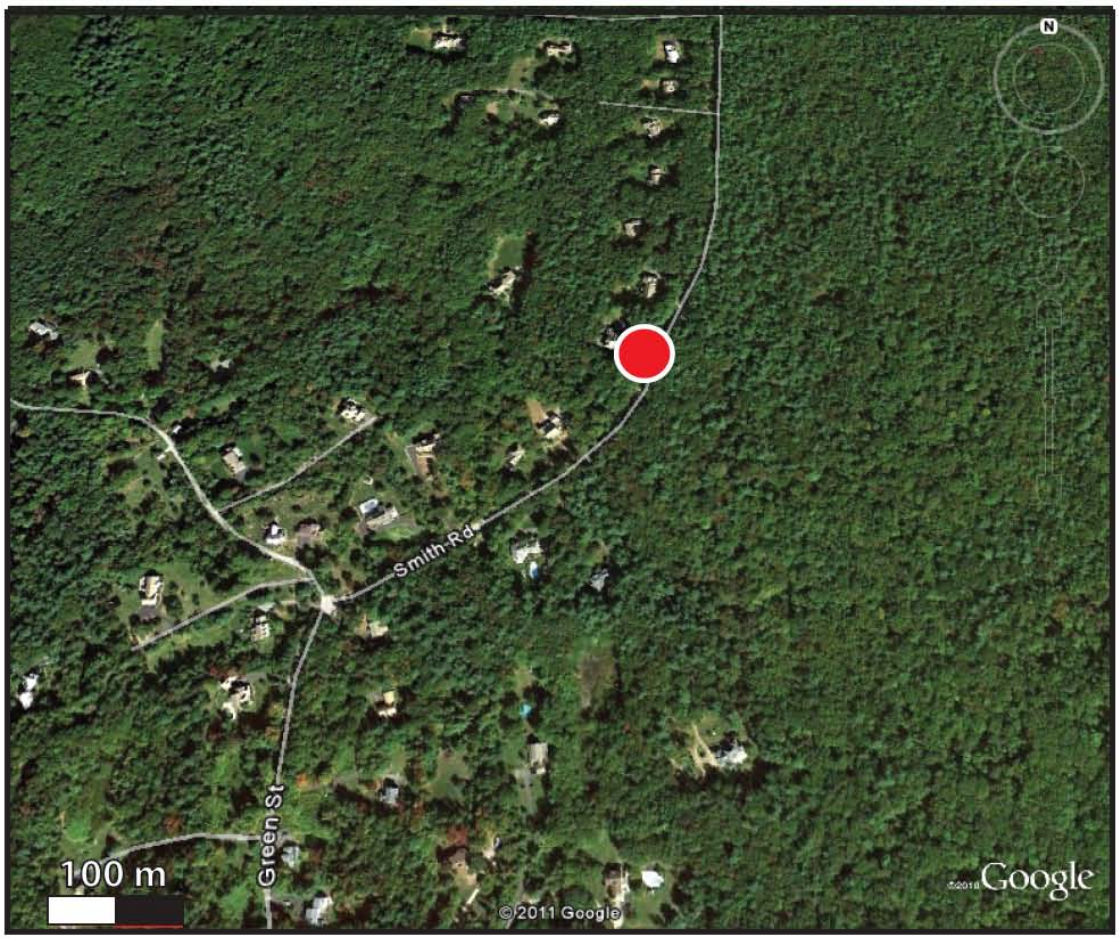

APPENDIX III
Sketch maps

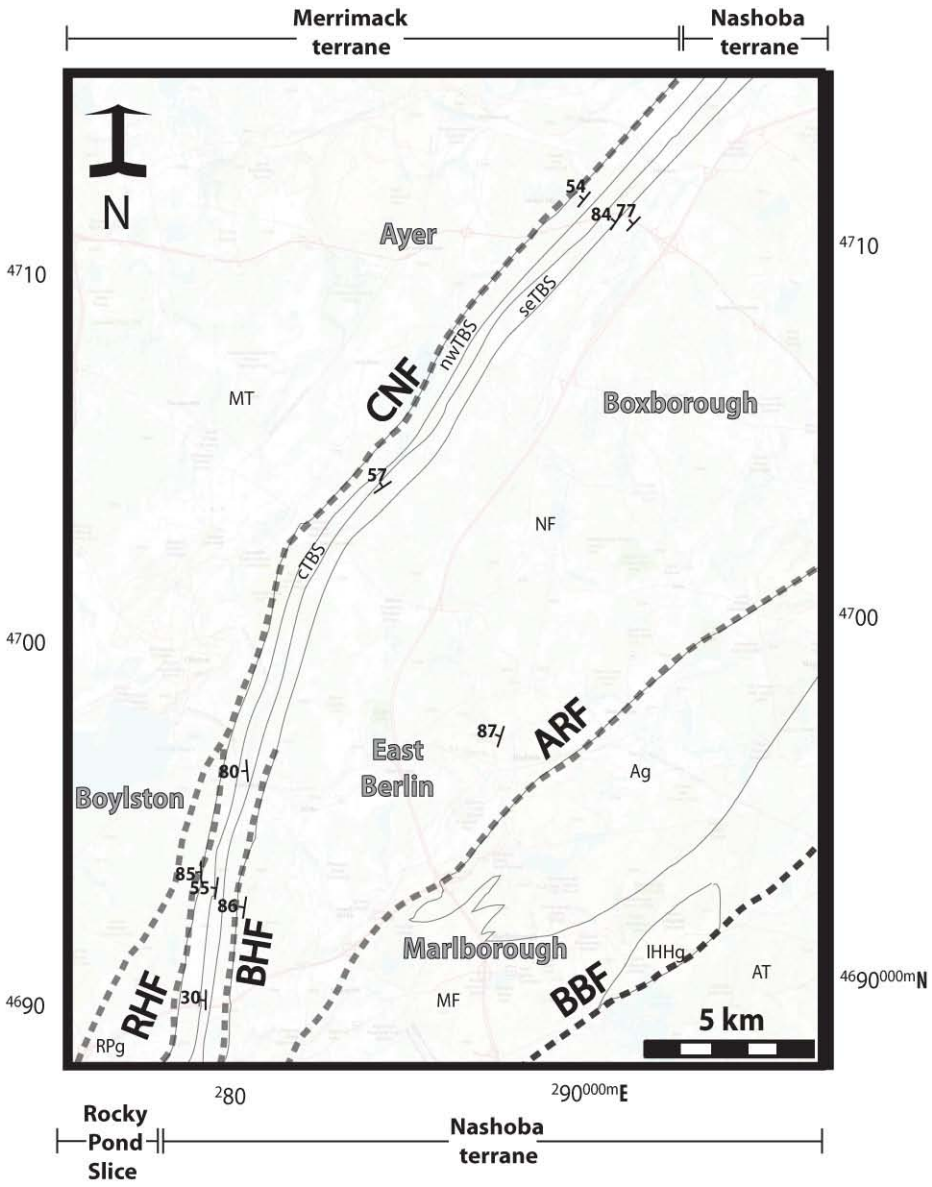

APPENDIX IIIA. Sketch map showing strike and dips measurements of foliations which were taken for this study. CNF = Clinton-Newbury fault; RHF = Rattlesnake Hill fault; BHF = Ball Hill fault; ARF = Assabet River fault; BBF = Bloody Bluff fault; MT = Merrimack terrane; nwTBS = northwest member of TBS; cTBS = central member of TBS; seTBS = southeast member of TBS; NF = Nashoba Formation; Ag = Ayer granite; MF = Marlboro Formation; IHHG = Indian Head Hill granite; AT = Avalon terrane

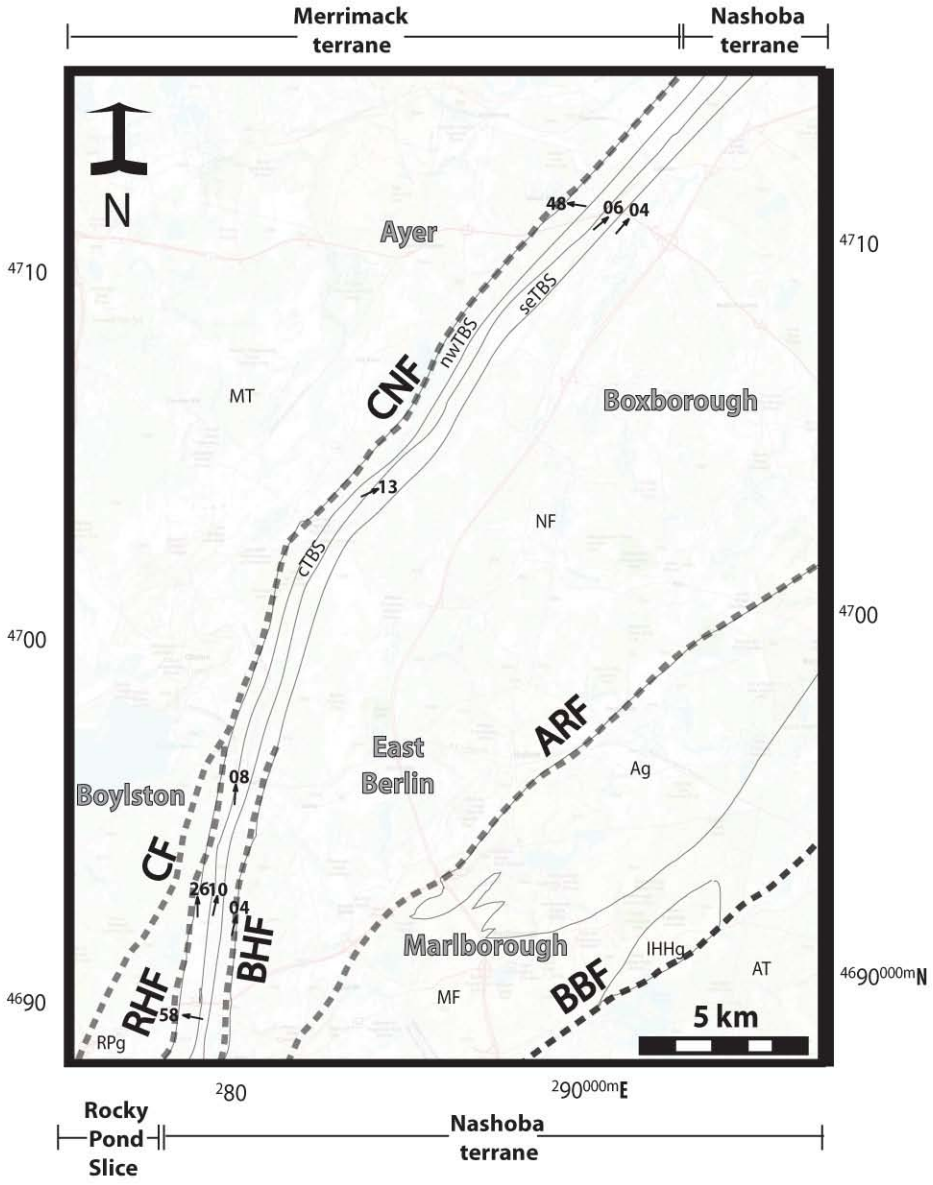

APPENDIX IIIB. Sketch map showing trend and plunge measurements of lineations which were taken for this study. CNF = Clinton-Newbury fault; RHF = Rattlesnake Hill fault; BHF = Ball Hill fault; ARF = Assabet River fault; BBF = Bloody Bluff fault; MT = Merrimack terrane; nwTBS = northwest member of TBS; cTBS = central member of TBS; seTBS = southeast member of TBS; NF = Nashoba Formation; Ag = Ayer granite; MF = Marlboro Formation; IHHG = Indian Head Hill granite; AT = Avalon terrane

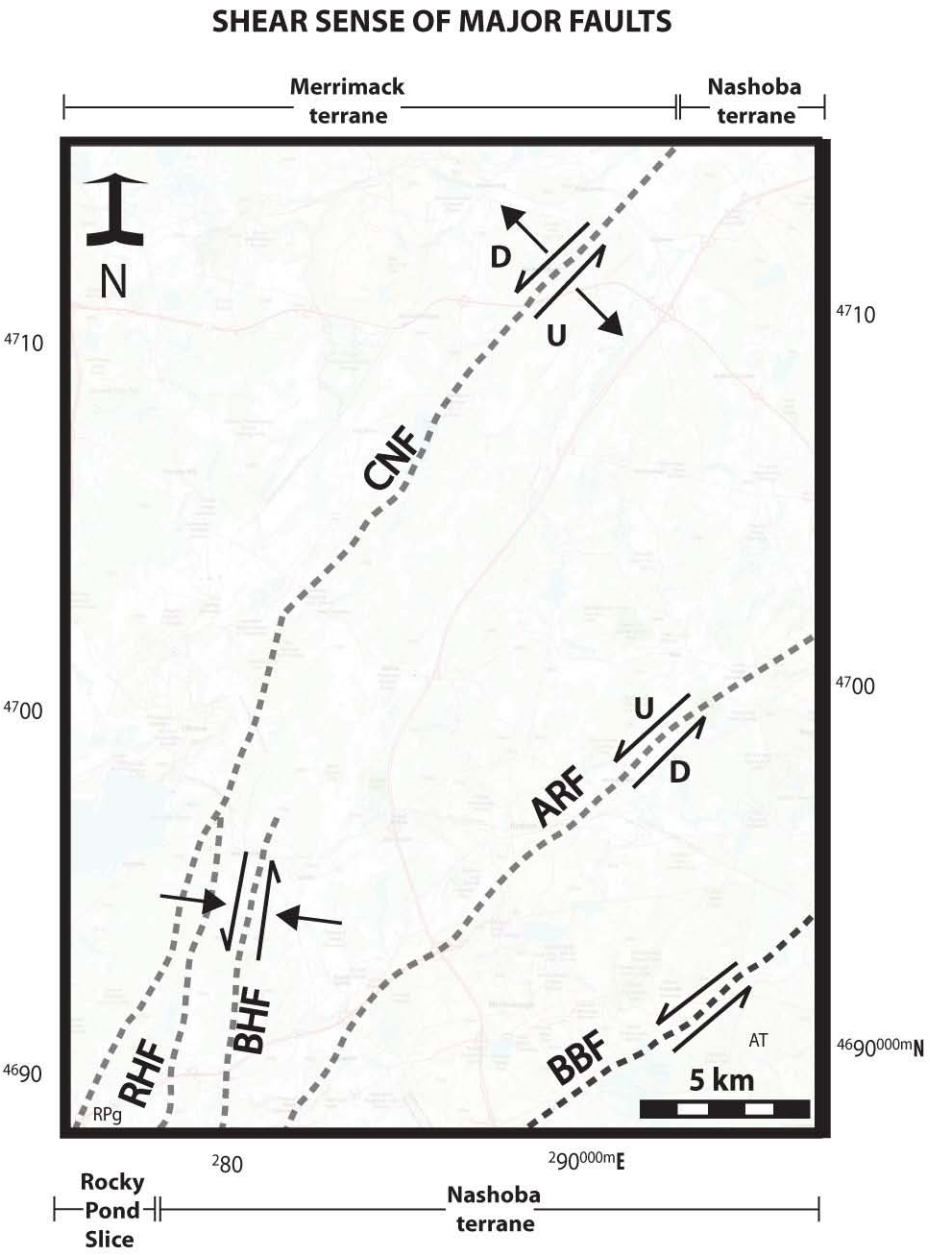

APPENDIX IIIC. Observed shear sense of major faults observed in this study, Goldstein (1994) and Markwort (2007).

METAMORPHIC ISOGRADS

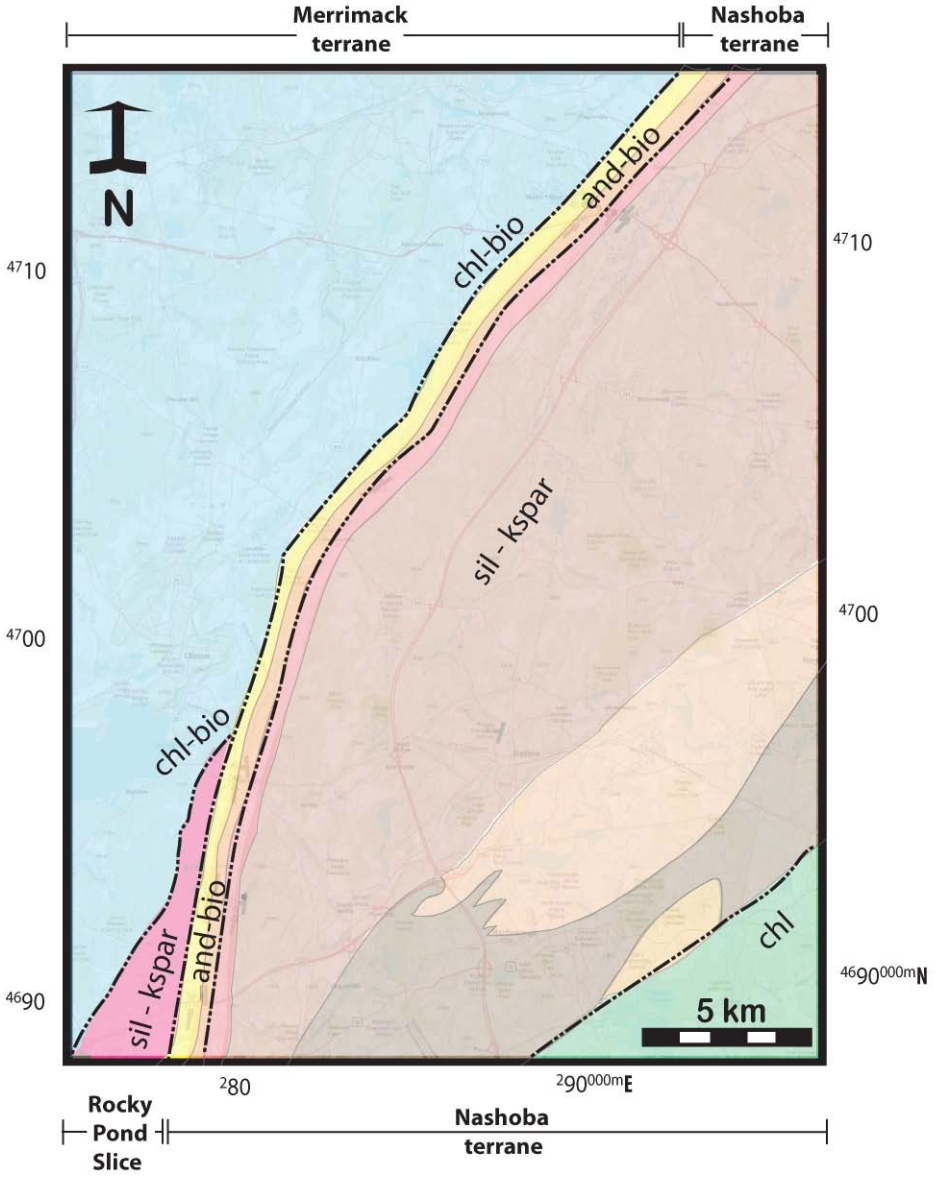

APPENDIX IIID. Simplified metamorphic isograd map of the field area.